



Politecnico
di Torino



ETH zürich

Politecnico di Torino

Master Degree in Micro and Nanotechnologies for ICT's

A.a. 2022/2023

Sessione di Laurea Ottobre 2023

Current-induced switching of in-plane magnets by Spin-Orbit Torques

Supervisors:

Prof. Dr. Pietro Gambardella

Prof. Carlo Ricciardi

Prof. Paolo Maria Eugenio

Icilio Allia

Candidate:

Natalia Boscolo

Meneguolo

(s300105)

Abstract

One of the possible tools that can be exploited for data storage nowadays are the Random Access Memories. The main advantage of this technology is that it allows to achieve almost identical writing and reading times, regardless of the position of the information inside the memory. One of the possible implementations of RAM is represented by the Magnetic RAM (MRAM), which relies on the magnetic properties of the materials in order to store data. MRAMs represent non-volatile types of Random Access Memories, i.e. functioning without the need of a constant power supply. The MRAM is based upon the possibility to manipulate the resistance value of a multi-layer structure according to the relative orientation of the magnetization between the ferromagnetic layers. This resistance manipulation allows obtaining a two state system (high resistance vs low resistance) that can be read as a 0/1 state in the digital framework.

Nowadays, almost the totality of the commercialized devices relies on systems where the magnetization pointing is out-of-plane of the multi-layer structures. However, it is possible in principle also to exploit systems displaying an in-plane magnetization. Indeed, the interest toward such systems has been recently growing given the possibility to exploit new physical phenomena for the information writing and reading that could lead to an increased efficiency and endurance of the devices.

It is such a system that has been taken into account and analysed in this thesis. Indeed, the main purpose was to verify the possibility to induce magnetization switching via Spin Orbit Torque (SOT) in in-plane ferromagnets.

To obtain an in-plane system Pt/Co bi-layers have been fabricated. In fact, by changing the thickness of such structures it is possible to tune the orientation of the magnetization (either in-plane or out-of-plane). On top of that, heavy metal (HM)/ferromagnetic (FM) bi-layers represent the perfect systems in order to be able to achieve the reversal of the magnetization based upon SOTs. We use the conversion of electric current into spin current in the HM, with a subsequent torque exertion over the FM magnetization. Pt represents a well establish material in the spintronics community because of its large spin-orbit coupling, which enables the spin-charge conversion mechanism, and allows the magnetization reversal based on SOT.

The chosen shapes for the devices under test were the Hall bars and Hall crosses. Such shapes are particularly suitable in order to perform harmonic Hall voltage measurements. However, not only electrical static characterization was carried out, but also time-resolved transport and optical characterization played an important role in the development of this thesis. In fact, the specific geometry of the in-plane magnetization makes these systems particularly interesting for time-resolved measurements. Moreover, the magneto-optical observation allows inspecting the magnetization switching of the sample eliminating the uncertainties due to spurious electrical signals.

The dimension of the presented devices is in the $\mu\text{m}/\text{nm}$ scale and the chosen shapes, beyond the Hall bars, include Hall crosses with central ellipses having three possible angles with respect to the x-axis of the system. Such a variety of shapes allowed to explore how the initial orientation of the magnetization in different directions in space can influence the reversal mechanism of the magnetization.

The results obtained with the magneto-optical technique reveal to be the most successful. It was possible to retrieve the specific condition parameters needed for the

switching (i.e. required voltage pulse amplitude and pulse length). On the other side, the time-resolved measurements did not lead to the desired results. Indeed, we are not sure about the magnetic nature of the observed signals with such a technique. The absence of clear magnetization switching signal during these measurements could be due to the inadequacy of both the samples and the setup itself. While the samples may be too small in the case of the ellipses, the setup was initially developed for out-of-plane magnetization switching investigations. This led to a measuring procedure not able to thoroughly analyse in-plane magnetization switching, since it is based on the detection of the anomalous Hall effect.

Overall, the presented thesis tries to provide an analysis of the current-induced magnetization switching in in-plane magnets, presenting not only the results obtained using different measurement setups but also their possible interpretations, with a final outlook on the in-plane technology and the possible steps that can be taken in order to improve its implementation.

Sommario

La memorizzazione dei dati nell'era moderna si basa principalmente sulle memorie ad accesso casuale (RAMs). Il vantaggio principale di questa tecnologia è che permette di ottenere tempi di scrittura e lettura quasi identici, indipendentemente dalla posizione delle informazioni all'interno della memoria stessa. Una delle possibili implementazioni della RAM è rappresentata dalla RAM magnetica (MRAM), nella quale la memorizzazione dei dati sfrutta le proprietà magnetiche dei materiali. Esse infatti si basano sulla possibilità di manipolare il valore della resistenza di una struttura multistrato in base all'orientamento relativo della magnetizzazione tra differenti strati ferromagnetici. Questa manipolazione della resistenza permette di ottenere un sistema a due stati (alta resistenza vs. bassa resistenza) che può essere letto come uno stato 0/1 in ambito digitale. Uno dei principali vantaggi delle MRAM è che rappresentano tipi di memorie non volatili, cioè funzionanti senza bisogno di un'alimentazione costante. Attualmente, la quasi totalità dei dispositivi MRAM commercializzati si basa su sistemi in cui la magnetizzazione è diretta fuori dal piano delle strutture multistrato. Tuttavia, in linea di principio, è possibile sfruttare anche sistemi che presentano una magnetizzazione nel piano (IMA). L'interesse verso tali sistemi è cresciuto di recente, data la possibilità di sfruttare nuovi fenomeni fisici per la scrittura e la lettura delle informazioni, che potrebbero portare a una maggiore efficienza e resistenza dei dispositivi.

È un sistema di questo tipo che è stato preso in considerazione e analizzato in questa tesi. Lo scopo principale era infatti quello di verificare la possibilità di indurre una commutazione della magnetizzazione tramite Spin-Orbit Torque (SOT) in ferromagneti in piano.

Per ottenere un sistema in piano sono stati fabbricati bi-strati di Pt/Co. Manipolando lo spessore di tali strutture è possibile regolare l'orientamento della magnetizzazione (in piano o fuori dal piano). Inoltre, i bi-strati di metalli pesanti (HM)/ferromagnetici (FM) rappresentano i sistemi perfetti per ottenere l'inversione della magnetizzazione basata su SOT. Infatti, assistiamo a una conversione della corrente elettrica in corrente di spin all'interfaccia tra HM/FM, con una conseguente coppia esercitata sulla magnetizzazione FM.

Il Pt rappresenta un materiale ben affermato nella comunità scientifica per il suo grande accoppiamento Spin-Orbit, fenomeno che consente il meccanismo di conversione spin-carica, portando a esperimenti di buona qualità quando entra in gioco l'inversione di magnetizzazione basata su SOT.

Le forme scelte per i dispositivi in esame sono state le barre e le croci di Hall. Tali forme si sono rivelate particolarmente adatte per eseguire misure di tensione armonica di Hall. Tuttavia, non è stata realizzata solo una caratterizzazione statica elettrica. Anche una caratterizzazione ottica e di trasporto risolta nel tempo hanno giocato un ruolo importante per lo sviluppo di questa tesi. Infatti, la specifica geometria dei sistemi fisici IMA rende questo tipo di dispositivi particolarmente interessanti per l'osservazione dell'evoluzione temporale della loro inversione della magnetizzazione. L'interesse di un'osservazione magneto-ottica è invece rappresentato dalla possibilità di ispezionare il campione eliminando le incertezze dovute alla presenza di segnali elettrici spuri. La dimensione dei dispositivi presentati è nella scala $\mu\text{m}/\text{nm}$ e le forme scelte, oltre alle barre di Hall, comprendono croci di Hall con ellissi centrali aventi tre possibili

angoli. Questa varietà di forme ha permesso di esplorare come l'orientamento iniziale della magnetizzazione in diverse direzioni dello spazio possa influenzare il meccanismo di inversione della magnetizzazione.

I risultati si sono rivelati positivi per quanto riguarda la tecnica magneto-ottica, consentendo di ottenere i parametri specifici che permettono di ottenere la commutazione in termini di pulsazioni di tensione attraverso le strutture studiate. D'altra parte, le misure risolte nel tempo non hanno portato ai risultati desiderati. Infatti, non siamo sicuri della natura magnetica dei segnali osservati. L'assenza di una commutazione di magnetizzazione durante queste misure potrebbe essere dovuta all'inadeguatezza sia dei campioni sia del setup stesso. Mentre per i primi le dimensioni scelte potrebbero risultare non ottimali (troppo piccole nel caso delle ellissi centrali delle croci di Hall), per il secondo l'osservazione principale è che il setup è stato inizialmente sviluppato per indagini sulla commutazione di magnetizzazione fuori dal piano. Questo ha portato a una procedura di misura che non è in grado di analizzare a fondo la commutazione della magnetizzazione nel piano.

Nel complesso, la tesi qui presentata cerca di fornire un'analisi dell'inversione della magnetizzazione indotta dalla corrente nei magneti in piano, presentando non solo i risultati ottenuti utilizzando diversi setup di misura, ma anche le loro possibili interpretazioni, con una prospettiva finale sulla tecnologia IMA e sui possibili passi da compiere per migliorarne l'implementazione.

Acknowledgements

This thesis, which has come to light, is the result of the contributions of many people who have guided me to this point today. It is my duty to acknowledge these people and give them the appropriate credit.

First and foremost, I would like to express my gratitude to Prof. Dr. Pietro Gambardella for providing me with the opportunity to gain experience in his lab. It was a place where I learned extensively from both theoretical and practical perspectives. The knowledge I acquired there will serve as invaluable luggage for my future experiences. I extend my heartfelt appreciation to Dr. Giacomo Sala. Without his guidance, I would have been utterly lost. He has served as a role model for me, representing a wealth of knowledge and an example of how a scientist should be, not only professionally but ethically as well.

I would also like to offer special thanks to Dr. Paul Noël. His assistance and guidance have been pivotal in helping me comprehend the subject matter, laying the groundwork for this experience.

I must not overlook my colleagues at the INTERMAG group. Without their support, this experience would not have been the same. They consistently offered their help and patiently endured my lack of experience. I wish to give a special mention to: Mingu, Marco, Pietro, Federica, Patrick, Jearin, Dominic, Aishwarya, Emir, Niklas, Richard, Benjamin and Yvonne.

My sincerest gratitude goes out to my family for their emotional and financial support.

I am deeply thankful for their unwavering encouragement of all my ideas, even the craziest ones.

I cannot fail to mention my friends who made my time in Switzerland extraordinary and unforgettable. The Zürich team: Gaetan (my Notfallkontakt who introduced me to the

Opernhaus, biking, train trips, photography, and so much more) and Roberta (my long-distance roommate, the finest pizzaiola in Switzerland, a special soul with whom I eagerly await sharing the next adventure). To my favorite hispanics in Winterthur (and beyond) Jorge and Mateo. A special nod to my steadfast friend in Geneva: Elisa. And I have certainly not forgotten Ines, Roberto, and Nicola – an invaluable addition to our journeys, always infusing them with more humor and joy.

Lastly, but certainly not least, *gracias Mati por tu apoyo, porque nunca dejaste de creer en mí.* I hope to be able to offer you at least a fraction of the support you've provided me with.

Contents

List of Figures	v
List of Acronyms	vii
1 Introduction	1
1.1 Context	2
1.2 Outline	3
2 Theoretical background	4
2.1 Ferromagnetism	6
2.1.1 Anisotropy	6
2.1.2 Exchange interaction	8
2.2 Spin magnetism	8
2.2.1 Spin-Orbit Coupling (SOC)	9
2.3 Magnetotransport and spin accumulation effects	10
2.3.1 Hall effects	10
2.3.2 Rashba Effect	12
2.3.3 Magnetoresistance (MR)	13
2.3.4 Thermoelectric effects	14
2.4 Magnetization switching	15
2.4.1 Spin Transfer Torque (STT)	16
2.4.2 Spin Orbit Torque (SOT)	17
2.4.3 Three types of structures	17
2.4.4 Switching protocol	21
3 Methods	22
3.1 Fabrication process	22
3.2 Harmonic Hall voltage measurements	23
3.2.1 Transverse and longitudinal resistance	24
3.2.2 Non-linear contributions	25
3.2.3 Field scan measurements	25
3.2.4 Angle scan measurements	26
3.2.5 DC pulse measurements	27
3.3 Time-resolved measurements	27
3.3.1 Setup structure	28
3.3.2 Measuring procedure	30
3.4 Magneto-optical characterization	31
4 Results	34
4.1 Magnetic properties characterization	35
4.1.1 Field and angle scans	36
4.1.2 DC pulse	42
4.2 Optical characterization	46
4.2.1 Non magnetic resistance changes due to electrical pulsing	46
4.2.2 Hall Crosses	47
4.2.3 Hall bars	48
4.3 Time-resolved characterization	53

4.3.1	Reference trace	53
4.3.2	Switching trace of Hall crosses	53
4.3.3	Switching trace of Hall bars	56
5	Conclusions and outlook	59
6	References	61
	Appendices	65
A	Photolithographic process for device fabrication	65
B	Masks used for sample fabrication	66
C	Electromigration	67

List of Figures

1	Big Data characteristics	1
2	Types of MRAMs	2
3	Types of SOT devices	3
4	Magnetic moment by current carrying loop	4
5	Schematic representation of diamagnetic, paramagnetic and ferromagnetic materials	5
6	Schematic representation of antiferromagnets and ferrimagnets	6
7	Magnetization loop	7
8	Spin Hall Effect schematics	10
9	Skew scattering vs side-jump scattering	11
10	Intrinsic Spin Hall Effect	12
11	Rashba Effect	13
12	Geometries of Nernst measurements	14
13	FL and DL torques	15
14	Damping and spin torque vectors	16
15	Type z magnetic device	18
16	Type y magnetic device	19
17	Type x magnetic device	20
18	\vec{M} precession for switching in three configurations	21
19	Fabricated devices	23
20	Possible planes of an angle scan measurement	27
21	Hall cross under TR measurement	28
22	Schematic of bias-T	29
23	Schematics of the TR set-up	30
24	Example of TR measurement	31
25	MOKE configurations	32
26	MOKE schematics	33
27	Type x and type y structures	34
28	Type x and y configuration schematics	34
29	Possible device's configurations	35
30	Hall bar type 1 and 2	35
31	Field scan of IMA samples	36
32	Angle scan plot of the first harmonics of xy and xx resistances	37
33	Second harmonic Hall resistance plot for a 0deg Hall cross	38
34	SOTs impact on magnetization	39
35	$R_{2\omega}^H$ angle scan	39
36	DL and FL fields evolution with the applied reading current	40
37	Comparison among angle scans	41
38	Switching in a Hall bar in y configuration	42
39	Switching in a 0° Hall cross in x configuration	43
40	Switching in a 0° Hall cross in y-configuration	44
41	DC measurements for switching performed at different external fields	44
42	DC pulse measurement of a 406 Hall bar in y-configuration	46
43	MOKE measurement of a 90 deg Hall cross in y configuration	48
44	MOKE images of switching in type 1 Hall bars in y configuration	49
45	MOKE images of switching in type 2 Hall bars in x configuration	51

46	MOKE images of switching in type 2 Hall bars in y configuration	52
47	Reference traces acquired during TR measurements	54
48	Hall cross TR switching traces	55
49	TR switching analysis with no sample	56
50	Hall bar contacted for TR measurements	57
51	TR switching measurement for a type 1 Hall bar	57
52	TR switching measurement for a type 2 Hall bar	58
53	Photolithographic process for device fabrication	65
54	Mask used for two step sample fabrication.	66
55	Mask used for one step sample fabrication.	67
56	Electromigration in 90deg Hall crosses	68

List of Acronyms

AHE Anomalous Hall Effect

ANE Anomalous Nerst Effect

DL Damping-like

FL Field like

FM Ferromagnet

HM heavy metal

IMA In-plane Magnetic Anisotropy

MR Magnetoresistance

PHE Planar Hall Effect

SHE Spin Hall Effect

SOC Spin Orbit Coupling

SOT Spin Orbit Torque

1 Introduction

We could define the 21st century as the era of big data. The definition of big data is still not too rigorous and we could try to give it a shape using the three V classification: 1) **volume**, the amount of available data; 2) **variety**, wide possibility of data and 3) **velocity**, both in terms of generation rate and required processing time.

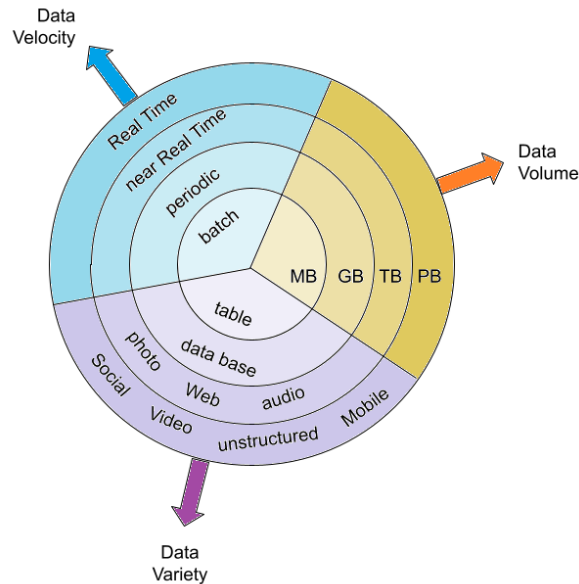


Figure 1: Big Data characteristics. Elaborated from: [Ender005](#)

Usually, the label big data addresses an extended group of information that can not be treated with a traditional processing software given the complexity that such a group entails and the statistical power required for its processing. However, even before the processing, one of the most important steps is represented by the preliminary storage of the obtained information. Given also the development of Artificial Intelligence and of the Internet of Things (IoT), the production of data is experiencing an extremely fast growth rate, which is forecast to increment exponentially over the next few years. According to 2020 estimation, almost 64.2 zettabytes were stored by that year. Such value will probably increase to 180 zettabytes by the 2025 [1]. The storage of all this information is posing new challenges to the scientific community.

Given the environmental sensibility that is developing nowadays, one of the most important requirements when dealing with the storage of data is to find an energetically efficient way to do it. Indeed, nowadays, we are experiencing the urgency to find a sustainable way to conjugate technology with our everyday life. For this reason the scientific community is trying to develop energetically efficient technologies. One of the ideal targets would be a no power-consuming storage technique. Spintronics may result helpful in such a demand. Non-volatile memory units already exist: the Magnetic Random Access Memory (MRAM). They allow retaining data even after cutting off the power supply. The basic concept underneath such a technology is the exploitation of the magnetic properties of matter. As a consequence, we are assisting to the flourishing of the domain that could allow us to obtain new paradigms of memories with better performance and lower consumption. An example of such a paradigm could be the development of an SOT in-plane

based MRAM. It is the underlying physical principles of such a kind of memory that have been studied and analysed in depth and that will be discussed in this thesis.

1.1 Context

The basic unit block composing the MRAM is the Magnetic Tunnel Junction (MTJ). An MTJ is constituted by a stack of layers. More precisely there is a thin insulating layer among a pair of nanomagnets, where one of the two serves as a reference (i.e. whose magnetization orientation is fixed, also said to be the pinning layer) and the other is free to change its magnetization direction. The relative alignment of the magnetization in the two nanomagnets (i.e. in a parallel or antiparallel way) allows to store a specific information.

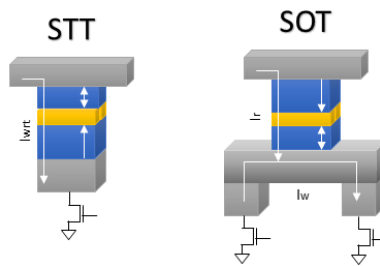


Figure 2: Spin Transfer Torque (STT) and Spin-Orbit Torque (SOT) MRAMs' architectures. In the left panel is presented a two terminal STT device. Despite allowing a high density technology, STT devices' writing latencies are limited to about 5-10 ns. In light gray are represented the metal contacts, while in blue are represented the ferromagnetic layers. The writing current (I_{wrt}) crosses the whole structure tunneling across the non-magnetic layer (yellow in the picture). In the right panel is presented instead a three terminal SOT device. Not only it is able to provide high endurance, but also it allows sub-ns operating regimes. The reading current (I_r) and I_{wrt} inside SOT structures follow two different paths (feature that allows to increase the endurance of the device itself). Elaborated from: [2]

The technological evolution has led to the use of Spin Transfer Torques (STT) first and Spin-Orbit Torques (SOT) afterwards as methods for the manipulation of the magnetization of the free magnetic layer of the stack, i.e. as writing technique. Despite STT devices being greatly compatible with the scaling down of the technologies, they display a low endurance. This is due to the high current density that tunnels through the structures during the writing process. In such a scenario SOT based devices could represent a better choice, being able not only to provide a better endurance with respect to STT counterparts, but also displaying a better access time and lower energy consumption.

A further differentiation could be made in the framework of SOT devices [3]. Indeed, by considering the orientation of the magnetization easy axis (i.e. preferential direction of the magnetization) we can distinguish three types of structures. Each one of this configuration has different properties, which lead to different advantages when thinking about their technological exploitation.

This thesis will focus on those configurations that present the magnetization placed in the plane of the device itself (i.e. displaying a 90° angle between the z-axis of the system and

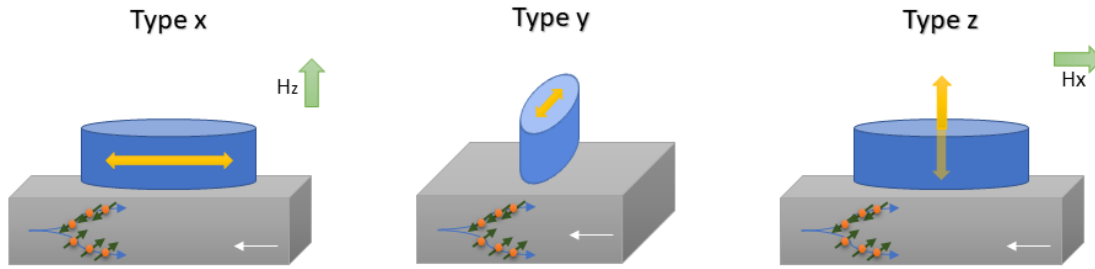


Figure 3: Types of SOT devices. The yellow arrow represents the easy-axis of the magnetization, the white arrow is the injected charge current, the dark green arrows represent the spin direction of the accumulated spins (orange spheres) the blue arrows represent the spin-polarized current splitting and the big light green arrows marked with H_x and H_z are the representation of the externally applied magnetic field. Elaborated from: [3]

the magnetization). It will be presented an analysis of how the switching (i.e. reversal of the magnetization direction) works in such systems. Not only we will discuss about the necessary conditions in order to induce such a phenomenon in the presented devices, but also about how the switching may be observed.

1.2 Outline

The thesis has been organized as follows:

- **Chapter 2** will present the basic concepts of ferromagnetism and spin magnetism. Then we will move on to the main effects exploited to probe the response of the analyzed samples to external stimuli (namely the Hall and the Nernst effects). As a last point, explanations about the differences among the three possible SOT devices configurations (namely type-z, type-x and type-y) will be given and about the actual switching requirements.
- **Chapter 3** will illustrate the used methods for sample fabrication outside and inside the clean room facilities of ETH. Also the instrumental setups exploited for the measurements will be thoroughly described, namely those for harmonic Hall voltage, magneto-optical and time-resolved measurements.
- **Chapter 4** will finally present the obtained results and their interpretation for each kind of possible structure fabricated.
- **Chapter 5** is a conclusion where the experience will be summed up and some possible continuations will be suggested along with some potential improvements to the methods exploited.

2 Theoretical background

At the basis of magnetism there are two fundamental concepts:

1. When a current flows in a wire generates a magnetic field. This idea is described by the Biot-Savart law [2.1], which takes into account μ_0 (the vacuum magnetic permeability equal to $4\pi \cdot 10^{-7} H m^{-1}$), and the differential element $d\mathbf{l}$ of wire crossed by the current having direction of the crossed path C. Also the distance of the wire element $d\mathbf{l}$ at a point l from the point where the magnetic field is measured, \mathbf{r}' , is taken in consideration.

$$\mathbf{B}(\mathbf{r}) = \frac{\mu_0}{4\pi} \int_C \frac{I d\mathbf{l} \times \mathbf{r}'}{|\mathbf{r}'|^3} \quad (2.1)$$

2. The current passing through a coil generates a magnetic dipole (Figure 4).

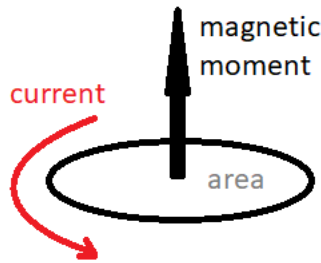


Figure 4: Magnetic moment by current carrying loop. The mathematical description is given by the formula $\mu = I \cdot A$ where μ is the magnetic moment, I is the flowing current and A is the area of the loop.

Acknowledging these concepts, we can apply them to the electrons orbiting around the nucleus of an element. Indeed, the orbiting electron (being a charge displacing in a loop) generates a magnetic field. As a consequence, we can interpret each orbiting electron as a microscopic coil, randomly oriented when in vacuum conditions. In such a way we can give rise to the concept of magnetic moment $\vec{\mu}$, noting that if all the local magnetic dipoles are gathered together into a global magnetic dipole, they lead to a universal polarization. We can now introduce the concept of magnetization, defined as the average value of the magnetic moments belonging to N particles contained in an infinitesimal volume dV (2.2).

$$\vec{M} = \frac{\sum_{i=1}^{dN} \vec{\mu}_i}{dV} \quad (2.2)$$

At this point we can distinguish the materials according to the behavior of their magnetization \vec{M} under the influence of an external magnetic field \vec{B}_{ext} :

- **Diamagnets** are those materials that experience repulsive forces when subjected to an external magnetic field. This is due to the fact that \vec{B}_{ext} induces inside of diamagnetic materials a magnetic field whose orientation is antiparallel to the external one. The internal field is called demagnetizing field \vec{B}_{dem} while the stray field represents the one generated by the material and exerted on the space surrounding it. The diamagnetic behavior may be found in all materials, however usually its contribution is so small that is easily overcome by other forms of magnetism.

- **Paramagnets** are instead weakly attracted by external applied magnetic fields since their magnetization orients parallel to the one of \vec{B}_{ext} (i.e. there is the generation of an internal field \vec{B}_{dem} which is parallel to the external one). The causes of this behavior may be understood if we look at the atomic structures of such materials. Apart some exception such as Cu, paramagnetic materials have in their orbitals unpaired electrons. Such electrons possess magnetic dipole moments, which act as small magnets. However, once the external magnetic field is suppressed, the paramagnets do not retain the magnetization, which instead is randomized by thermal motion.
- **Ferromagnets (FMs)** are materials, on the other hand, in which the external magnetic field is able to orient the magnetization, which is then maintained upon the removal of the external field itself. The majority of such materials can be found among the transition metals (e.g. Fe, Co, Ni) and the rare earths (e.g. Gd, Tb). The reason of their behavior is the presence of many unpaired electrons in their d and f -shells respectively. The long-range exchange interaction taking place in ferromagnets, keeps the ferromagnetic order even in absence of externally applied magnetic fields.
- **Antiferromagnets (AFMs)** are materials where neighbouring atoms and molecules have magnetic moments regularly aligned having one opposite direction with respect to the other. However, such an ordering of the moments exists for temperatures below the Néel Temperature (T_N), above which the material behaves paramagnetically.
- **Ferrimagnets (FiMs)** are materials in which we can find, as in AFMs, an antiparallel orientation of the neighboring magnetic moments. In this case the magnetic moments oriented antiparallely have also different order of magnitude (Figure 6), allowing a net magnetization to arise. However, such features disappear once the critical temperature (called Curie Temperature, T_c) is crossed. Above T_c there is the loss of the spontaneous magnetization of the system.

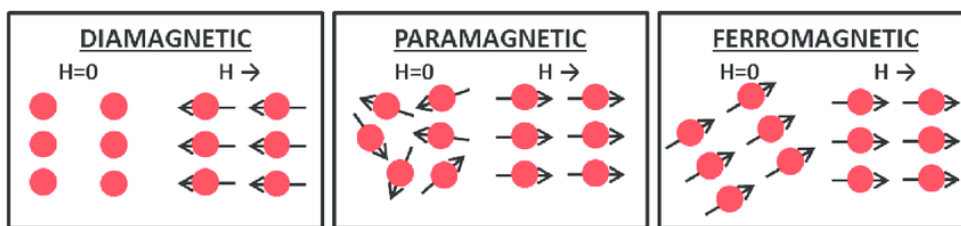


Figure 5: Schematic representation of diamagnetic, paramagnetic and ferromagnetic materials under no field conditions ($H = 0$) and under an applied magnetic field ($H \rightarrow$). The black arrows represent the magnetic moments of the atoms (red dots). Source: [4]

An important remark that has to be done is that the magnetization usually is not homogeneous throughout the space. It is instead fragmented into domains. Within each domain the magnetization is constant in amplitude and direction. The transition from one domain to the other happens through a rotation of the domain, in a structure called domain wall. Given the geometrical properties of the sample and its magnetization such domain walls can assume different profiles [5]. The width of the domain wall is determined by the equilibrium between the minimization of the total exchange energy and

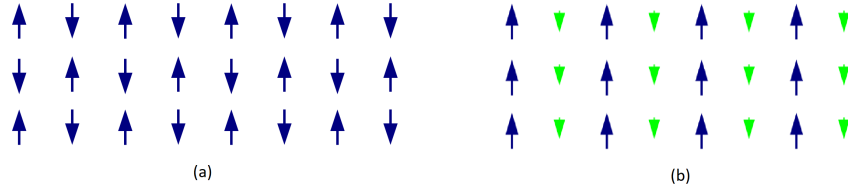


Figure 6: Schematic representation of antiferromagnets (a) and ferrimagnets (b). We can observe that in both cases the atoms' magnetic moments (represented by the arrows) have antiparallel orientation but in the case of Ferrimagnet (FiM)s they have also different amplitude (graphically represented by changing dimensions of blue and green arrows).

the anisotropy energy (Equation 2.4). Furthermore, external magnetic fields (\vec{B}_{ext}) applied on ferromagnetic materials can lead to the growth of those domains that display the magnetization parallel to \vec{B}_{ext} , or to the nucleation (i.e. generation) of new regions with such an orientation of the magnetization. According to the spatial scale that we are taking into account there are different kinds of phenomena that influence the magnetization pattern (i.e. domain distribution). We could distinguish such phenomena into short and long range. Among the short range interactions we can quote the micromagnetic exchange energy and the magnetocrystalline anisotropy (2). The micromagnetic exchange energy represents the exchange energy (described in detail in 2.1.2) applied to atomic length scales, which involves the nearest neighboring atoms. On the other side, among the long range interactions, we could include the magnetostatic interaction. Such an interaction generally depends on the shape of the system and favors the in-plane alignment (i.e. co-planar to \vec{B}_{ext}) of moments in thin film because of the dipole pattern assumed by long-ranged magnetic fields.

2.1 Ferromagnetism

Let's now focus on ferromagnetic materials. Their fingerprint is given by the magnetization loop. Indeed, what we can observe is that the magnetization has an hysteretical behavior, i.e. according if we are coming from a condition where a positive or a negative field was applied the value of the magnetization changes. According to the orientation of the material's magnetization (\vec{M}) with respect to the applied magnetic field (\vec{B}_{ext}) of the system we can have two main kind of magnetization loops: the hard loop (\vec{M} perpendicular to \vec{B}_{ext}) and the soft loop (\vec{M} parallel to \vec{B}_{ext}) (Figure 7). While hard loops are usually exploited in sensing applications, the easy loops are at the basis of memory devices (thanks to the possibility to clearly distinguish two separate states in their plot).

2.1.1 Anisotropy

Given the possibility of the magnetization to orient itself in space, we can introduce the concept of easy axis of a material. It is defined as the preferential direction in which the magnetization lays. The property of having a preferential direction of \vec{M} is called magnetic anisotropy. Such a fundamental property defines material's parameters like coercivity and remanence. The immediate consequence is that the magnetization loop is affected by the magnetic anisotropy. Therefore, we can easily understand that magnetic anisotropy is a key point when dealing with the design of magnetic devices.

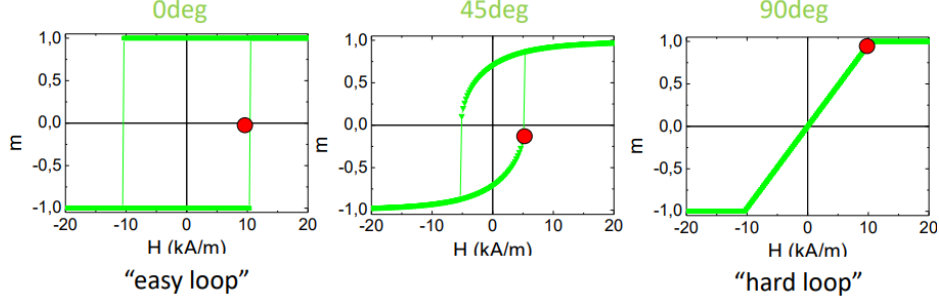


Figure 7: Plot of the magnetization versus applied magnetic field. It is possible to appreciate three different behaviours according to the angle between the magnetization and the direction of the applied field. When the two are parallel the loop is named as easy, when they are transverse the loop is defined as hard. We define as remanence magnetization (m_r) the value of the magnetization at zero applied magnetic field. The coercive field (H_c) is instead the one needed to force the magnetization to zero. Source: *Magnetic Nanostructures* course slides by L. Buda-Prejbeanu.

The anisotropy field (H_a) represents the field needed to saturate the magnetization of a uni-axial crystal in its hard direction.

The contribution to the magnetic anisotropy may come from:

1. the sample shape (**shape anisotropy**). It can be observed in non spherical objects and finds its origin in the magnetostatic energy (the one that arises when a magnetic material finds in presence of a magnetic field). It is due to the fact that the demagnetizing field (\vec{B}_{dem}) inside the material changes its value according to the direction taken into account. Indeed, the charge distribution on the surface of an object (and the dipoles that subsequently form) influences the magnitude of the demagnetized field along the different spatial directions. If we look at the theoretical discussion, we will find out that \vec{B}_{dem} is given by the product between the magnetization and the demagnetizing factor N (direction dependent with N_a, N_b, N_c the demagnetizing coefficients in the three axis directions such as $N_a + N_b + N_c = 4\pi$). Indeed, the magnetic flux density \vec{B} is related to the magnetic field strength \vec{H} by $\vec{B} = \mu_0 \vec{H}$. \vec{H} is described in Equation 2.3, where also the magnetization intensity I_i with $i \in [x, y, z]$ is direction dependent.

$$H_x = -N_a \cdot I_x, H_y = -N_b \cdot I_y, H_z = -N_c \cdot I_z \quad (2.3)$$

2. The crystal lattice of the material and the μ -scale texture (**magnetocrystalline anisotropy**). Among all the listed causes of magnetic anisotropy, Magnetocrystalline Anisotropy (MCA) represents the only intrinsic one. It may be observed by performing magnetization measurements along different crystallographic orientations of the material. The result will be magnetization curves reaching saturation for different values of applied field according to the chosen direction. The cause of this phenomenon may be found in the interaction of the crystal lattice with the spin magnetic moment of the material (more details will be given in 2.2.1).
3. Forces and tension experienced by the material (**magnetoelastic anisotropy**). Actually, the anisotropy constants giving the value of the anisotropy energy (Equation 2.4) depend on the strain. Practically speaking, magnetizing a material coincides also with changing its dimensions. As a consequence, is also possible to

perform a measure of the induced strain as a function of the applied magnetic field. This is mainly due to the stress anisotropy (i.e. change in stress intensity according to the crystallographic direction), which through the magnetoelastic coupling leads to variation of the magnetization in the different directions. The magnetoelastic coupling is defined as the change in the crystal lattice induced by a spin order. Indeed we can assist to a modification of the spin waves due to the interaction of the magnetic moments with the lattice [6].

4. The coupling between Antiferromagnet (AFM)s and Ferromagnet (FM)s which causes the antiferromagnetic material to induce a change in the magnetization of the ferromagnet (**exchange anisotropy**) [7].

The energy associated to the uniaxial anisotropy is defined as:

$$E_a = k_1 \sin^2 \theta + k_2 \sin^4 \theta \quad (2.4)$$

In Equation 2.4 the coefficients k_1 and k_2 are called anisotropy constants and they depend on the temperature conditions and on the composition of the sample. Usually higher order terms are neglected. θ represents the angle of the magnetization with the z-axis.

2.1.2 Exchange interaction

Another concept that will be useful for understanding the framework of this thesis is the one of exchange interaction. Indeed, along with the magnetic anisotropy, the exchange interaction represents one of the main features controlling the magnetic properties of transition metal compounds [8].

The exchange interaction is a quantum effect taking place among indistinguishable particles (in our case we are interested into electrons). For the Pauli's exclusion principle, we know that two fermions (class to which electrons belong) can never assume the same quantum state. As a consequence, the quantum mechanical wave function associated to two electrons in the same atom, has to be antisymmetric. It means with either symmetric local component and antisymmetric spin component or vice versa.

The simplest model to describe such a system is the classical Heisenberg one, according to which the system is defined by means of the Heisenberg Hamiltonian, which for a two particles system writes as:

$$\hat{H} = J_{12}(\vec{S}_1 \cdot \vec{S}_2) \quad (2.5)$$

In Equation 2.5 J_{12} represent the coupling constant between spins (equal to J for neighboring particles, zero otherwise), S_1 the spin momentum of the first electron while S_2 the spin momentum of the second electron.

2.2 Spin magnetism

Magnetic fields do not represent the only possible way to manipulate the magnetization of a material. Nowadays, what is mostly exploited for technological purposes is the spin magnetism that gave rise to spintronics (i.e. spin electronics). As a matter of fact, the changes in magnetization can be also obtained by taking advantage of the spins of electrons in atoms. The main advantages of such technologies is the possibility to reduce the power consumption required by devices based on such principles. Indeed, in such conditions is looming the possibility to act in close proximity of the core magnetic element of

a device, if not even within it [9].

To understand the origin of spin magnetism, we have first to make a distinction. The angular momenta associated to an electron may be of two types:

1. Orbital magnetic moment, due to the precession of the electron around the nucleus of the atom.
2. Spin magnetic moment, due to the precession of the electron around its own axis.

Both of those momenta lead to ferromagnetic properties in the material since they give rise to a current loop (i.e. charge moving in circle), which for the Ampere's law generates a magnetic field. It is the second type of momentum that finds at the origin of the spin magnetism.

In this frame work, we can define a magnetic system as a system where may be distinguished a spin polarization (i.e. a majoritarian orientation of the spins). In transition metals such a spin polarization is given by the competition between an atomic-like exchange interaction (which would tend to align the spins) and an interatomic hybridization (which on the other side would tend to reduce the spin polarization).

The main consequence of such a property of a system, is the possibility to exert torques over magnetic moments of FM only by induction of currents. It is on this principles hat are based almost all of the nowadays spintronic devices.

2.2.1 Spin-Orbit Coupling (SOC)

One of the most important points in the following discussion will be the Spin Orbit Torque effect and its exploitation for the characterization of the proposed samples and their properties. More details about this phenomenon will be given in 2.4.2, however it is important to already present the relativistic interaction underlying this concept: the Spin Orbit Coupling (SOC). SOC (also known as Spin Orbit Interaction), appears when the spin of a moving particle interacts with the electric potential surrounding such particle. Such potential could be caused by different effects (e.g. impurities and Coulomb interaction with the nucleus) [10]. Put in other words, SOC is the interaction between the spin of an electron and the orbital moment mediated by an electric field that is perceived as magnetic by the electron. Under this perspective we could define the SOC as the expression of the interchangeability between the electric and the magnetic fields in reference systems moving with respect to each other. The energy contribution brought to the system by this phenomenon may be expressed as follows:

$$E_{SOC} = \lambda_{SOC} \vec{S} \cdot \vec{L} \quad (2.6)$$

In equation Equation 2.6 λ_{SOC} is the coupling constant and \vec{S} and \vec{L} are respectively the spin and orbital momenta of the electron. Its main consequence is that spin currents are generated as a result of electric currents, with an additional induction of a torque on material's magnetization [11].

Different forms of Spin Orbit Interaction are possible according to the symmetry of the interaction (consequently giving rise to torques with different order of magnitudes) [10]. The main causes of Spin Orbit Interaction in bulk FM system can be classified as extrinsic or intrinsic. The former includes the contribution coming from the nuclear potential and the band structure. The latter, instead, refers to the presence of impurities.

2.3 Magnetotransport and spin accumulation effects

In FM heterostructures the changes in voltage (and consequently structure's resistance) that may be observed subsequently to the action of Hall and magnetoresistive effects give a good indication about the magnetization orientation. Such measures are not only at the basis of the analysis proposed in the following but of the spintronics in general, allowing the detection of spins through electrical measurements.

In the following we will therefore analyze the main effects that can be induced in heterostructures, caused by both electrical and thermal events.

2.3.1 Hall effects

We could start by explaining what the Ordinary Hall Effect (OHE) is. The Ordinary Hall Effect represents a general property of conducting materials, a consequence of the transverse Lorentz force induced by externally applied magnetic fields \vec{B}_{ext} . What happens is that the Lorentz force acts on the conduction electrons of the material, deviating their trajectory toward the edges of the material. For this reason OHE results to be proportional to the z component of the external magnetic field ($\propto B_z = \vec{B}_{ext} \cdot \cos\theta_B$ with θ_B the angle between the external field and the xy plane).

Given that, now it is possible to define the general family of Hall effects. The Hall effects include all those phenomena of different origin that have as a final consequence the deviation and subsequent accumulation of spins at the edges of a material and at the interfaces in a heterostructure.

Spin Hall Effect (SHE) One the most important phenomenon of conversion of charge current into spin current is the Spin Hall Effect (SHE). The spin current may be defined as the flow of electrons carrying spin information [12]. The SHE is a transport phenomenon. In an analogous way to the Ordinary Hall Effect, the SHE consists into the accumulation of opposite spin electrons at the two sides of a non-magnet (schematically shown in Figure 8). Therefore it is said to be a spin accumulation effect.

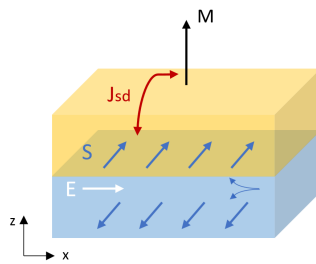


Figure 8: Spin Hall Effect schematics. We have a spin accumulation (blue arrows) on the two opposite surfaces of the non-magnetic layer (blue in the picture). \mathbf{E} represents the internal electric field while \mathbf{M} is the magnetization of the FM (yellow layer in the picture), in this case pointing out-of the plane. \mathbf{J}_{sd} represents the exchange interaction between the magnetization and the non-equilibrium spins (which is the cause of SOTs). Elaborated from: [13]

The origin of the SHE can be localized in the bulk of the material. Such nature opposes it to the Rashba effect (which will be treated more in detail in 2.3.2). In the bulk, the spin-dependent scattering events induce the net accumulation of spins at the edges of the material. Such scattering events may be distinguish in three main contributions [14]:

- **Skew scattering or Mott-skew scattering** [15]. Considered as an extrinsic contribution, the skew scattering leads to different scattering cross-section of electrons accordingly if they are spin-up or spin-down. Such an inelastic scattering is caused by the interaction with impurities in the lattice. More precisely, what happens is that the force acting on the spins ($\vec{F} = \nabla(\vec{s} \cdot \vec{H})$ with \vec{s} spin and \vec{H} magnetic field induced by flowing charges), according to the direction of the spin itself and of the magnetic field, deviates electrons either toward the left or the right side, resulting in a collective scatter of the spin-up electrons in one direction and spin-down in the other.
- **Side-jump mechanism.** Also the side-jump scattering is considered as an extrinsic phenomenon, however, it is a purely quantum mechanical effect. Considering the quantum description of the electron as a wavepacket, when in proximity of an impurity the electron will experience a slight shift of its original trajectory (Figure 9). Adding to this behavior also a low scatter density, we will assist to an accumulation of electrons on the edges of the material. Indeed, a low scattering density means the absence of interfaces between different scattering events.
- **Intrinsic contribution** [16]. Last but not least, we have to account also for a purely band structure contribution. Here the Bloch electrons, accelerated by longitudinal electric field (\mathbf{E}), according to their \mathbf{k} vectors and the direction of \mathbf{E} will experience a distortion of the Fermi surface (Figure 10). This will lead to the acceleration of the electrons in a direction depending on \mathbf{k} and \mathbf{E} . The main consequence of such a precession motion is the rise of a spin population.

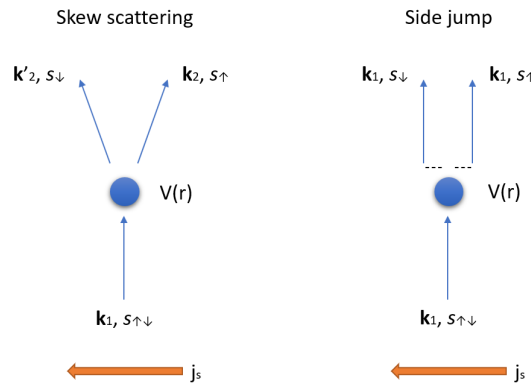


Figure 9: In the case of a skew or a side-jump scattering, after the interaction with the impurity, the momentum \mathbf{k} of the electron differs, representing the main difference among the two mechanisms. In the first case the electron coming with speed $V(r)$ and momentum \mathbf{k}_1 , according to if it has spin-up or spin-down can be scattered and get a momentum \mathbf{k}_2 or \mathbf{k}'_2 respectively. In the second case the momentum is preserved. Elaborated from: [14]

Anomalous Hall Effect (AHE) In ferromagnets, the Ordinary Hall Effect (OHE) and the SHE are not the only Hall effect that takes place. Indeed, because of the Spin Orbit Interaction (2.2.1), in a FM we can observe an anomalously large transverse voltage, which gives rise to the Anomalous Hall Effect (AHE) [17]. The reasons for this effect are also traceable back to the scattering events that were listed among the reasons leading to

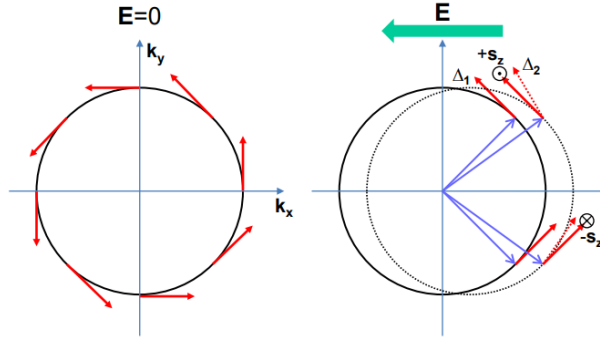


Figure 10: As shown in the left panel, when the \mathbf{k} vector has a $+\mathbf{y}$ component, the spin (red arrow) is along $-\mathbf{x}$ (and vice versa). By applying an external electric field (green arrow, right panel) along $-\mathbf{x}$, we have a distortion of the Fermi surface and a gain in speed by electrons along $+\mathbf{x}$, with a spin polarization component along $+\mathbf{y}$. The result is the exertion of a torque on spins, which will force them to precess around the field itself. Source: [14]

the SHE. However, it is still not clear which is the amount of influence of each scattering component in the overall effect. The AHE depends on the out-of-plane magnetization component (i.e. $\propto m_z = m \cdot \cos\theta$). It is said to be a magnetotransport effect.

Planar Hall Effect (PHE) As for the Anisotropic Magnetoresistance (AMR), the PHE stands from the orbital-dependent electron scattering. Indeed, electrons are scattered more or less according to how the electron current is oriented with respect to the material's magnetization. The Planar Hall Effect (PHE) is the transverse manifestation of the longitudinal magnetoresistance effect (described in 2.3.3). The name planar is due to the fact that such a scattering is also co-planar to the in-plane magnetization component (i.e. $\propto m_x \cdot m_y$). The PHE is classified as a magnetotransport effect.

2.3.2 Rashba Effect

The Rashba effect represents a second type of contribution able to change local electric currents into spin currents [18], belonging as a consequence to the spin accumulation effects class. The reason behind this phenomenon is the breaking of the crystal symmetry at the interface between two materials. Indeed, a net electric field is experienced by electrons when moving in asymmetric crystal-field potentials (i.e. in asymmetric lattices). In other words, the electric field is a consequence of the different work functions of the two materials constituting the interface. The magnetic field standing from the electric one is called Rashba field (Equation 2.7) [19], and couples orbital and spin momenta of the two materials [20]. In the Rashba field equation $\hat{\mathbf{z}}$ is a unit vector perpendicular to the surface of the material, \mathbf{k} the linear momentum, α_R is the Rashba constant (material dependent) and $\boldsymbol{\sigma}$ the spin angular momentum.

$$H_R = \alpha_R(\hat{\mathbf{z}} \times \mathbf{k}) \cdot \boldsymbol{\sigma} \quad (2.7)$$

If we take into account a non-magnetic/FM interface, the magnetic material's local magnetic order is affected by the spins induced by the Rashba field thanks to the exchange interaction (2.1.2). The result is an effective field exerted on local magnetic moments [21].

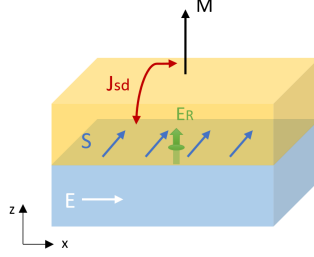


Figure 11: Schematics of the Rashba effect. The interfacial electric field \mathbf{E}_R causes the polarization of the spins \mathbf{S} of the conduction electrons of the flowing current at the interface. Those electrons were dragged at the interface by the external electric field \mathbf{E} . Elaborated from: [13]

The Rashba SOC (which will be a useful concept when analysing Spin Orbit Torque (SOT)s), is therefore the result of the interfacial electric field (directed perpendicularly w.r.t. the interface itself), which gives rise to the Rashba magnetic field [22].

2.3.3 Magnetoresistance (MR)

In ferromagnetic metals we have to consider that there is not only a classical component to resistivity due to the finite scattering time of travelling electrons (because of the presence of impurities, grain boundaries, phonons). Also, material properties such as composition, structure and size influence what is called the Magnetoresistance (MR) of ferromagnets. Among the contributions to the MR we can find:

- **The ordinary Lorentz MR.** It can be understood taking into account that electrons have a cycloidal motion when undergoing a magnetic field. As a consequence, applying an external magnetic field, we assist to an increase of the longitudinal resistance, which is $\propto B_{ext}^2$. Given the dependence on B_{ext} , such an effect is present not only in ferromagnetic but also in paramagnetic state.
- **The spin-disorder MR** on the other side is a property of exclusively FM. It coincides with the decrease of the resistance with a linear proportionality to B_{ext} . The cause of this phenomenon may be found in the decrease of the electron-magnon scattering due to the suppression of spin-disorder induced by low energy magnons.
- **The Anisotropic Magnetoresistance (AMR).** What we observe in this case is a maximum in the resistivity of the FM when the magnetization (\vec{M}) is oriented in the direction parallel to the one of an injected current (\vec{j}). Instead, the minimum of the resistance is achieved with a perpendicular orientation of the magnetization to the current. Such an observation finds its reason in the Spin Orbit Interaction and how the atomic orbitals orient themselves depending on how the magnetization is directed. A larger scattering cross-section is observed when \vec{j} and \vec{M} are parallel and a smaller when the two are perpendicular.
- **The Unidirectional Spin Hall Magnetoresistance (USMR).** In addition to the linear effects, also the non-linear ones have to be taken into account as contributions to the measurements performed. Among those we can find the USMR, representing the increase of the longitudinal resistance of the device when the spin accumulation is parallel to the magnetization of the FM layer of the structure.

The whole class of MR contributions belongs to the magnetotransport effects family.

2.3.4 Thermoelectric effects

A further step in the discussion is represented by taking into account also the effects produced by temperature gradients. Higher temperature is associated with a larger phonon density, which translates into a greater interaction with free electrons, i.e. more scattering events. In presence of a temperature gradient (∇T), we assist to a flow of electrons from warmer to cooler regions because of the larger kinetic energy possessed by the electrons in the warmer region, which translates into a higher velocity. In conclusion, we can obtain the generation of an electrical current from a ∇T , a phenomenon called the Seebeck effect. There also exist a thermal equivalent to the spin Hall effect called the Spin Seebeck Effect (SSE). More generally there exists a whole group of effects that represent the thermal equivalents of the Hall effects. This new group of phenomena is called as the one of Nernst effects. We can list: the ordinary Nernst effect (ONE), the Anomalous Nernst Effect (ANE), the Planar Nernst Effect (PNE) and the Spin Nernst Effect (SNE). To find a physical explanation to their nature we can apply the same reasoning that we made for the respective Hall effects. Speaking about correspondences, we can also find a thermal analogous to the MR: the Magneto-thermopower (MTP). With thermopower we define the redistribution of electrons due to a ∇T [23].

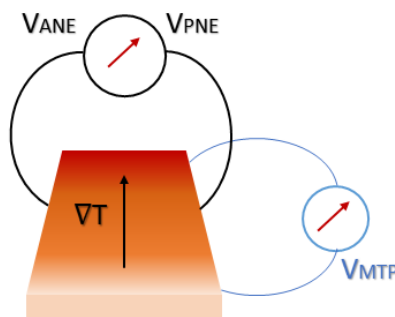


Figure 12: Given a specific temperature gradient, the measurement geometries of anomalous and planar Nernst effects are shown, along with the magneto-thermopower. The electric field that is generated by the Anomalous Nernst Effect (ANE) has a symmetry given by $\mathbf{E}_{ANE} = -\alpha_{ANE} \nabla T \times \mathbf{M}$, where α_{ANE} represents the ANE coefficient.

2.4 Magnetization switching

The main topic of the thesis was the induction of a magnetization (\vec{M}) reversal in in-plane magnetic devices through means of a current. In order to achieve such a behavior we can exploit the exertion of a torque on material's magnetization, namely the spin torque effect. Before moving on to any further details about which kinds of spin torque effects we can find in a FM, it is worth to spend few words on how the magnetization dynamics works, i.e. the physics behind the reorientation of \vec{M} . For this kind of description it comes into help the Landau-Lifshitz-Gilbert (LLG) equation (2.8).

$$\frac{d\vec{M}}{dt} = -\gamma_{eff}\vec{M} \times \vec{B}_{eff} + \alpha_{eff}\vec{M} \times \frac{d\vec{M}}{dt} \quad (2.8)$$

The terms γ_{eff} and α_{eff} in the LLG equation represent respectively the effective gyromagnetic ratio and the effective Gilbert damping factor. Furthermore, we can distinguish two terms on the right-hand side of 2.8. The first term represents the precessional torque, which causes the precession of the systems magnetization \vec{M} around the external magnetic field \vec{B}_{eff} . Indeed, we are talking about a system's magnetization since we are applying a macrospin assumption. It means that we are assuming \vec{M} to be constant in magnitude, therefore constituting a single magnetic moment for the whole system thanks to the coupling of the different electrons spin momenta generated by the action of the exchange interaction. On the other side, the second term in the right-hand side of 2.8, represents a damping torque. This one causes an orientation of \vec{M} towards \vec{B}_{eff} . While the first term was of conservative kind, since during the precession the angle Θ between \vec{M} and \vec{B}_{eff} is kept constant, on the contrary this second term takes into account the dissipative phenomena, since we may observe a variation of the angular momentum, which for $\Theta = 0$ displays the minimum of the potential energy.

We can therefore split the torque contribution into the so-called Field like (FL) torque, represented by $\vec{T}_{FL} = \vec{M} \times \vec{B}_{eff}$, and the so-called Damping-like (DL) torque, given by $\vec{T}_{DL} = \vec{M} \times \frac{d\vec{M}}{dt}$.

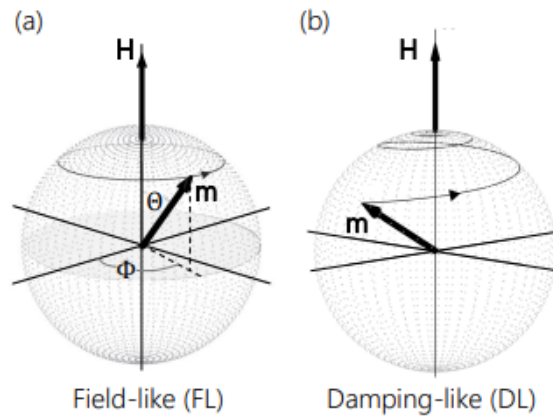


Figure 13: FL (a) and DL (b) torques acting on magnetization. What we assist to is an initial precession of the magnetic moment under the effect of an external magnetic field. The magnetic moment aligns to the field after a short time, in a damped spiral motion. Source: [24]

So far, have been identified two possible types of spin torque effects: 1) the Spin Transfer Torque and 2) the Spin Orbit Torque. At the basis of the first effect we find the interaction

of the magnetization of the system with an injected spin-polarized current. On the other side, in the second case, the magnetization is affected by the transfer of orbital angular momentum from the lattice to the spin system (mechanism mediated by the SOC).

2.4.1 Spin Transfer Torque (STT)

By Spin Transfer Torque we define a torque exerted on the magnetization by a polarized spin current, which causes its reorientation (a schematic representation is given in Figure 14). Usually such a torque is exerted by non-equilibrium conduction electrons on FM. Its cause may be found in the variation to which is subjected the current of spin angular momentum [25]. Changes in current could be due for example to the crossing of spin-polarized electrons of non-uniform magnetic distributions (such as domain walls). What happens in the majority of the cases (e.g. in Magnetic Tunnel Junctions), is a transfer of momentum from one FM to another.

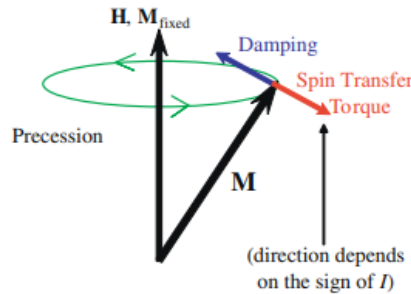


Figure 14: Damping and spin torque vectors. \mathbf{M}_{fixed} is the magnetization of the fixed layer while \mathbf{M} is the one of the free layer. The geometry taken into account is the simplest one, with \mathbf{M} assumed to be able to move as a macrospin (i.e. non taking into account the moments on a μ -scale). \mathbf{H} is the magnetic field and is assumed to be fixed along with \mathbf{M}_{fixed} . We note that in case of absence of damping and spin transfer torques, with a \mathbf{M} even slightly tilted away from the \mathbf{M}_{fixed} , the magnetization starts to precess under the action of the FL torque. The damping component (red arrow in the picture) contributes to the alignment of \mathbf{M} to \mathbf{M}_{fixed} , which represent the low-energy configuration. If also a current is introduced in the system, we have the emergence of a spin transfer torque component, which direction depends on the sign of the current. In case the damping and the STT components are in the same direction the result is a faster spiraling of \mathbf{M} towards \mathbf{M}_{fixed} . On the other side, oppositely directed damping and STT components can result in a decreased effect of the damping (case STT weaker than damping) or a spiraling of \mathbf{M} away from the low energy configuration (case STT stronger than damping). Source: [25]

Let's take into account a practical example. Consider two FM layers with a metal layer in between. Let's assume one of the two FM layers has a fixed magnetization. By injecting a current directed from the reference to the free layer, this current will become spin-polarized (the reference layer acts as a spin-filter). The electrons reaching the free layer travelling across the metal layer will induce an orientation of the magnetization parallel to the one of the reference layer. Those electrons, having non-collinear spin to the free layer, will induce a torque on free-layer electrons, resulting in a parallel alignment of the magnetization of the two FM layers. On the other side, by applying a current having opposite polarity, electrons will flow from the free layer to the pinning one. The electrons having spin anti-parallel to those of the reference layer will be reflected at the interface

with the metal and sent back to the free layer. The result is an antiparallel alignment of the magnetization in the two FM layers.

We can therefore conclude that thanks to STT we are able to manipulate the magnetization without any need of external magnetic fields.

2.4.2 Spin Orbit Torque (SOT)

As already mentioned in the introduction to this section, at the basis of SOT we find the SOC. Also in this case the torque generated by the transfer of the angular momentum (leading to a spin accumulation and a subsequent deterministic switch of the magnetization) can be divided into two contributions: 1) the FL torque ($\mathbf{T}_{FL} \propto \vec{M} \times \hat{\mathbf{y}}$ with $\hat{\mathbf{y}}$ versor of the y-axis and perpendicular to the current injected in the system) and 2) the DL torque ($\mathbf{T}_{DL} \propto \vec{M} \times (\hat{\mathbf{y}} \times \vec{M})$).

The first observation of the SOT were made on heavy metal (HM)/ferromagnet structures. It is for this reason that the explanations given in the following about this physical phenomenon take as a reference system such a bilayer.

The spin accumulation at the interface between a HM and a FM can be ascribed to two key players: the SHE and the Rashba-Edelstein effect [26].

1. **Bulk SHE.** In this case the torque is generated by the exchange interaction that develops between the perpendicular spin component and the magnetization, causing a transfer of angular momentum from the former to the latter. The spin current is pumped by the heavy metal toward the ferromagnet. The spin polarization on the other side results to be oriented in-plane, perpendicular to the current flow.
2. **Rashba-Edelstein effect (REE).** In this case we have an interfacial spin accumulation which is due to the breaking of inversion symmetry subsequent to in-plane moving carriers. The generated torque is dominated by the FL component when the spins align perpendicularly to the momentum (i.e. exchange interaction among spin accumulation and FM's magnetization is weaker than the Rashba SOC). On the other hand, the torque is dominated by the DL component when we have an out-of-plane spin accumulation.

2.4.3 Three types of structures

As also mentioned in the introduction, three possible structures of devices can be implemented by injecting an in-plane current across the device (called CIP configuration). What distinguishes those three types of structures is the preferential orientation of the magnetization in space. Given the diversity among those three configurations, they display also three different magnetization switching mechanisms enhanced by three different initial conditions.

Type z The type z structure is characterized by the magnetization pointing perpendicularly to the material's plane. The name refers to the fact that the magnetization is oriented along the z-axis of the reference system taken into account.

In this kind of structure a symmetry breaking of the system is required in order to achieve bipolar switching. Such condition may be achieved by applying an external magnetic field along the x-axis. Actually, what may be observed is a maximum torque for an external applied magnetic field in the same direction of the current injected into the substrate.

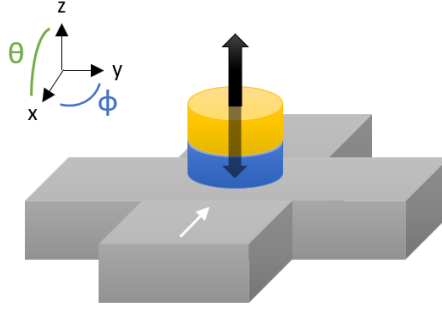


Figure 15: Type z magnetic device. The structure is made by a thin cobalt layer (blue in the picture) with strong perpendicular anisotropy and Rashba interaction induced by asymmetric Pt (grey) and AlO (yellow) interface layers. The black arrow represents the magnetization while the white one the injected current. Elaborated from: [27]

Such a behavior is induced by a spin accumulation along $\mathbf{B}_R \times \mathbf{M}$. $\mathbf{B}_R = \alpha_R(\hat{\mathbf{z}} \times \mathbf{j})$ is the Rashba field that arises at the interface between the HM and FM constituting the device. The causes of such an accumulation may be traced back to two main effects:

1. applied magnetic field parallel to \mathbf{j} leads to a spin polarization component orthogonal to current's plane, because of the action of \mathbf{B}_R combined with the spin-dependency of the mobility. The result is a net spin accumulation parallel to the $\hat{\mathbf{z}}$ component of $\mathbf{B}_R \times \mathbf{M}$, mediated by the $s - d$ exchange.
2. SHE in Pt causes an absorption of spin current with a subsequent diffusion in Co. However, this component is part of a more complex mechanism, since the SHE is not able on its own to justify the intensity of the switching field. It is thought that the vertical gradient of \mathbf{B}_R at Pt/Co interface could induce additional spin currents that add up to the SHE one.

We could be interested in understanding the critical current J_C needed for the switching. It has been proved [28] that for a magnetic layer having perpendicular magnetization (the so-called PMA sample) and featuring in-plane current generated by SHE, J_C takes the form of:

$$J_C = \frac{2e M_s t_F}{\hbar \theta_{SH}^{eff}} \left(\frac{H_K^{eff}}{2} - \frac{H_x}{\sqrt{2}} \right) \quad (2.9)$$

In Equation 2.9 e represents the elementary charge, \hbar the Dirac constant, θ_{SH}^{eff} the effective spin Hall angle (measure of the conversion efficiency between charge currents and pure spin currents, material dependent) and M_s saturation magnetization, t_F thickness, H_K^{eff} effective anisotropy field all referred to the ferromagnetic layer. In order to have an idea about the order of magnitude of J_C let's take into account perpendicularly magnetized Co dots (system used to give the first proof of such a structure in 2011). For dots with lateral size of 500 nm, the switching is observed by pulsing across the structure currents of 1.9 mA with 15 ns pulse length. This translates into a current density of about $10^8 \text{ A}\cdot\text{cm}^{-2}$ [27]. It is important to note that as far as the lateral size of the dot is increased, also the critical current proportionally decreases. If instead we manipulate the pulse length, the critical current results to be inversely proportional to it.

On the other side, if we are interested in the switching times, the time scale for type z structures results to be really fast, with a magnetization dynamics being < 1 ns.

Type y The type y structure, as the name itself says, displays the magnetization \vec{M} oriented along the y axis of the reference system. The current needed for achieving the switching is injected along the x-axis. In such a way there is a 90° angle among the two. This kind of configuration (among with the type x one), constitutes the In-plane Magnetic Anisotropy (IMA) devices, since \vec{M} finds in the plane of the structure.

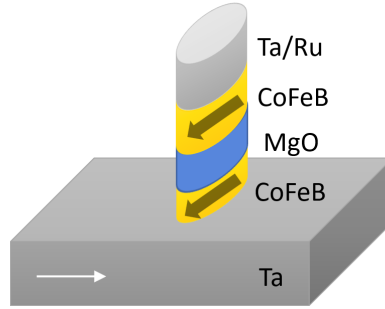


Figure 16: Type y magnetic device. The structure is constituted (starting from the bottom) by Ta(6.2nm)/CoFeB(1.6nm)/MgO(1.6nm)/CoFeB(3.8nm)/Ta(5)/Ru(5). The Ta bottom layer has the shape of a $1\mu\text{m}\times 5\mu\text{m}$ strip. The white arrow refers to the injected current. Elaborated from: [29]

If we move to the analysis of the switching mechanism, we will discover that there is no need to apply an external magnetic field in order to enhance the process. This is because the physical phenomenon upon which the mechanism is based is the giant SHE. We assist to the generation of spin torques due to a spin current in the transverse direction to the one in which the charge current has been injected in the material. Those torques lead to the reversal of the magnetization after an initial precession. As shown in [29] for Ta-based samples, a further proof of this explanation is given by the fact that we are able to exclude the Oersted field as responsible phenomena for the switching. Indeed, the Oersted field displays an opposite polarity with respect to the observed switching and results to be smaller with respect to the coercive field of the material. On top of that, since the switching phase diagram is consistent with a thermally assisted DL spin torque and in contrast with any other current generated effective field, we can also exclude any contribution due to FL originating from the REE.

Also in this case we could be interested to compute the critical current value J_C needed in order to be able to observe a switching event in such a structure. It has been proven [29] that it is given by:

$$J_C = \frac{2e}{\hbar} \frac{\alpha M s t_F}{\theta_{SH}^{eff}} \left(H_{K, in}^{eff} + \frac{H_{K, out}^{eff}}{2} \right) \quad (2.10)$$

In this case, in 2.10 α represents the Gilbert constant, $H_{K, in}^{eff}$ the in-plane effective anisotropy field and $H_{K, out}^{eff}$ the out-of-plane one. As far as the order of magnitude of such a current is concerned, also in this case the dimension of the structure plays an important role. Indeed, the reduction of the dimensions leads to a decrease of J_C . The same effect is given also by the decrease of the demagnetizing field of the FM free layer. For example, for a structure of 100×350 nm of Ta(6.2nm)/CoFeB(1.6nm) J_C is about $6 \cdot 10^8 \text{A} \cdot \text{cm}^{-2}$.

If we are interested instead in switching times τ_S we could argue that they are comparable to those that may be encountered for STT-PMA (Perpendicular Magnetic Anisotropy) devices given the similar geometry of the structures. Indeed the switching is obtained after many initial precessions. τ_S results therefore to be in the time scale of tens to few ns [30].

Type x As last, we will present the type x structure, in which (as the name suggests) \vec{M} is directed along the x-axis of the system and parallel to the injected current.

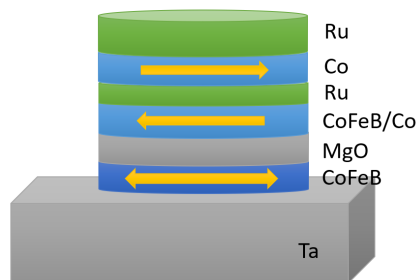


Figure 17: Type x magnetic device. The MTJ structure used for the first studies was grown on a Ta channel. Elaborated from: [3]

The configuration displays an SOT switching mechanism. We assist to the action of SOT generated by the HM on the ferromagnetic free layer, mediated by the SOC [31]. What peculiar in such a structure is that the bipolar switching is achieved by applying an external magnetic field along the z direction, H_z (analogous to the initial conditions needed by the type z structure). The sign of H_z directly affects the switching direction, which suggests that the reversal of the magnetization is due to the damping-like component of the SOT.

In this case the critical current J_C is in the order of $2 - 3 \cdot 10^{11} \text{ A} \cdot \text{m}^{-2}$. Unfortunately, despite the similarities in the leading switching mechanisms between type z and y devices, J_C can not be determined using Equation 2.9. This is because while type z structures have uniaxial anisotropy, type x configurations display two different anisotropy values if we are considering xy or xz planes. However, we can note that J_C depends on H_z with a linear inverse proportionality.

Also in this case, the switching takes place soon after the application of the current, with switching times of $< 1 \text{ ns}$ [31]. This shows that type x and z structures are better in term of fast control of the magnetization with respect to the type y configuration.

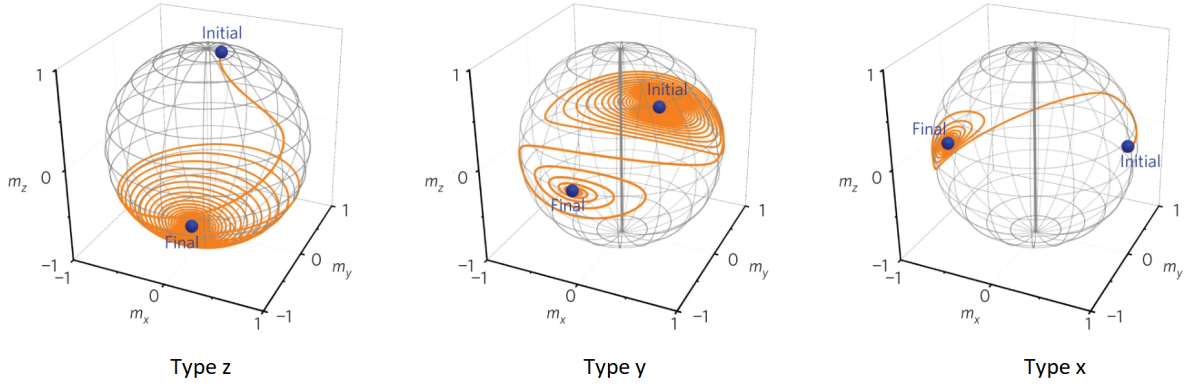


Figure 18: \vec{M} precession for switching in the three configurations. The length of the required precessions in initial and final state before completing the switching affect the switching time τ_S . Source: [3].

2.4.4 Switching protocol

As presented in the previous paragraph, we need to have a current flowing across the samples in order to induce the reversal of \vec{M} . The technique usually employed consists into sending current pulses across the investigated structures. As seen, the parameters of such pulses (namely the pulse length and the amplitude) in association with an externally applied magnetic field can lead to a successful switching or not.

As far as IMA samples are taken into account, the magnetization dynamics is driven by the SOT mechanism.

In order to trigger the magnetization reversal, usually the procedure consists into sending set and reset pulses through the device. In such a way the set pulse will trigger the switching while the reset will restore \vec{M} original position. After each pulse, the value of the sample's resistance is measured (more precisely the transverse resistance R_H). This allows to be able to distinguish the two states by the variation in R_H .

3 Methods

In the following chapter we will discuss about the methods exploited in order to fabricate and characterize the investigated devices.

As already stated in the previous chapter, the main concern of this thesis was the study of the magnetization switching and in order to do that were mainly exploited electric measurements based on Hall effects. For this purpose, the geometry chosen for the devices has been either the Hall bar or the Hall cross having at the center an ellipse which could assume different spatial orientations. The main difference among the two configurations is that bars allow to measure both transverse and longitudinal resistance, while crosses only the transverse one. On the other hand, Hall crosses with ellipses at their center allow to observe the behavior of the magnetization in a circumscribed point, avoiding the dubiety that could arise generating simultaneously many different nucleation points. In the following (3.2) we will get more into detail about the physics of the measurement.

3.1 Fabrication process

The starting point in the fabrication of the devices was the evaporation on a cleaned Si/SiO₂ substrate of the following stack: Cr/Pt/Co/Cr/Si₃N₄. This step was performed by Dr. Giacomo Sala and samples with different relative thicknesses were realized. In Table 1 are reported the thicknesses of the different deposited stacks.

Sample name	Cr (nm)	Pt (nm)	Co (nm)	Cr (nm)	Si ₃ N ₄ (nm)	\vec{B}_{ext}
405	2	3	3	2	5	no
406	2	3	4	2	5	no
407	2	3	3	2	5	yes
411	2	5	3	2	5	no
412	2	5	4	2	5	no

Table 1: Table of samples composition. For sample number 407 it has been chosen to apply an external magnetic field during the growth procedure.

For the realization of the HM/FM bi-layer has been chosen to use Pt/Co, already well established materials in the scientific community for this kind of researches. The main advantage of Pt is that given its large atomic number, it allows to exert a quite large spin orbit torque on the FM layer. In addition to that, it is also possible to further maximize the SOC exerted on Co by enlarging Pt resistivity (which may be achieved by increasing the growing temperature or the growing pressure [32]). On the other side, Co allows to tune the magnetization easy axis by manipulating its thickness. Indeed, by increasing the thickness the samples changes from out-of-plane to in-plane magnetization anisotropy. The underlying reason is that by increasing the film thickness the contribution given by shape anisotropy overcomes the one due to the interface. As a consequence, the magnetization of the sample is forced in-plane. In our case we can see the transition to in-plane samples for a Co thickness of 3 nm.

After the evaporation, the clean room process needed to obtain the desired device shape was performed. According to the specific devices fabricated, the operating procedure consisted into a photolithographic process performed once or twice. In the case of the two

step process, the first one aimed to obtain the general Hall bar or Hall cross shape, while the second one was performed in order to obtain the central ellipse and the central bar respectively for the Hall cross and bar. In A we can find all the specific steps constituting the procedure.

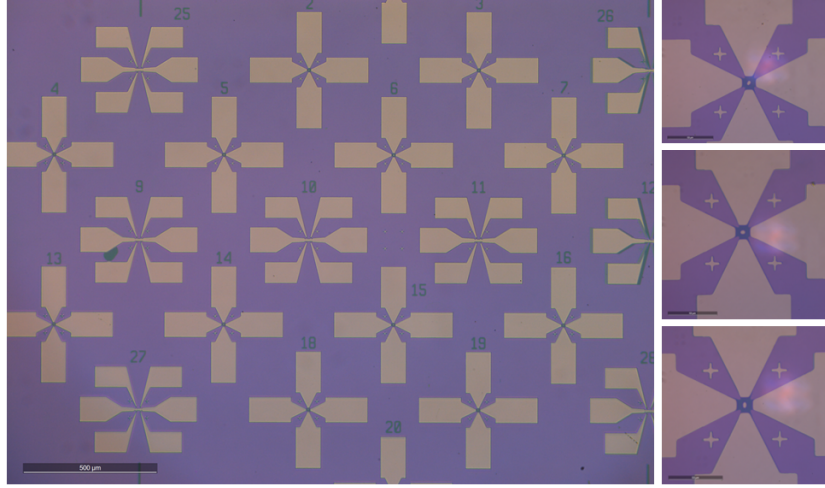


Figure 19: Result of the whole nanofabrication process. On the three right panels is presented a close up of the three possible orientations of the central ellipses of the Hall crosses. Their dimension is fixed and they display a $6 \mu\text{m}$ long axis and a $3 \mu\text{m}$ short axis.

3.2 Harmonic Hall voltage measurements

As mentioned in the previous chapter, the effect exploited in order to induce magnetization reversal of the proposed samples is the SOT effect, standing from the interaction between the spin accumulation (given by the action of SHE and Rashba effect) and the magnetization of the FM layer. In order to measure such an effect one could imagine to exploit different techniques. One among the possible ones consists into the injection of an AC current across the sample and a subsequent measurement of the Hall effects induced in it. The technique is said to be the Harmonic Hall voltage measurements technique. The basic concept consists into sampling device's Hall voltage that is modulated by the action of SOTs. The procedure consists into injecting an AC current across a Hall bar. The consequence will be the generation of an AC SOT, which will cause the FM magnetization \vec{M} to oscillate too. The subsequent transport effects taking place in the device under test will have two components: the first one at the same frequency ω of the injected current (said to be the first harmonics), and one with double the frequency (i.e. 2ω , said to be the second harmonics). According to which harmonics is taken into account also the information that can be extracted differ.

The convenience of such a technique is a better signal-to-noise-ratio with respect to the DC current injection method. This last method on the other side relies on the comparison of the effects induced by the injection of opposite polarity currents.

It is important to keep in mind that the basic assumption that applies when dealing with the measurements that will be presented is the one of the macrospin approximation. It means we are assuming that the magnetization can be consider as homogeneous through out the whole sample, neglecting the possibility of the fragmentation of the domains.

We can further distinguish two types of possible macrospin measurements: the field scan and the angle scan. In the first case the result is obtained by sweeping \vec{B}_{ext} value while keeping fixed the spatial position of the sample (and as a consequence also the angles θ and φ). In the second case the opposite conditions apply: the angular orientation of the sample is changed through out the measurement while the magnetic field is kept constant.

Another important remark is that when dealing with this kind of measurements, we not only obtain information about spin orbit torques inside the studied devices. We get as well details about the magnetoresistive and current-induced effects taking place in the sample. We will provide some useful techniques for the differentiation of the different contributions inside the measure.

3.2.1 Transverse and longitudinal resistance

Before getting into detail about the functioning of the field and angle scan techniques, it is worth to define the actual parameters that are measured: the transverse and the longitudinal resistance.

As we mentioned before, the devices that we are focusing on are either Hall crosses or Hall bars. Such shapes are chosen in order to be able to see how in FM the transverse and the longitudinal voltages change according to how the magnetization is oriented in space. Such changes are due to Hall and magnetoresistive effects explained in the previous chapter. Such effects can be not only of the first order, but can also get to higher orders because of the presence of secondary effects of thermal nature (e.g. Joule effect) and current-induced torques.

The main contributions to the measured transverse resistance (R_H) are those coming from the Hall effects. Given the transverse resistivity ρ_H

$$\rho_H = \rho_{AHE} \cdot m_z + \rho_{PHE} \cdot m_x \cdot m_y + \rho_{OHE} \cdot B_z \quad (3.1)$$

(where we can find contributions coming from the Ordinary Hall Effect (OHE), the Anomalous Hall Effect (AHE) and the Planar Hall Effect (PHE)) the transverse resistance R_H writes as

$$R_H = R_{AHE} \cdot \cos\theta + R_{PHE} \cdot \sin^2\theta \cdot \sin(2\varphi) + R_{OHE} \cdot \vec{B}_{ext} \cdot \cos\theta_B \quad (3.2)$$

The OHE is a consequence of the transverse Lorentz force produced by \vec{B}_{ext} acting on conduction electrons, then deviated towards the edges of the material. The AHE represents the interaction between electrons and magnetization due to SOC and spin-dependent scattering. The PHE is caused by the anisotropic scattering of conduction electrons from localized d -orbitals.

On the other side, the longitudinal resistance of the device takes into account the magnetoresistance effects.

In this case we get:

$$\rho_m = \rho_0 + \rho_{AMR} \cdot m_x^2 + \rho_{SMR} \cdot m_y^2 + \rho_{AIMR} \cdot m_z^2 \quad (3.3)$$

where MR is the Ordinary Magnetoresistance, AMR the Anisotropic Magnetoresistance, SMR the Spin Hall Magnetoresistance and AIMR the Anisotropic Interface Magnetoresistance.

The associated resistance will be:

$$R = R^z + (R^x - R^y) \cdot \sin^2\theta \cdot \cos^2\varphi + (R^y - R^z) \cdot \sin^2\theta \cdot \sin^2\varphi \quad (3.4)$$

3.2.2 Non-linear contributions

As we already mentioned in 2.3.3, higher order effects may arise, leading to non linear contributions to the resistance measured across the device. As a consequence, we should focus ourselves not only on the 1st harmonic of the transverse and longitudinal resistance but also on their 2nd harmonic.

For the analysis, we exploit the method based on the injection of an AC current $I_0 \sin(\omega t)$, which allows to give rise to time dependent periodic oscillations of the magnetization \vec{M} around its equilibrium point. As a consequence, the voltage across the structure will be time dependent (i.e. $V(t) = R(t) \cdot I_0 \sin(\omega t)$) and analogously the resistance $R(t)$ (in this case taking into account both the transverse and longitudinal components). Therefore, we get the following expression: $R(t) = R(B_0 + B_I(t))$, where B_0 includes the static contribution (i.e. the ones due to the external field, to the effective anisotropy and the demagnetizing field), while $B_I(t)$ gathers all the current induced fields ($B_{FL} + B_{DL} + B_{Oe}$). The natural consequence is that we can rewrite the voltage as $V(t) \approx I_0 \cdot [R_0 + R_\omega \sin(\omega t) + R_{2\omega} \cos(2\omega t)]$. The three resistance components represent respectively the 0th, the 1st and the 2nd harmonics contributions. While the 1st harmonic represents the transverse and longitudinal resistance that can be obtained with a DC measurement, the 2nd harmonic coincides with the contributions due to current-induced fields.

$$R_{1\omega}^H = R_{AHE} \cdot \cos\theta + R_{PHE} \sin^2\theta \cdot \sin(2\varphi) \quad (3.5)$$

Equation 5: First harmonics transverse resistance.

$$R_{2\omega}^H = (R_{AHE} - 2 \cdot R_{PHE} \cdot \cos\theta \cdot \sin(2\varphi)) \frac{d\cos\theta}{dB_I} \cdot B_I + R_{PHE} \cdot \sin^2\theta \cdot \frac{d\sin(2\varphi)}{dB_I} \cdot B_I \quad (3.6)$$

Equation 6: Second harmonics transverse resistance.

The current-induced second order component may be detected exploiting the field-scan and angle-scan measurements.

3.2.3 Field scan measurements

Let's start by analysing the field scan measurement technique first.

This kind of measurement is performed by sweeping an externally applied magnetic field (\vec{B}_{ext}) and keeping fixed the angle at which is orientated the device under test. In such a way, what we obtain is the plot of the device's resistance (either transverse or longitudinal according to the chosen angle) vs \vec{B}_{ext} . Regardless if we are dealing with in-plane

or out-of-plane \vec{M} samples, the main attractiveness of this technique is to allow a quite easy characterization of samples having a large anisotropy. Indeed, to be able to realize a proper measure taking into account the angle dependency of the magnetization, we have to saturate it along all the possible space direction (included the easy and the hard axis). However, if the sample's anisotropy is large, to achieve the saturation along the hard axis would require to apply a really high \vec{B}_{ext} . This can be avoided in the field scan measurement.

Now we will focus on the signal detection in IMA systems, which are those of our interest.

As we already know from the theoretical background, the SOT signal used to characterize the sample is made up by two components: a FL and a DL component. What is prevailing in the field scan measurement is the FL component. This may be explained by the fact that when the magnetization is tilted away from its equilibrium position by means of a \vec{B}_{ext} , the magnetization itself becomes more susceptible to the action of an in-plane field. Remember that since the DL torque pushes \vec{M} to orient toward the external magnetic field with a dissipative motion where the angular momentum is not conserved, it will lead to the appearance of some out-of-plane components on top of the in-plane ones.

Also thermoelectric signal comes into play when dealing with field scan measurements. In this case we can observe a ∇T_z contribution to the transverse resistance that has the same behavior as T_{DL} (i.e. $\cos\varphi$ symmetry) but with reversed sign. We remind that φ is the angle in the xy plane between the magnetization's in-plane component ($\vec{M}_{||}$) and the x-axis. On the other side, thermal contribution to the longitudinal resistance coincide with the USMR signal ($\sin\varphi$ symmetry).

The major difficulty is represented by the separation of the T_{DL} term from the ∇T_z one. A possible way to address this issue could be done by performing xy scan measurements with fields much higher with respect to the anisotropy one (which instead has a direct impact on T_{DL}). In this way one could minimize the relative influence of \vec{B}_{ani} on the second harmonics measurement and as a consequence minimize the contribution of T_{DL} over the ∇T_z one.

3.2.4 Angle scan measurements

The main advantage of angle scan measurements is that they allow to probe linear and non-linear effects depending on the magnetization, thanks to the possibility to vary schematically the magnetization vector. Indeed, by changing the angle of the applied magnetic field, we can see what happens to the magnetization's angle exploiting the rotational form of the Hall resistance and of the magnetoresistance.

The angle scan measure may be obtained by rotating the magnetic field in the three possible planes: xy , zx and zy . The combination of the information coming from those three measures allows to obtain the magnetotransport coefficients of the material in the three directions, enabling a full analysis.

xy scan The xy plane scan is especially useful for isotropic in-plane samples. The first harmonics obtained with such a measure allows to evaluate the Anisotropic Magnetoresistance (AMR) and the PHE. Their ratio coincides with the aspect-ratio of the investigated Hall bar. On the other side, the second harmonics allows to estimate the non linear effects, allowing a quantification of the SOTs.

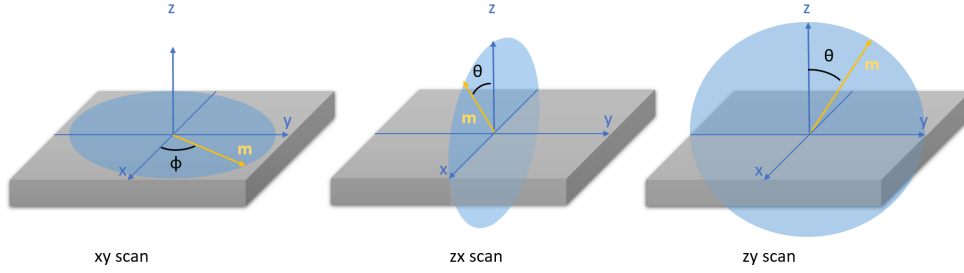


Figure 20: Possible planes of an angle scan measurement.

zx scan This technique reveals to be more suitable for the detection of SOTs in Perpendicular Magnetic Anisotropy samples, since they depend on the angle of the magnetization. As far as IMA samples are concerned, the first harmonic of the transverse resistance $R_{1\omega}^H$ can give information about AHE. On the other side, the first harmonics of the longitudinal resistance $R_{1\omega}$ gives information about the variation of the magnetoresistance.

zy scan In zy plane measurements the second harmonics component of the transverse and longitudinal resistances reveal to be interesting for IMA samples. In $R_{2\omega}^H$ both the damping-like and field-like components are present, with comparable magnitude and angle symmetry.

3.2.5 DC pulse measurements

Another possibility given by the harmonic Hall voltage setup is to perform DC pulse measurements. This kind of experiments allow to pulse a current through the device and sample its resistance soon after. This kind of measurement is particularly useful in order to investigate the magnetization reversal of the devices under test. Indeed, as already said, the magnetic state of the specimen is associated to a specific resistance value and when the magnetic state changes, also the magnetization does. The \vec{M} switching is associated specifically to a low or a high resistive state, which allows to built a two state system that can be exploited in nowadays digital applications.

What is done in DC pulse measurements is actually a sweep of current pulses at a fixed external magnetic field. The current sweep has to be done taking into account the limits of current density endured by the sample itself. Usually, to avoid to put too much stress on the device, the sweep starts at zero current, increases up to the maximum value and then decreases to the minimum, repeating the loop at least twice. As a result, if the parameters chosen enable to achieve a switching behavior, we should be able to observe a loop going from high (or low) resistance value, then switching abruptly to the low (or high) one and by reversing the current sweep the opposite behavior. Multiple current loops are performed in order to be sure that the resistance loops plotted close and that the behavior is always the same in time. In such a way we are sure that we are not observing events having thermal origin.

3.3 Time-resolved measurements

The next step is represented by the study of the dynamics of magnetization on its magnetic time scale (usually ns). Indeed, the harmonic Hall voltage measurements are able to

provide useful information about the magnetic properties of the samples (such as SOT strength) however they do not provide any information about the behavior in time domain. For this purpose, during this thesis has been used a time-resolved (TR) measurement setup (described in [13]).

As for the harmonic Hall voltage measurements, also the TR setup bases its detection upon signal standing from Hall effects. In this case however, the measurement does not present the detection problem present instead in the previously discussed technique. It means that in this case we can rely on Anomalous Hall Effect (AHE) for the detection since during the switching (depending on the magnetization trajectory while \vec{M} reverses) out-of-plane components can arise (preserving the $\cos\theta \cdot R_{AHE}$ term in Equation 3.5).

By sending pulses across the sample we are therefore able to trigger magnetization reversal and read it via Hall effects.

The basic idea of this setup is to send same amplitude and opposite polarity pulses along the longitudinal arms of a Hall cross in order to analyze the evolution in time of its magnetization switching. This technique addresses the problem of current shunting. While in DC measurements the shunting of the current (i.e. deviation from the main longitudinal path towards the transversal arms) is avoided by increasing the resistance of the transverse arms, this is not possible for RF setups. This approach would induce additional reflections of the current. As a consequence, is exploited the combination of two voltage pulses having same amplitude but opposite polarity. In such a way, if the structure is symmetric, the two pulses will reach at the same time the center of the device forcing there a virtual ground. Such condition enables to direct the whole current through the main longitudinal channel, avoiding shunting of current components across the transverse arm.

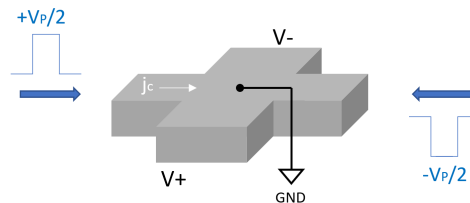


Figure 21: Injection in a single Hall cross of two pulses of opposite polarity ($\pm V_P/2$) that meet in the center of the structure generating a virtual ground, whose consequence is the propagation of the current along the longitudinal arm and avoiding current shunting towards the transverse arms.

3.3.1 Setup structure

The main building blocks of this setup are:

1. **Pulse generator** - The pulse generator provides the voltage pulses needed to perform the measurement. Because of the specifics of the used pulse generator (Kentech RTV40), the voltage range goes from -35V to +35V with a maximum pulse length of 20ns. As all the building blocks, also the pulse generator can be set up exploiting a Graphic User Interface (GUI) of the measurement software developed in MATLAB. The specific values chosen for voltage and pulse length depend on the fragility of the samples. However, it is important to keep in mind that shorter pulses need usually higher voltages in order to induce magnetization switching.

2. **Oscilloscope** - The oscilloscope has the aim of sampling the output signal. It is triggered by an attenuated portion of the pulse coming from the pulse generator. Its parameters may be controlled through the instrument itself or through the interface of the measuring software.
3. **Pick-off T** - The oscilloscope is activated by a trigger, which is provided by the voltage pulse used also to perform the measurement. This is allowed by the pickoff-T that splits the signal in a primary part directed towards the device under test and a secondary smaller one (attenuated by 20 dB), which instead is directed towards the scope.
4. **Balun** - After the pickoff-T we find the balun, which splits the voltage in $+\frac{1}{2}$ V and $-\frac{1}{2}$ V.
5. **Bias-T** - Each balun is connected with two bias-tees, whose purpose is to split the incoming current into DC and RF components. This split allows to perform not only the TR measurement (which needs RF signals) but also the DC one (such as the field scan). The DC component of the bias-T is directed towards the lock-in amplifier.

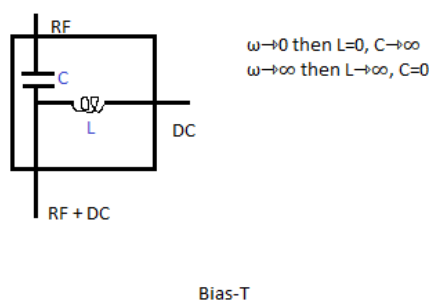


Figure 22: Schematic of bias-T. For low frequencies (i.e. ideally ω approaching 0) only the DC component is let across the bias-T. On the other hand, for high frequencies (i.e. ideally ω approaching ∞) only the RF component survives at the output.

6. **Lock-In Amplifier (LIA)** - The LIA (Zurich Instruments MFLI) measures $V+$ and $V-$ coming from the transverse arms of the device under test as an AC signals, being in the range of tens of Hz. The instrument improves the signal-to-noise ratio of the measured signal by multiplying it by a reference sinusoidal signal and then integrating it over a certain period (which is larger with respect to the period of the measured signal itself). This technique ensures the attenuation of all the parasitic signals that may contribute to the measure. Since the LIA works with voltages, it is paired with a current-to-voltage converter.
7. **Voltage Controller Current Source** - This device converts the incoming current into a voltage that is provided to the LIA.
8. **Amplifier (SAV-331+)** - The amplifier is an active component and as such needs an external power supply. Therefore, it is provided to it not only the RF signal that has to be amplified but also the DC power supply component by exploiting a couple of bias-tees.

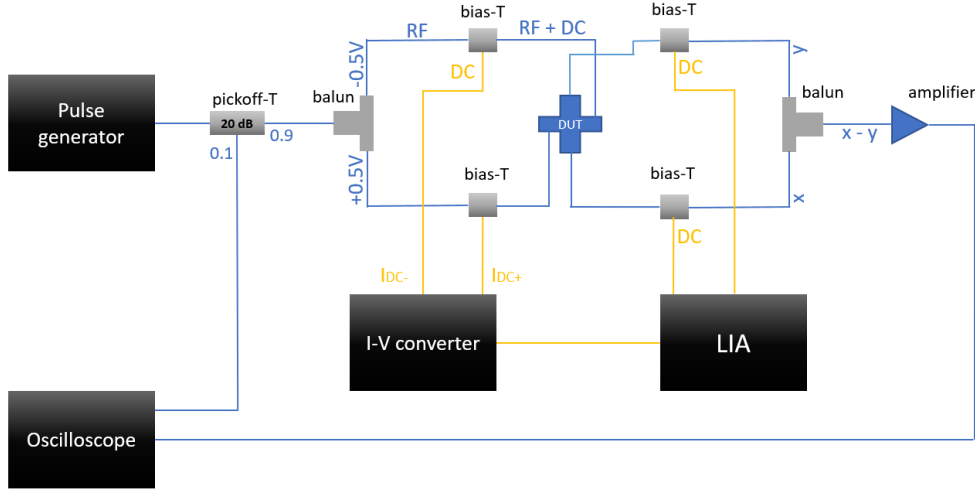


Figure 23: Schematics of the TR set-up. In blue are indicated the signals coming from the different ports. In case of the pickoff-T the numbers refer to the percentage of impinging signal that is transmitted in the two different branches. The blue cross represents schematically the device under test (DUT).

3.3.2 Measuring procedure

The procedure to measure the time-resolved switching of the magnetization of a device relies on the acquisition of two main signals: the reference one and the switching one. The reference trace represents the voltage vs time window in which the switch takes place. Sampling a reference trace, instead of using the directly acquired signals, is necessary in order to be able to cancel out the non-magnetic contributions to the plots. Indeed, the reference trace is obtained by a differential technique, which enables to improve the quality of the final results by removing the unwanted contributions (i.e. those not changing with the variation of the magnetic properties of the device under test).

In case of PMA samples such a reference looks like a rectangle and the height of such a rectangle gives a measure about the amplitude of the magnetization state. On the other side, as will be discussed deeply in chapter 4, in IMA samples the reference trace is flat because of no energetic difference among the two magnetic states along the two possible magnetization's orientations. The basic idea beneath the reference trace is to acquire two background signals, one for positive \vec{B}_{ext} and the other for negative \vec{B}_{ext} applied. The two background signals are associated to the two opposite equilibrium states in the two possible configurations of the magnetization: before and after the switching. Such a background signal is obtained by injecting repeatedly pulses having same current magnitude and direction. After obtaining the two background signals, they are subtracted one from the other giving in this way the net magnetic signal.

As far the switching trace is concerned, it represents the time evolution of the magnetization of the device. Also in this case the signal is obtained by injecting a train of current pulses having same amplitude, however the main difference is that now the polarity of such pulses is reversed every other pulse. In this way, at each couple of set-reset pulses the current reverses its direction and analogously also the magnetization. The average of several of such pulses (between 200 and 1000) gives the switching traces.

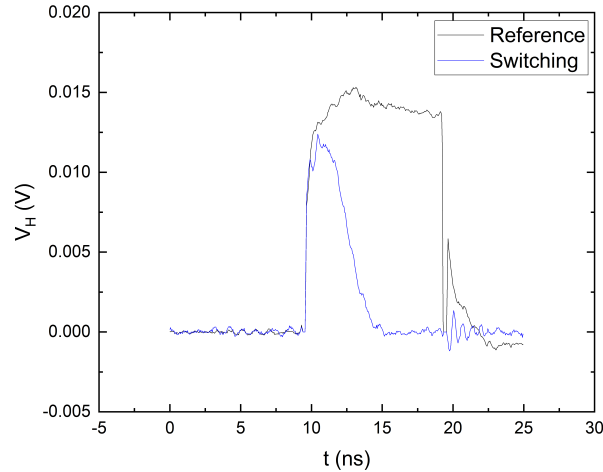


Figure 24: Example of TR measurement of a PMA sample made by a Hall cross with a GdCoFe dot at its center. Despite being PMA, we report this result in order to have a clear idea of how the TR measurement traces look like. We can clearly distinguish among the reference and switching trace. We can also appreciate the \vec{M} reversal dynamics, with the switching trace passing from the high to the low state inside the reference trace boundaries.

3.4 Magneto-optical characterization

Some additional measurements were performed with a home-built wide-field polar Magneto-optical Kerr Effect (MOKE) microscope. The basic idea is that the polarization of the light reflected and transmitted by a material depends on its magnetic state. This specific property allows to image the magnetization direction inside samples and is often exploited in order to observe the domain walls motion and to study their velocity. What specifically is exploited in the imaging techniques of ferromagnets are the linear effects on magnetization due to the changes induced in the light-wave crossing a material, following the law given by the formula $\vec{D} = \epsilon\vec{E}$. \vec{D} represents the displacement field, ϵ is the complex dielectric permeability tensor and \vec{E} is the electric field making up the electromagnetic radiation represented by light. More specifically, the Kerr effect is the one that arises when the light is reflected by the material (the Faraday effect instead concerns the transmitted component). According to the direction of the magnetization in the investigated material we can have three possible MOKE configurations:

- The polar MOKE, exploited for PMA samples (i.e. having \vec{M} pointing out-of-plane) and sensitive to the condition when the light impinges perpendicularly to the sample's surface, giving in such a way the largest signal.
- The longitudinal MOKE is instead used for imaging IMA samples. The best result is obtained with oblique incidence of the light since the signal's magnitude is proportional to $\sin\theta$ (where θ is the incidence angle).
- The transversal MOKE configuration presents the plane of incidence of light perpendicular to material's magnetization. The most important difference with respect to the two previous configurations is that now the amplitude of the light can change according to the incidence angle. To have the best results the light should be polarized

at 45° with respect to the plane of incidence.

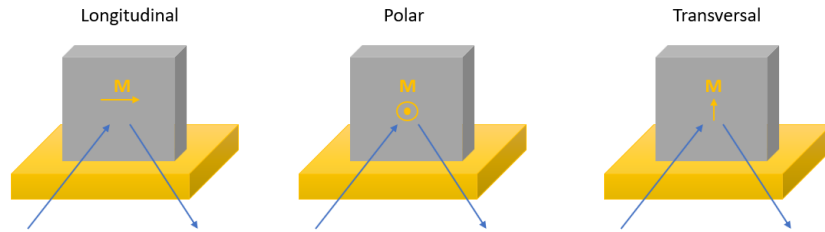


Figure 25: Three possible MOKE configurations: longitudinal, polar and transversal. The blue arrows represent the impinging light while the yellow one represents the magnetization of the material (gray box in the illustration). Elaborated from: [33]

The light source used for the setup is a LED emitting in the blue frequency ($\lambda = 450 \pm 24$ nm). Its beam is collected and focused by lenses on the aperture diaphragm. The light is then filtered by a field diaphragm and passes through a polarizer. Afterwards the light is focused in the samples thanks also to a beam splitter and to objective lenses. The light is then reflected by the sample with a rotated polarization. It finally reaches a water-cooled CMOS camera passing through an analyzer (whose purpose is to filter the transversal components of the polarization). The Kerr rotation is given by the ratio between the transversal and longitudinal component of polarization. In addition to the optical part, we may find in the setup also the coils needed to generate the in-plane and out-of-plane fields. A current pulser (AGILENT 8114A-100V/2A) serves to nucleate and drive the domain walls. The final picture is obtained by taking differential MOKE images in order to enhance the contrast. The whole setup is interfaced by using a LabView Graphic User Interface.

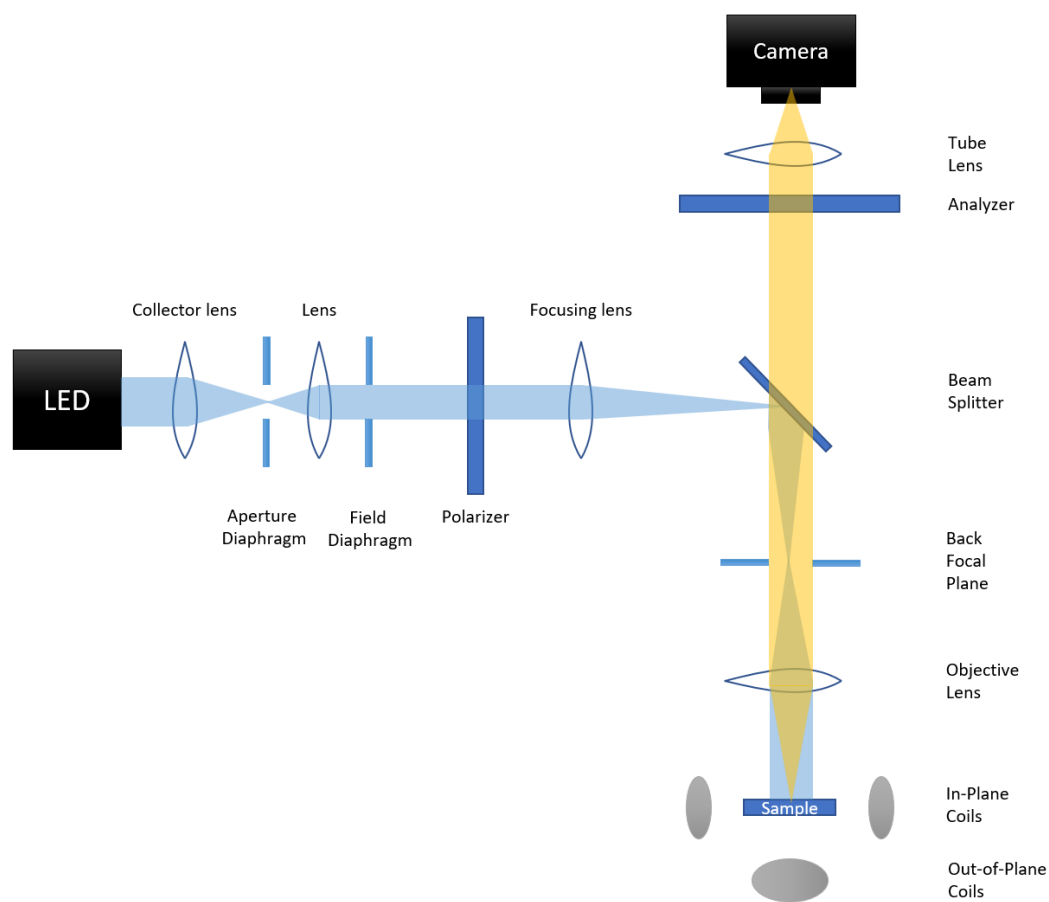


Figure 26: MOKE schematics. The blue light beam represents the illumination light path while the yellow one is the image-forming path. Elaborated from: [33]

4 Results

As mentioned in the introduction (3), according to the orientation of the magnetization and the subsequent switching mechanism, we can have three possible types of structures. Since in this thesis we are dealing with in-plane magnets, we will limit our discussion to two of those structures: the type x and the type y (Figure 27). Both the configurations have been investigated during this experience in order to see the fundamental differences from a physical standpoint of view among the two.

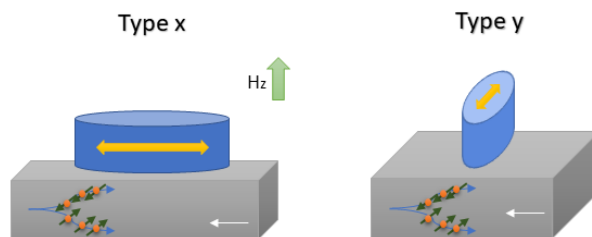


Figure 27: Type x and type y structures for SOT switching.

In type x configuration analysis the device is oriented in such a way that the injected current and the easy axis of the anisotropy are parallel one to the other during the measurement (Figure 28).

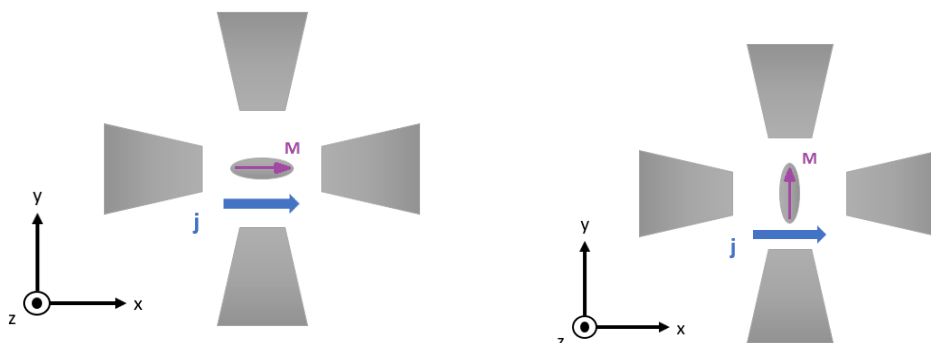


Figure 28: The left panel depicts type x configuration schematics. Both the injected current and anisotropy easy axis are along the x-axis direction. In the right panel instead is represented the type y configuration schematics. In this case, while the injected current (white arrow) is directed along the x-axis direction, the magnetization has its easy axis (yellow arrow) directed along the y-axis.

In the y configuration the injected current and the anisotropy easy axis are perpendicular the one to the other and co-planar. This last one represents the configuration that revealed to be the best choice for the analysis carried out, giving the most interesting results. Indeed, this layout allows to exploit Unidirectional Spin Hall Magnetoresistance (2.3.3) in order to have a reference for the resistance variation subsequent to a magnetization switch [34].

4.1 Magnetic properties characterization

As already mentioned in the methods (43), the fabricated devices displayed four possible configurations: either Hall bars or Hall crosses with 0° , 90° and 45° oriented central ellipses (Figure 29).

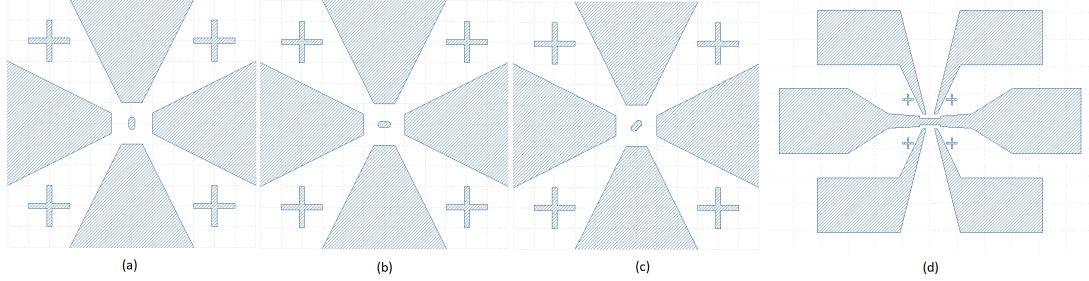


Figure 29: Mask design of the four possible device's configurations. (a) Hall cross with 90° ellipse; (b) Hall cross with 0° ellipse; (c) Hall cross with 45° ellipse; (d) Hall bar.

On top of that, the Hall bars were of two different types, according to their geometrical parameters. For sake of simplicity we will refer to such structures as type 1 and type 2 Hall bars. The first type of Hall bars that we will analyse had an investigated magnetic channel of $38 \mu\text{m}$ in length and $12 \mu\text{m}$ in width. In the second case the length was $20 \mu\text{m}$ and the width $5 \mu\text{m}$. In both cases the thickness of the Pt plus Co layer was equal to 7 nm .

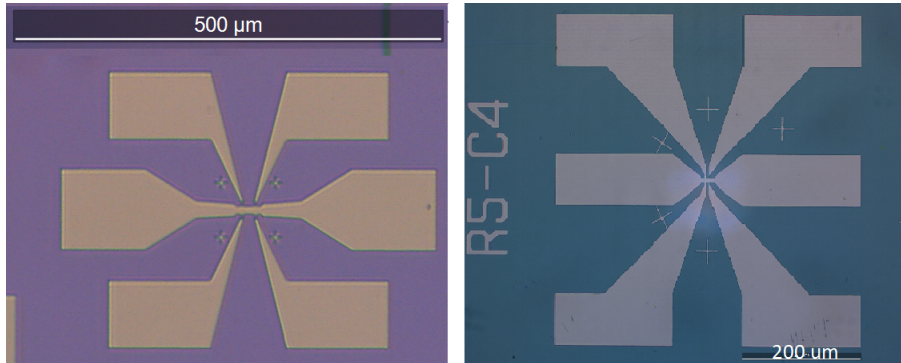


Figure 30: Hall bar type 1 (left side image) and type 2 (right side image).

Regardless on the shape of the device and on the investigated configuration, the first step in the analysis is to check that the device is an in-plane magnet. A static field scan measurement of the Hall resistance vs the externally applied magnetic field can be exploited for this purpose. It is a harmonic measurement and as such it can give information not only about the first order effects but also about the higher order ones. However, to get the information that we are looking for, one has to focus on the first harmonic. This measurement was done both along the x-axis and the z-axis of the sample (Figure 31). In case of an in-plane magnet we may observe that along the x-axis the Hall resistance stays more or less constant around a certain value. The only deviation is observed in proximity of the zero field point. This behavior coincides with what expected: indeed, with an in-plane applied magnetic field (\vec{B}_{ext}), we have that the magnetization \vec{M} displays angle $\theta = 90^\circ$ and angle $\varphi = 0^\circ$ (remember that θ is the angle between the z-axis and \vec{M} while φ is the angle between the x-axis and \vec{M} in the xy plane). As a consequence, while the

magnetization is forced along the x-axis because of the presence of an external field, we can easily see from Equation 3.5 that the Anomalous Hall effect (AHE) and the Planar one (PHE) will not give any contribution. The resistance deviation observable at zero field (and in the around of this point) is due to the fact that the absence of field leads to a breakage of the magnetization into several domains. As a result, we assist to the arising of contributions due to AHE and PHE, with a subsequent increase of the measured resistance. As soon as \vec{B}_{ext} is applied once again, the previous state is restored.

On the other side, along the z-axis we may observe that the magnetization orients slowly along the external magnetic field by reorienting its domains. As a consequence, also the Hall resistance increases slowly up to the saturation point for high positive and negative magnetic fields. In this condition we have an alignment $\vec{M} \parallel \vec{B}_{ext}$ of the global magnetization (in our case it was achieved for fields $\vec{B}_{ext} \geq 1$ T in magnitude for all the analyzed samples).

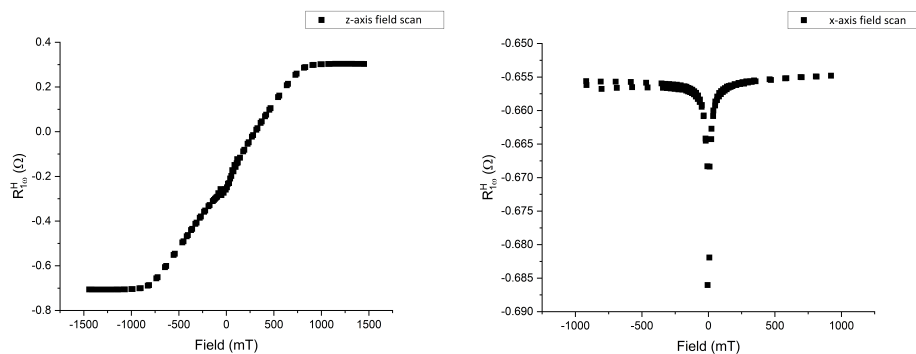


Figure 31: Field scan of IMA Hall bar of type 406 (1). On the left panel we report the field scan along the z-axis, also said to be the out-of-plane (OOP) configuration. We may observe the hysteretical behavior of the curve in the nearby of the zero field point because of the randomization of the magnetization. On the right panel we report the x-axis field scan, also said to be the in-plane (IP) configuration.

Once we are sure about that orientation of the magnetization of the device under test is the desired one, we can proceed with its static characterization.

4.1.1 Field and angle scans

Analysing the resistance vs applied field traces that we obtain performing the field and angle scan measurements we can get different kind of information according not only to the chosen harmonics order but also to the resistance taken into account, namely the longitudinal or the transverse one.

As already shown in Equation 3.5, from the first harmonic of the Hall resistance (the so-called transverse resistance) we can get information about the influence of the AHE and of the PHE on device's behavior. Given the dependence of $R_{1\omega}^H$ from θ and φ angles, the orientation of the ellipses in the Hall crosses in principle leads to different results. As long as a field scan is performed along the x or y-axis, being that θ is always 90° in all the possible devices (because of the IMA nature of the samples), we can conclude that there can be no significant observation of the AHE. If some contributions by AHE are observed it is because of the non-ideality of the samples, which leads to a magnetization not perfectly lying in-plane but deviating a bit out of it.

Let's consider for instance a Hall cross having a central ellipse aligned along the x-axis.

The θ and φ angles will be respectively 90° and 0° . As a consequence, we should get no remarkable information from $R_{1\omega}^H$, since in the formula $R_{1\omega}^H = R_{AHE} \cdot \cos\theta + R_{PHE} \cdot \sin^2\theta \cdot \sin 2\varphi$ both right hand side terms cancel out.

In the case of ellipses aligned to the y-axis the θ and φ angles will be both 90° . However, because of the dependence on $\sin 2\varphi$ of the R_{PHE} term in Equation 3.5, also in this case $R_{1\omega}^H$ will not give any notable information.

Only the Hall crosses with central ellipses having $\varphi = 45^\circ$ could reveal to be interesting if taking into account $R_{1\omega}^H$, since the term referred to the PHE survives in Equation 3.5.

On the other side, performing the angle scan measurement and looking at the first harmonics angle scan of both the longitudinal and transverse resistances, we will see that the curves are not perfectly symmetric if there is a preferential direction of the magnetization anisotropy. Indeed, this kind of measurement represents a good tool in order to understand the behavior of the anisotropy of a device. For instance, it is the case of Figure 32. We may notice that for both $R_{1\omega}^{xy}$ (i.e transverse resistance) and $R_{1\omega}^{xx}$ (i.e. longitudinal resistance), the curves are respectively decreasing in the slope and flattening in correspondence of 180° angle. This means that the magnetization lies preferentially along the x-axis.

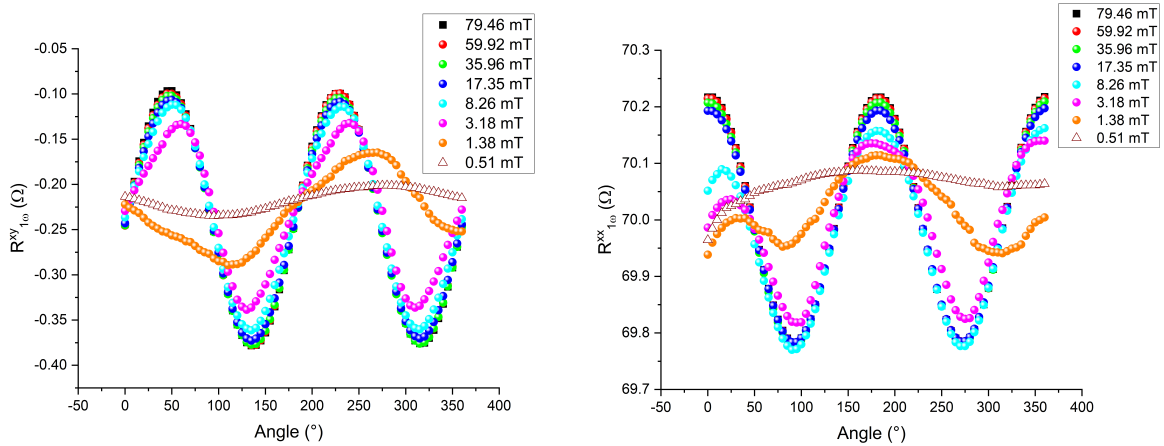


Figure 32: Angle scan plot of the first harmonics of xy (left panel) and xx (right panel) resistances for a 406 Hall bar. It is possible to see that with the decrease of the externally applied field the curves start to display a more relevant asymmetry according to the angle at which the measurement is done. This is because the external field suppresses the anisotropy of the sample, forcing its magnetization to follow it and align to it.

Let's now focus instead on the second harmonic of the Hall resistance ($R_{2\omega}^H$). Indeed, we can retrieve from this signal information about the Spin-Orbit Torque's FL and DL components. More precisely, according to Equation 4.1 we can see that we are able to distinguish the FL plus Oersted field contribution from the DL plus Anomalous Nerst Effect (ANE) one.

$$R_{2\omega}^H = R_{FL+Oe} \cdot (2\cos^3\varphi - \cos\varphi) - 0.5 \cdot (R_{DL} + R_{ANE}) \cdot \cos\varphi \quad (4.1)$$

By looking for instance at the curves obtained for 0° Hall crosses (i.e. central ellipse with the major axis parallel to the x-axis) (Figure 33), we can identify two regimes: the low

field and the high field one. While the torque information can be extracted from the low field condition, the high field results instead to be useful for understanding the action of thermal effects, more precisely of the ANE.

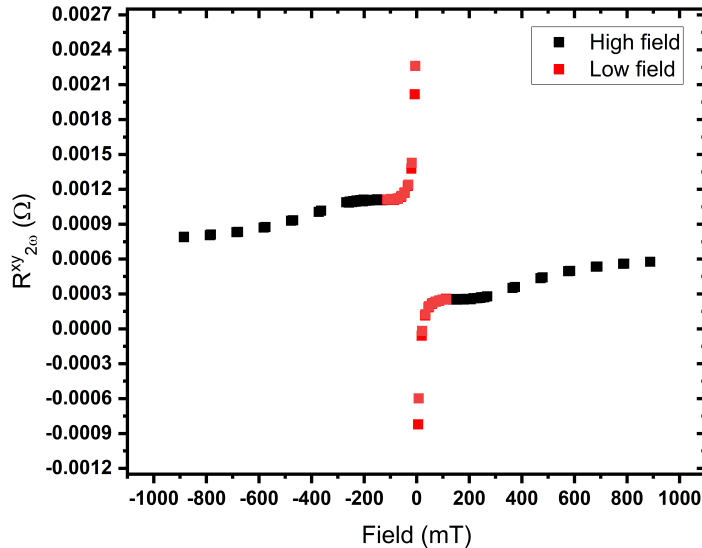


Figure 33: Second harmonic Hall resistance plot for a 0° Hall cross of type 406 (1). The low field points (in red) refer to the SOT contribution to the magnetization, while the high field ones (in black) refer to the thermal contribution. Because of the geometry of the sample the magnetization tends to be aligned along the long axis of the sample which coincides with the x-axis for this measure. Also the applied magnetic field was directed along the x-axis. Surprisingly, the transition between the low and high field regions is not linear but presents a saddle point. In addition, we can see that thermally assisted \vec{M} reversal leads to a smaller $\Delta R_{2\omega}^{xy}$ with respect to a SOT assisted one (i.e. $\Delta R_{2\omega}^{xy}$ at the extremes of the high field region is $< \Delta R_{2\omega}^{xy}$ at the extremes of low field region).

To better understand how does the action of SOTs affects magnetization Figure 34 could result useful. After an AC current has been injected into the HM/FM system, the magnetization starts to oscillate around the equilibrium point because of the subsequent current-induced torques. This reasoning results to be valid as long as \vec{B}_{ext} is not too high. Indeed, if it is not the case, the magnetization tends to align to the external field direction, suppressing the SOT effects [35].

Upon the injection of an AC current $I = I_0 \sin(\omega t)$ the magnetization starts to oscillate around an equilibrium point. The equilibrium point is given by a balance among the different fields acting on the magnetization itself: the external (\vec{B}_{ext}), the demagnetizing (\vec{B}_{dem}), the anisotropy field (\vec{B}_{ani}) and those induced by Spin-Orbit torques (namely \vec{B}_{DL} and \vec{B}_{FL}).

The extraction of the FL and the DL components from Equation 4.1 can be done by observing the angle scan measurement along the xy plane [36]. By fitting with Equation 4.1 the obtained $R_{2\omega}^H$ second harmonic curves for different values of \vec{B}_{ext} , we are able to retrieve the coefficients corresponding to R_{FL+Oe} and $R_{DL} + R_{ANE}$. Exploiting then the field dependent relations (4.2) [35] it is possible to find out the value of the FL SOT component. The DL SOT component is instead obtained by considering how $R_{2\omega}^H$ changes

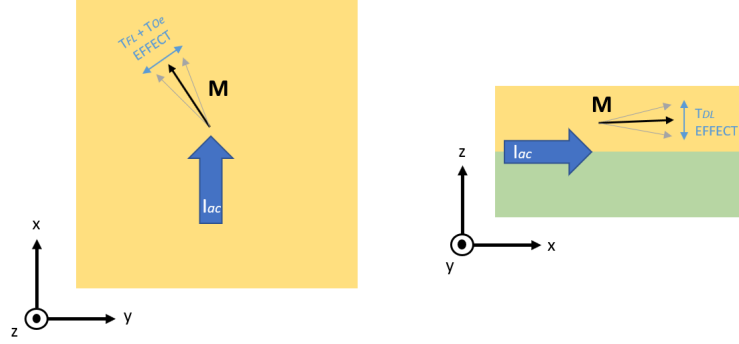


Figure 34: SOTs impact on magnetization. On the left panel is represented a top view of the sample (xy plane) while the right panel represents its cross section (zy plane). While on the left we may see that the main contribution to magnetization in-plane oscillation upon AC current injection is given by field-like and Oersted components, on the right is made explicit that the damping-like component plays a major role when dealing with an out-of-plane oscillation of the magnetization. The yellow layer represent the ferromagnetic Co and the green one represents the non magnetic Pt layer. Elaborated from: [35]

according to the value of the external field (because of this the angle scan is performed at different values of \vec{B}_{ext} in a range between 1.5 T and 0.5 T (35)). To finally decouple DL from ANE contribution we can still take advantage of the field dependent relations (4.3).

$$R_{FL+Oe} = \frac{1}{2} \cdot \frac{R_{PHE}}{B_{ext}} \cdot B_{FL+Oe} \quad (4.2)$$

$$R_{DL} + R_{ANE} = \frac{R_{AHE}}{B_{ext} + B_{dem} + B_{PMA}} \cdot B_{DL} + R_{ANE} \quad (4.3)$$

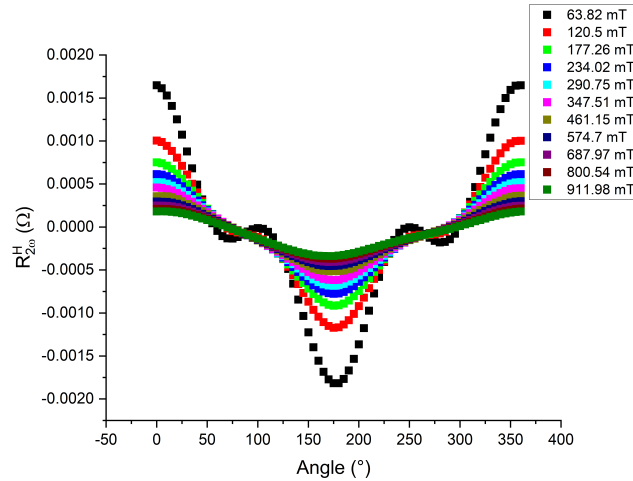


Figure 35: $R_{2\omega}^H$ angle scan of a type 1 Hall bar made out of 406 sample.

While the DL contribution is a dynamic effect due to the oscillation of the magnetization, the thermal one (ANE) represents a static contribution. As a consequence, only the thermal component is left in the measured signal since at high fields the dynamic contribution vanishes being the magnetization forced to align to the external field direction.

The preliminary step for performing the SOT component extraction is represented by realizing the out-of-plane field scan along the z-axis. Thanks to the subsequently obtained curves it is possible to extract the values of the demagnetizing field \vec{B}_{dem} and of the resistance R_{AHE} , which are required as starting point to solve equations 4.2 and 4.3. The two extracted parameters represent respectively the external field amplitude for which the magnetization reaches saturation and the resistance value associated to the saturated magnetization.

It is also possible to see the evolution of the FL and DL fields with the applied reading currents (I_{read}) by repeating the SOT analysis for several I_{read} values (36).

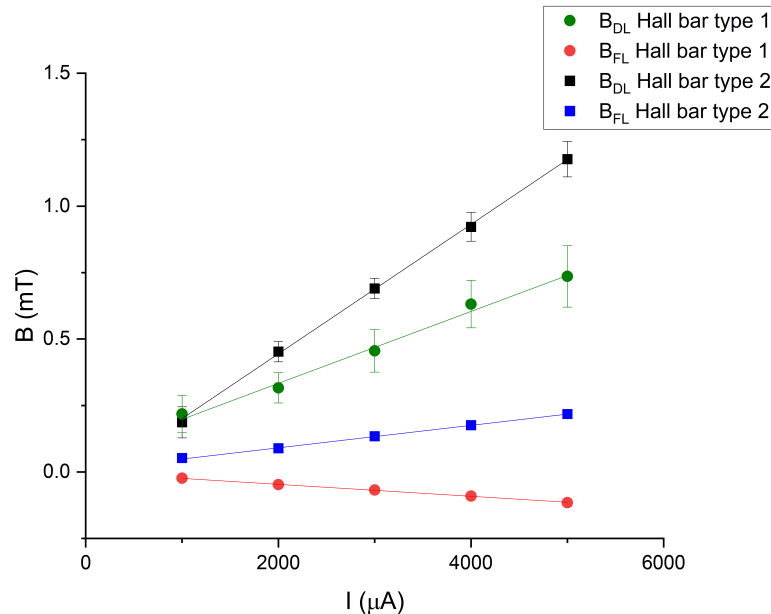


Figure 36: DL and FL fields evolution with the applied reading current of Hall bars of two types both obtained from 406 sample. The difference among the two kinds of Hall bars is their aspect-ratio: for type one it is $= 3$ while for type two $= 4$. We can see that in type 2 Hall bars the SOT fields result to be stronger with respect to type 1 devices at same injected current. This could be explained by the fact that across type 2 Hall bars flows a larger current density with respect to type 1 given the smaller dimension of the structure. As a consequence, in type 2 devices more SOTs are produced given that the charge-spin conversion efficiency (exclusively material dependent) is the same in the two cases. We may further notice that the FL curves change sign in the case of the two Hall bars. This may be due to the fact that we have not subtracted the Oersted field component from the FL coefficient. This component is affected by the direction of the current flowing across the device.

Such an analysis gives the best results if the measures are carried out on Hall bars instead of Hall crosses. The reason may be found in the fact that they can provide a larger magnetic volume with a subsequently clearer signal.

To conclude, we can summarize the main points concerning the performed field and angle scan measurements.

First of all, the field scan analysis has been performed for all possible geometries: the three types of Hall crosses and the Hall bars. The main interest of the field scan measurement is first of all the possibility to confirm that the investigated device is an in-plane

magnet. Second, it gives a reference for the switching measurements performed during the DC pulse procedure (4.1.2).

According to the specific geometry, the switching reference is sought in a different signal. For the y-type geometries (such as the 90° Hall crosses) the signal of interest is the second harmonic of the longitudinal resistance ($R_{2\omega}^H$). For the x-type instead (such as the 0° Hall crosses) we could take advantage of the odd symmetry Planar Hall effect (OPHE) [37]. This technique consists into measuring the first Hall resistance ($R_{1\omega}^H$) upon injection of a DC current across the sample first with one polarity and then with the opposite one. The difference among the two resulting measurements gives the reference.

As far as the angle scan is concerned, the main objective of this kind of analysis is the understanding of the orientation of the magnetization (i.e. anisotropy easy axis) and extraction of the SOT components. In this case all the kind of devices except for 45° Hall crosses have been analyzed. This because we wanted to focus first on more simple geometries and move to more complex only after being sure on the possibility to observe the switching in more basic structures. For the same reason we limited the analysis only to 406 samples.

The main outcome of the angle scan analysis is that in all the cases the magnetization resulted to be preferentially oriented at 180° . Additionally, the angle-scan plot does not reach the same $R_{1\omega}^{xy}$ peak value in the ranges $0^\circ - 90^\circ$ and $180^\circ - 270^\circ$. This is because the amount of energy needed to switch the magnetization from 0° to 180° and vice versa is different.

The SOT extraction on the other side, as already said, results to be meaningful only for Hall bars. The obtained values for two types of Hall bars having different aspect-ratios (36) are consistent with literature results [38].

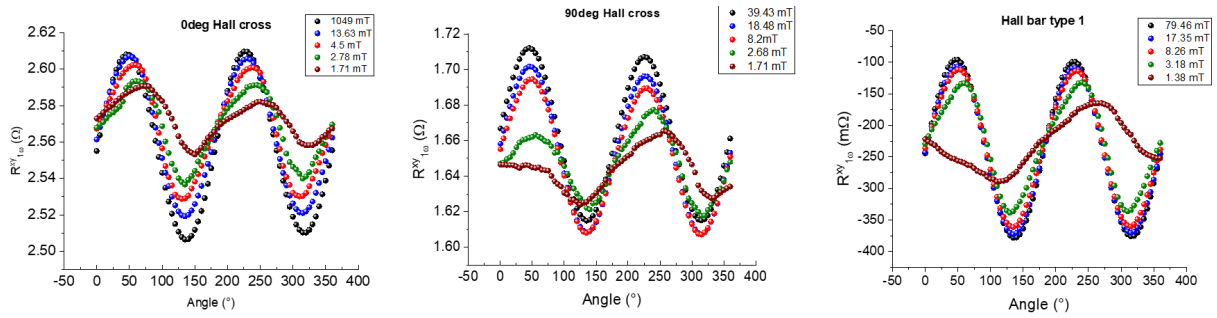


Figure 37: Comparison among angle scans of 0° and 90° Hall crosses and a type 1 Hall bar. The angle is measured with respect to the current direction, assumed to be initially along the x-axis (i.e. at 0°). We can see for the plot referred to the 90° Hall cross a temperature drift lead to a shift of the curves, as a consequence they are not all centered around the same point.

4.1.2 DC pulse

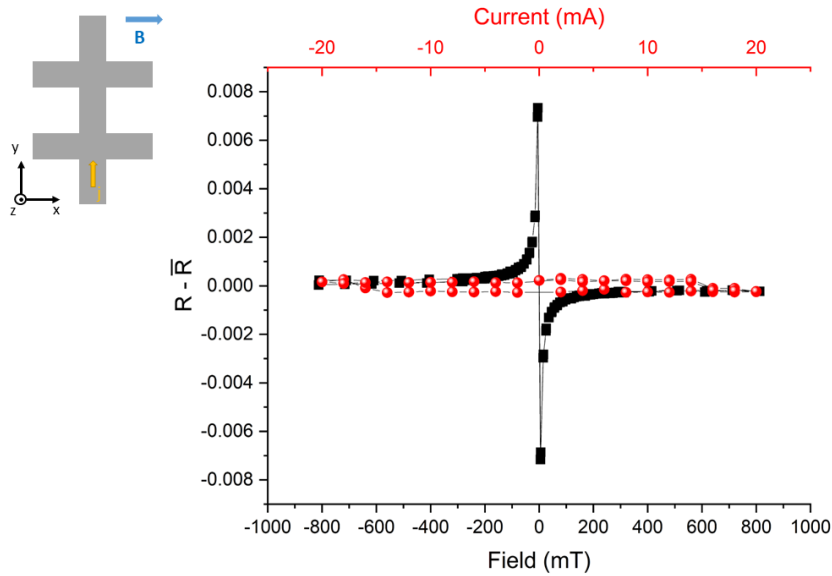


Figure 38: Switching in a type 1 Hall bar made of sample 406 in y configuration (i.e. current injected along the y-axis while an almost zero magnetic field is externally applied along the x-axis). A representation of the configuration is reported on the top left corner. Black trace represents the $R_{2\omega}^{xx}$ vs externally applied field and red one is the $R_{2\omega}^{xx}$ vs applied current pulses. The resistances are normalized in order to center the two plots in the same point and enable a comparison.

The switching in static conditions is performed by realizing DC pulse measurements. It means that DC pulses are sent across the structure and afterwards is checked the value of the resistance across the device. The switching resistance is chosen according to the used reference, i.e. if for instance we are exploiting the Unidirectional Spin Hall Magnetoresistance (USMR) trace as reference for the ΔR associated to the \vec{M} reversal also the switching signal will be observed in the second harmonic of the longitudinal resistance ($R_{2\omega}^{xx}$).

Indeed, when the magnetization switching takes place, the samples passes from a low resistance to a high resistance phase or vice versa. The difference among those two resistances is what we can define as magnitude of the switching. Thanks to this information we can also understand which is the dominant effect in the switching. For example, taking into account $R_{2\omega}^H$, we could have a switching dominated by either SOT or thermal effects. In the first case the resistance variation would be comparable with the separation of the two curves constituting the $R_{2\omega}^H$ vs field graph in the center of the plot (i.e. low field regime), while in the second case it would be comparable with their separation at the edges of the plot (i.e. high field regime) (Figure 33).

The $R_{1\omega}^H$ is not taken as reference for the magnetization switching in our case since in in-plane magnets no appreciable change is introduced in the first harmonic of the Hall resistance. This is because not only in principle we can not observe the AHE, but also the PHE for a 180° magnetization reversal is not clear. This last point can be easily understood if we look at the angle scan measurement. Indeed, we can notice that the resistance value is the same at φ equal to either 0° or 180° . It is because of those difficulties that we came up with the idea of realizing time-resolved measurements, which will be discussed

in the following (4.3).

It is interesting to notice that both in the case of 0° Hall crosses (Figure 39) and Hall bars (Figure 38) the switching resulted to be comparable with the ANE instead of the SOT events.

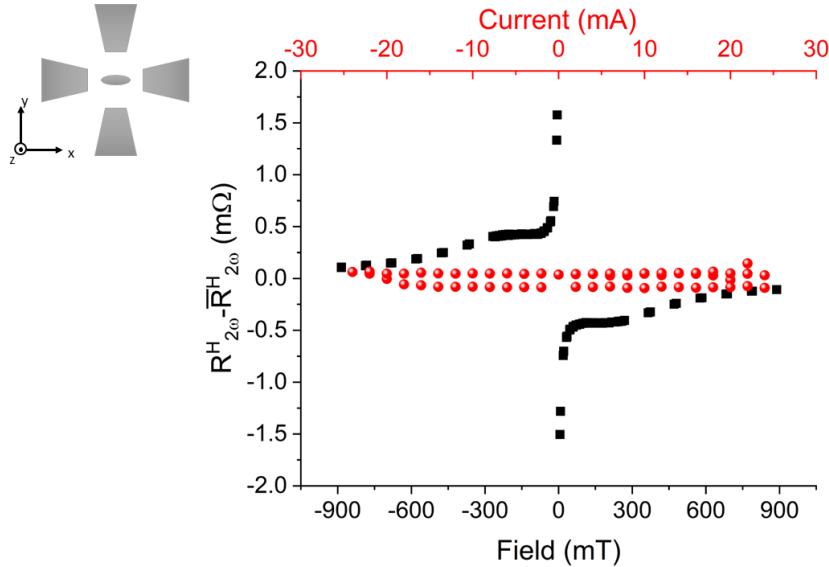


Figure 39: Switching in a 0° ellipse in x configuration. A representation of the configuration is reported on the top left corner. Black trace represents the $R_{2\omega}^H$ vs externally applied field along x-axis and red one is the $R_{2\omega}^H$ vs applied current signal. The resistances are normalized in order to center the two plots in the same point and enable a comparison.

What further may be noticed from Figure 38 and Figure 39 is that the Hall crosses need a higher current to switch, which suggests a more difficult reversal of the magnetization process. The traces for the switch of Hall crosses in y-configuration are not commented because the obtained traces did not allow to distinguish the presence of two different discrete resistance levels (Figure 40).

As already said in the introduction, in the y-configuration, in order to observe the magnetization reversal, there is no need to assist the process with an external magnetic field. As a consequence, it was crucial to demagnetize the coils of the instrumental setup in order to ensure an almost zero \vec{B}_{ext} . In Figure 41 we may see that with an increase of the magnetic field we quickly lose the information about magnetization reversal. We get a complete loss of information when the external field reaches the value of the coercive field (in our samples about 4mT). On top of that, also the reading current sent across the sample has an impact on the quality of the result.

Indeed, the read out is achieved by measuring the voltage induced by spin accumulation [39]. The injection of spin-polarized current not only leads to the accumulation of spins at Pt/Co interface, but also leads to the split of the spin-up and spin-down Fermi energies (i.e. chemical potentials). According to the magnetization orientation in Co, its chemical potential will align to the Fermi level of either the spin-up or spin-down electrons. This will give rise to an interface voltage that then is exploited for the read out.

The larger will be the reading current and the larger will be also the injected spin-polarized current, leading to a better read out. The upper limit to the read current is given by the

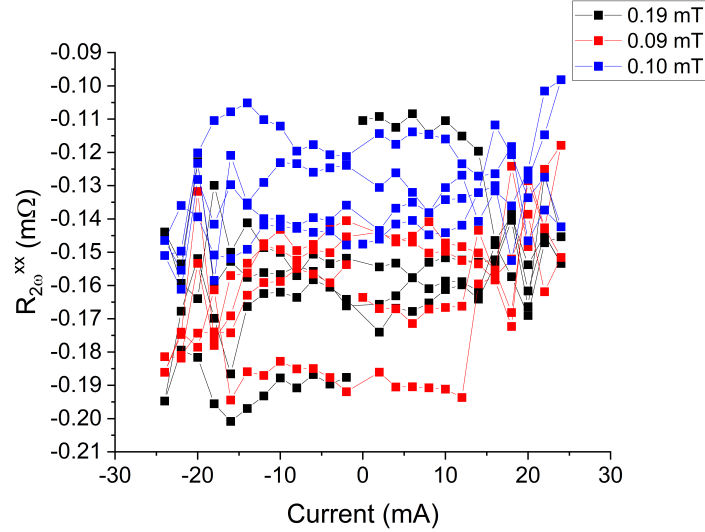


Figure 40: Switching in a 0° ellipse in y-configuration. What is reported are only the traces resulting from the DC pulse measurements. As we may see there is no clear switching behavior.

capability of the sample itself to stand large current densities, which is directly affected by the resistance of the same device.

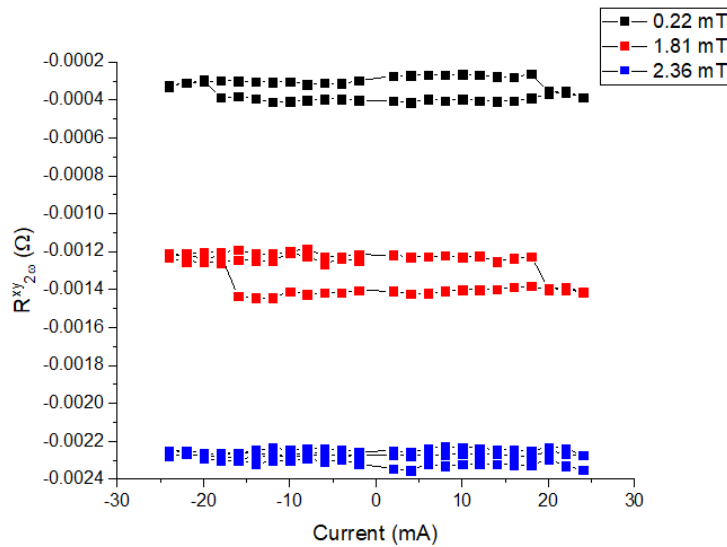


Figure 41: DC measurements for switching 0° ellipses in x configuration performed at different external fields. We may notice that the curve corresponding to the highest \vec{B}_{ext} is also the one displaying the worst difference among the two resistive states associated to before and after switching conditions.

To sum up, we have observed the switching in 0° and 90° Hall crosses and in Hall bars. The configurations in which the switching was observed was of the x-type for the Hall crosses while both x and y-type for the Hall bars. When dealing with both x and y-configuration an external magnetic field was applied with a few mT amplitude, however while for x-type structure such field was oriented along the z-axis, for the y-type structures the external magnetic field was oriented along the x-axis and with an amplitude value as

close as possible to 0mT.

In all the three cases the resistance variation associated to the magnetization reversal is comparable to the one introduced by thermal effects, namely the Anomalous Nernst effect (ANE). The fact that the switching is comparable to the ANE instead of the SOT contribution is still not completely clear. First of all, the ΔR for switching evaluation is smaller with respect to the expected value at low field considering only the SOT contribution because probably the magnetization \vec{M} is not fully nucleated leaving some regions not concerned by switching. As a consequence, we assist to the decrease of the expected ΔR . An explanation could be represented by the Joule heating taking place in the investigated structures. Heating leads to a decrease of the effective magnetization M_{eff} . This is because value of the saturation magnetization M_S contributing to M_{eff} is inversely proportional to the temperature due to the increase of spin-wave excitation at higher temperatures [40]. Less M_{eff} results into less available magnetic volume for switching.

In addition to that, also a not fully in-plane magnetization (but featuring out-of-plane components before and after the switching) leads to a decrease in the observed ΔR .

However, we are sure about the beneficial role of the temperature in the process up to a certain extent. Indeed, many precessions are needed in y-configuration magnetization reversal before completing the switching (18). As a consequence, thermal assistance reveals to be useful to achieve the switching since it enhances the misalignment of the magnetization from its equilibrium point [41].

Finally, we can comment on the \vec{M} orientation at the beginning of the DC pulse procedure. The weak applied external magnetic field \vec{B}_{ext} does not affect \vec{M} initial direction as soon as it is $< 4\text{mT}$ (value of the coercive field of the analysed devices). Therefore, \vec{M} results to be initially randomly oriented and fragmented into domains. The DC pulsing starts with a current equal to 0 mA and then progressively increases. After some current pulses have been injected in the devices and the magnetization is saturated in one specific direction, we can start to consider the data as valid for the current loop associated to the magnetization reversal (as may be seen in Figure 42).

Being the magnitude of ΔR associated to the magnetization reversal not comparable with the ongoing SOT effects, some doubts about the actual magnetic behavior of the sample raised. We decided to face this issue by exploiting a magneto-optical characterization technique.

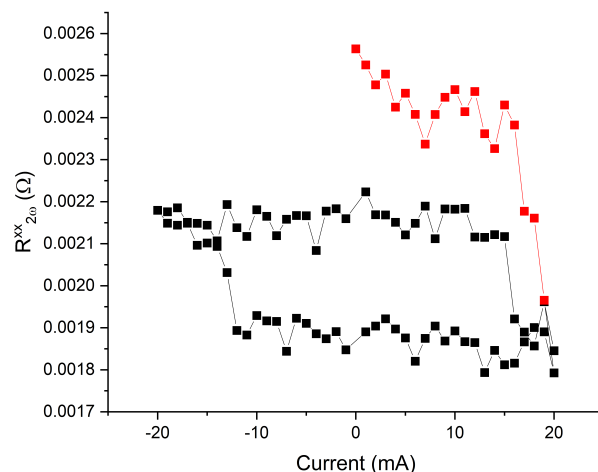


Figure 42: DC pulse measurement of a 406 Hall bar in y-configuration with an external field applied along the x-axis direction with amplitude equal to 0.04mT. The red points measurements feature a randomly oriented magnetization. \vec{M} needs to be first saturated before starting to consider the DC pulse measurements as representative of the \vec{M} switching.

4.2 Optical characterization

The next step to be sure about the switching behavior of the devices is to perform magneto-optical measurements using a Magneto-optical Kerr Effect (MOKE) microscope. Indeed, Hall resistance variations may be caused also by ongoing thermal effects. In the following we will first contextualize the analysis giving some information about non-magnetic changes in Hall resistance and then we will follow by presenting the results for each investigated structure.

4.2.1 Non magnetic resistance changes due to electrical pulsing

When studying the magnetization switching in ferromagnets it is important to keep in mind that there could be a change in the measured resistance due to non-magnetic events. Indeed, the shape taken by the plot of the resistance versus the number of current pulses sent through a device not always represents an unambiguous distinction mark among magnetic switching or thermal events [42, 43].

Elements such as the chosen substrate and the shape of the device can greatly affect the transverse resistance of magnetic devices leading to its changes by effects having non-magnetic nature. Indeed, substrates for devices featuring better capabilities to dissipate heat (i.e. having larger thermal diffusivity) allow to exploit a broader spectrum of amplitudes for applied pulses. This possibility leads to an increased chance to observe through electrical measurements an actual magnetic switching event in the investigated sample. As mentioned before, also the shape of the device has a fundamental role. Depending on the shape of the pulse and on its amplitude, around the corners of a structure we can assist to the local decrease in resistivity because of thermal annealing (induced by the increase in temperature due to Joule heating) or to an increase of resistivity because of electromigration (C). The main consequences are formation of hillocks in the first case and

of voids in the second. Also current crowding effects taking place at the corners of devices can induce changes in the measured transverse resistance uncorrelated to the changes in the magnetic properties of the device under test. Last but not least, also training effects can be observed when trying to characterize the switching behavior of magnetic samples. It means that the measured signal stabilizes only after having sent multiple times the same current pulse across the structure.

The permanent change in the system's structure because of events such as electromigration is characterised by the impossibility to restore transverse resistance's original state even after many hours of relaxation.

4.2.2 Hall Crosses

In the first place we analysed both the 0° and 90° Hall crosses in y-configuration. To perform such a measurement the procedure is constituted by the following steps:

1. Application of an external magnetic field in order to saturate the sample's magnetization in one specific direction, which will represent the initial condition for the switching.
2. Removal of the external magnetic field in order to enable the reversal of the magnetization (we quickly remind that y-configuration switching is field-free).
3. Sent positive pulses of voltage across the device to ensure its \vec{M} is parallel to the reference direction.
4. Send negative polarity pulses to observe the switching phenomenon.

The exact switching parameters are not known *a priori*. Since this procedure is quite different from the DC pulse static one, entailing different specifications of the devices making up the two setups, it is not possible to exploit the parameters that allowed former switching in harmonic Hall voltage measurements for MOKE observations. However, this kind of measurement reveals to be useful not only to confute the presence of switching. Additionally, since the pulser used both in the magneto-optical and in the time-resolved setups is the same, we can additionally prove that the \vec{M} reversal can be observed through TR measurements (since the two approaches exploit the same pulsing technique).

Unfortunately, no switching could be observed in the Hall crosses before reaching the burning condition of the devices, i.e. causing their failure by electromigration (C). Despite the trial of several combination of different pulse voltages (in a range from 20V to 45V) and pulse lengths (in a window going from 20ns to 50ns), every choice revealed to be the wrong one not being able to affect the magnetic state of the samples.

An explanation to this behavior may be found in the fact that the ellipse configuration has been chosen in order to limit the magnetization switching to a specific spot, avoiding the simultaneous nucleation of multiple domains in different places. This is done in order to obtain better measurements results. As a consequence, the magnetic system is etched in the shape of an ellipse and all around the ellipse is present only a Pt layer. Such a layer is not able to sustain the currents induced by pulses larger than 40V at 20ns. Because of the fragility of those structures and their proven inadequacy for TR measurements, the analysis of the 45° Hall crosses was not attempted at all. Given the above reported conclusions for the Hall crosses, in the further the discussion will focus only on Hall bars, which revealed to be more promising. Because of this, where fabricated new devices in the

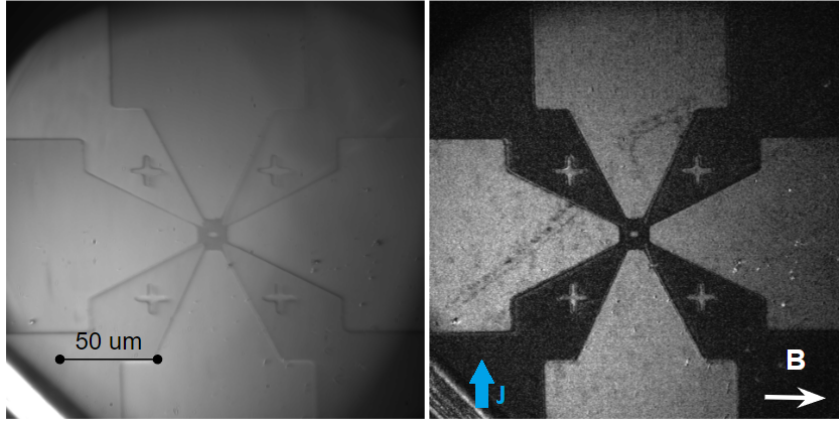


Figure 43: MOKE measurement of a 90° Hall cross in y -configuration. The black part is saturated along the negative direction of the external magnetic field, while the white part is direct along the positive \vec{B}_{ext} . The coercive field (i.e. the one that leads to a full saturation of the magnetic domain) is achieved at about 49 Oe (where 10 Oe = 1 mT).

shape of Hall bars but having different geometrical parameters compared to the previously realized Hall bars.

4.2.3 Hall bars

As already mentioned, the analysis carried out on Hall bars has exploited two different types of structures having different geometrical parameters. The type 1 Hall bars (having bigger geometrical parameters and an aspect-ratio of about 1.7) and type 2 Hall bars (having smaller geometrical parameters and an aspect-ratio equal to 1.4).

Type 1 Hall bars The type 1 Hall bars are those having bigger geometrical parameters. As may be noticed in Figure 44, to trigger magnetization reversal in type 1 Hall bars are needed relatively high values of voltage of applied pulses. Fixing the pulse length at 20 ns, the first sign of switching is observed at 35V. However, to observe a complete magnetization reversal across the whole channel of the device, we have to increase the pulse voltage up to 55V. In addition to that, if we look closely to what is happening, we may notice that the switching starts at one edge of the structure (the right one in the case of 44), extending afterwards to the rest of the structure as successive voltage pulses are injected in the Hall bar and their amplitude is increased.

A justification to this behavior may be given considering that initially applied pulses are not strong enough in order to lead to a complete reversal of the magnetization across the whole structure, despite the initial saturation of \vec{M} along one specific direction. Thanks to the first pulse we achieve the nucleation of a domain having switched magnetization. Then, with successive pulses, we assist to a domain wall motion event, with the expansion of the switched domain.

Type 2 Hall bars On the other side, type 2 Hall bars present switching parameters that suggest to be easier to reverse their magnetization if compared to the type 1 devices. According to the orientation of the magnetization with respected to the impinging light beam we assist to two different patterns arising in the MOKE images.

We quickly remember that in the longitudinal MOKE we have the magnetization lying

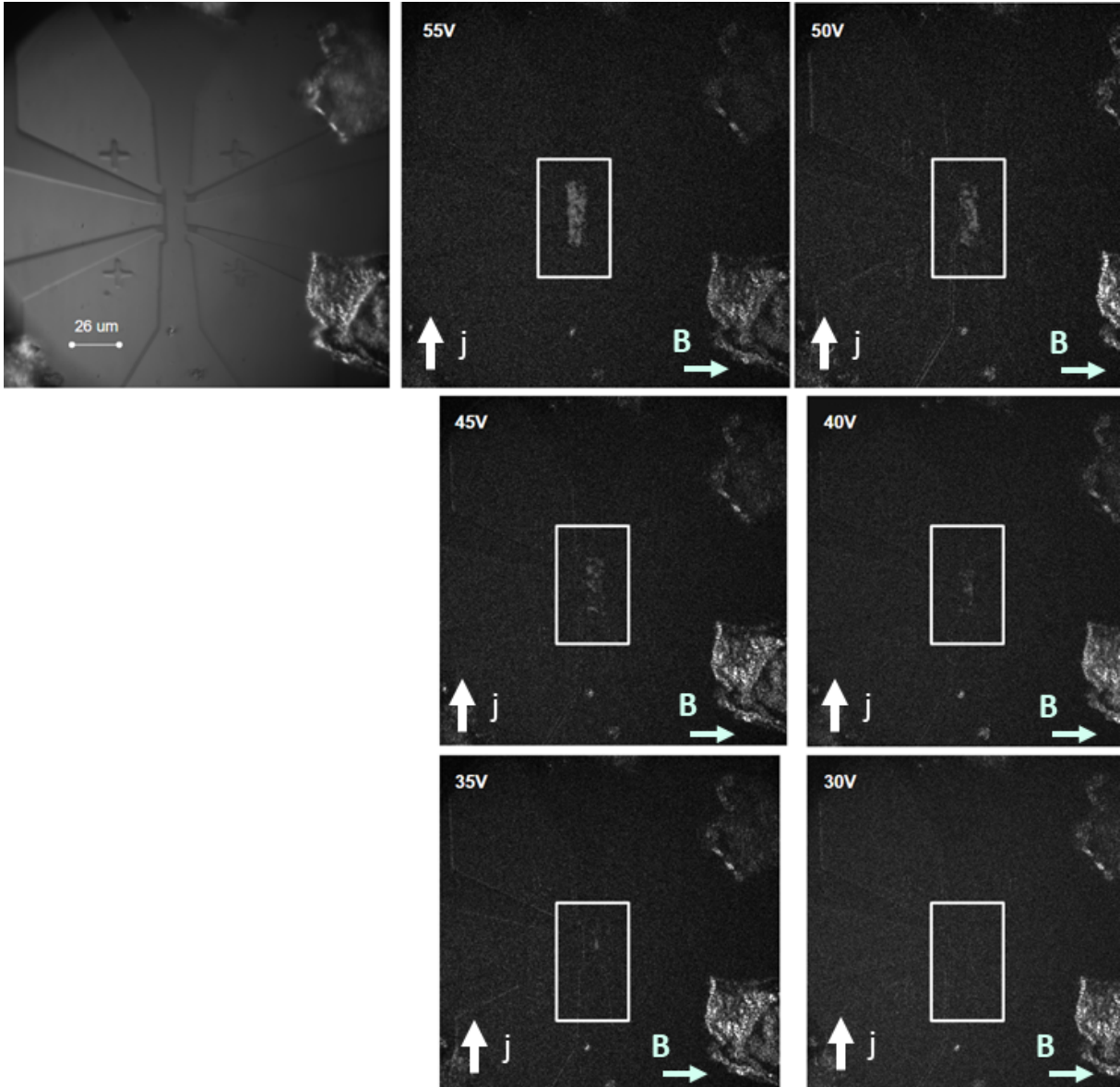


Figure 44: MOKE images of switching in type 1 Hall bars. Are reported the result for different pulses amplitudes at 20ns pulse length. The measurements have been performed in y-configuration, i.e. injected current perpendicular to the external field (whose value is approximately 3 Oe). The white window highlights the region where the switching is observed.

along the direction of the light beam, while for transversal configuration the two are perpendicular (25). In both cases, we may see that a complete switching of the structures is achieved already for 30V pulses, well below the threshold previously seen for type 1 Hall bars. A reason could be found in the dimension of the structure itself. Indeed, the Spin Orbit Torques reveal to be inversely proportional to the saturation magnetization M_S and to the thickness t_{FM} of the ferromagnet (remember from 2.10 that the critical current $J_C \propto (\theta_{SH}^{eff})^{-1}$ where $\theta_{SH}^{eff} \propto M_S \cdot t_{FM}$ [44]). Dealing with smaller devices, leads to less magnetic volume to be switched. As a consequence, the SOT action results to be more effective.

Additionally, if we take into account Figure 36 we may appreciate the difference in mag-

nitude for the DL and FL fields for the two types of structures given the same current conditions. This translates into the need of a smaller voltage amplitude pulses for type 2 Hall bars in order to achieve the same results as for type 1.

Let's now see the difference in the results between the longitudinal and transversal configurations.

Given the results obtained for the angle scan measurements (37), we could assume that the magnetization has its preferential direction along the arm of the Hall bar (i.e. along the x-axis).

We may notice that in transversal configuration (Figure 46) the total switching covers completely the whole structure, while in the longitudinal configuration (Figure 45) the switching area is limited to one side of the magnetic channel of the Hall bar.

The explanation to longitudinal configuration half-structure switching could be given considering the phenomenon as mainly assisted by the Oersted field (\vec{B}_{Oe}). Indeed, as previously explained, the x-switching results to be enhanced if an external magnetic field is applied along the z-axis direction. In our case, given the injection of a current along +x-axis, the \vec{B}_{Oe} presents both a component along the -y ($-|B_{Oe}^y|$) and the z-axis (B_{Oe}^z). The B_{Oe}^z will have a positive sign on the top of the channel (coinciding with the black region in 45) and a negative sign on the bottom part of the channel (coinciding with the white region in 45). Since during the performed measurement was applied an almost zero external magnetic field along the x-direction, it makes sense that the Oersted field plays a not negligible role in the switching reversal of the magnetization of the structure.

On the other side, the images obtained for what we supposed to be the transversal configuration cast some doubts. Indeed, it is true that what the MOKE technique images is the change of the magnetization state of the material without giving any information about the actual direction of the magnetization. Therefore, in the case that the magnetization is not perfectly aligned with an axis (having also some off-axis components that reverse their orientation too when pulses are sent) also the imaged contrast would change.

If the assumptions made in the longitudinal configuration hold, also in this case we should see the presence of two regions in the magnetization having opposite direction, given by the contribution of the Oersted field. On the contrary, the pictures (46) suggest us that reversal of the magnetization is complete.

One could try to explain this by assuming that the magnetization actually is not directed perfectly along x. As a consequence, while in the longitudinal configuration we see the x axis component of \vec{M} (undergoing x-type switching), in the so-called transversal configuration we are actually looking at the components along the y axis, directed along the MOKE's beam path because of the 90° rotation of the sample. Therefore, it is still a longitudinal configuration imaging. The \vec{M} components that we are now investigating undergo a y-type switching, resulting in the complete change in contrast. This assumption could also explain why in harmonic Hall voltage DC pulse measurements we were observing a change in resistance smaller with respect to what we would expect from an SOT switching. It could be due to the fact that what we were inspecting was the reversal of the projection of the magnetization along the y-axis.

However, this assumption is still not a fully satisfactory explanation of why such a difference in contrast among the two types of measurements (46 and 45).

To summarize the results obtained during the magneto-optical analysis we can first of all point out that successful switching was observed only in Hall bars and not in Hall crosses (regardless on the orientation of the central ellipse).

Focusing now only on Hall Bars, we have seen that type 1 structures (having larger geo-

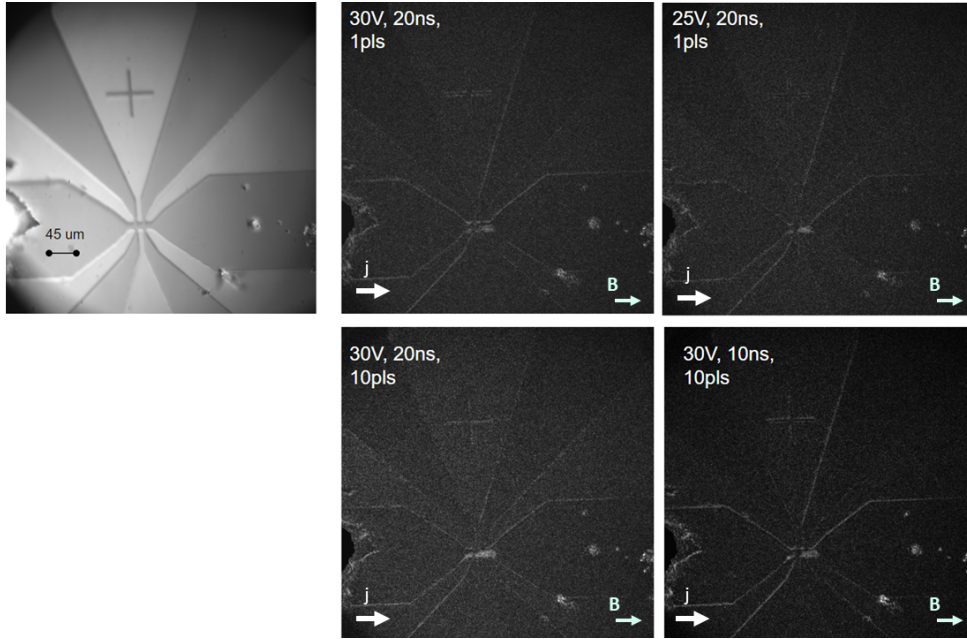


Figure 45: MOKE images of switching in type 2 Hall bars. Are reported the result for different pulses amplitudes and pulse lengths, as well as in the case on a single pulse and of a train of 10 pulses. The measurements have been performed in x-configuration. The external field value is approximately 2.68 Oe.

metrical parameters) need higher voltages in order to achieve the complete magnetization reversal (55V vs 30V at 20ns long voltage pulses). We have traced back this observation to the inverse proportionality existing between SOTs and M_S , t_{FM} parameters.

Additionally there is also a difference in the switching according to the sample orientation. While in we may observe a full \vec{M} reversal for vertically oriented Hall bars (even if is needed domain wall motion assistance for bigger structures), for the horizontally oriented structures it is not the case. The reason is due to the possible off-axis direction of \vec{M} . The reversal of the x-axis component of \vec{M} is assisted by the Oersted field, leading to the displayed contrast by the devices analysed.

In both configurations the measuring procedure consisted into the initial saturation of \vec{M} along a specific direction: while the black parts of the obtained images have the magnetization directed along the -x direction, the white parts are directed along +x. On top of that, during the measurement \vec{B}_{ext} was applied along +x direction, with an almost zero amplitude (namely about 0.25mT).

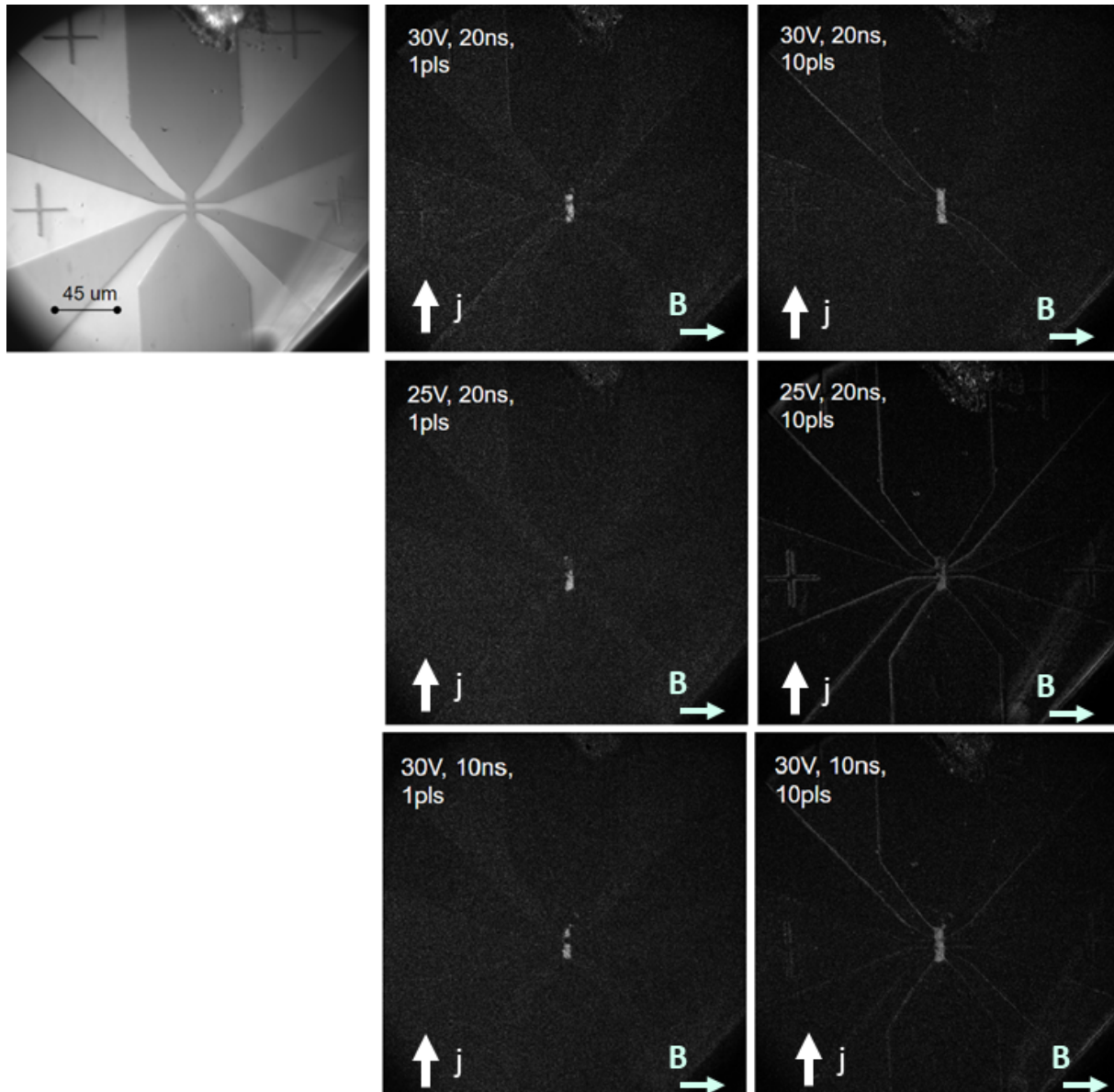


Figure 46: MOKE images of switching in type 2 Hall bars. Are reported the result for different pulses amplitudes and pulse lengths, as well as in the case on a single pulse and of a train of 10 pulses. The external field value is approximately 2.68 Oe.

4.3 Time-resolved characterization

As already said, one of the main interests of this thesis was the possibility to explore the time-evolution of the magnetization switching in a time-resolved setup (introduced in 3.3).

Measurements have been carried out for both Hall crosses and Hall bars, since it was not known *a priori* if it was possible to achieve the reversal of \vec{M} in the two different devices. However, as demonstrated with the magneto-optical analysis, Hall crosses revealed to not be a suitable structure for observing the investigated phenomenon. Despite that, the results obtained for the Hall crosses represent a good reference in order to evaluate the quality and reliability of the outcomes coming from Hall bars analysis.

4.3.1 Reference trace

We quickly recall that the TR measurements rely on the acquisition of first a reference trace and then of the switching trace. The reference is obtained by subtracting from the transverse voltage measured in the before-switching state of the magnetization (sampled with a positive background magnetic field while positive polarity voltage pulses are sent across the device), the transverse voltage associated to the after-switching state (obtained by applying a negative background magnetic field but still pulsing positive polarity signals). In the specific case of IMA samples we expected to obtain a flat reference window. This is because the setup samples a signal where it is not possible to separate the first from the second order effects. As a consequence the $R_{1\omega}^H$ contribution will be the dominant one in the resulting plot. We recall that $R_{1\omega}^H = R_{AHE} \cdot \cos\theta + R_{PHE} \cdot \sin^2\theta \cdot \sin(2\varphi)$. By taking into account the angle scan of IMA samples (32), we can conclude that the transverse resistance of the device when its magnetization is both at 0° and 180° should have always the same value. The direct consequence is that it is not possible to distinguish the before-switching state from the after-switching one, leading to a normalized reference (i.e. the difference among the two sampled reference traces) that results to be a flat curve. However, if we look at the real curves obtained from the measurements (Figure 47), we may notice that they are not completely flat but present some spikes and fluctuations. The explanation of such a behavior may be found in the following points:

- the large spikes at the edges of the raw reference data are caused by the inductive coupling effects between the wire bonds and the electric contacts of the circuit board;
- the distortion of the pulse is caused by the fact that the device itself is not suitable for Radio-Frequency (RF) operation;
- possible high-frequency oscillations are introduced by the voltage amplifier.

4.3.2 Switching trace of Hall crosses

According to the previous discussion, what we would expect as an outcome of Hall cross TR analysis would be two flat traces, one representing the reference and the other representing the switching. This last consideration is valid as long as no switching takes place and subsequently no contributions to both the AHE and PHE are present (which is what seems to be observed during the MOKE imaging). In fact, if the switching would have taken place following an in-plane trajectory a contribution given by the PHE would have led to a deviation from the reference trace, while on the other side switching with

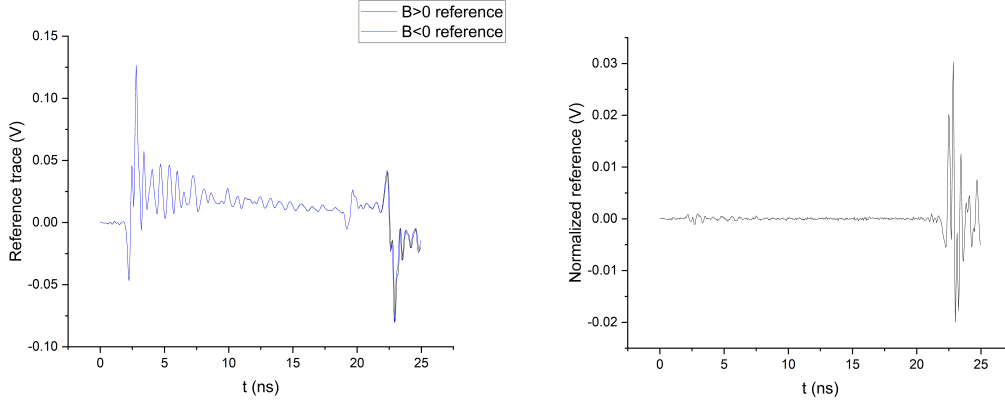


Figure 47: Reference traces acquired during TR measurements. In the left panel are presented the raw traces acquired for both positive and negative background fields, we can see that they are almost coincident. In the right panel instead is presented the normalized reference obtained by subtracting the negative background signal from the positive one. What we are interested in is the time window finding between the rising and the falling edges of the pulse, since it is where the magnetic information can be found. The trend of the normalized reference is almost flat except for the final spike. This behavior could be due to changes in the inductive coupling between the wire bonds and the electric contacts if \vec{B}_{ext} is positive or negative. Indeed, the coupling strongly depends on the value of \vec{B}_{ext} , not allowing the annealing of such a contribution in a differential read-out.

out-of-plane trajectory components would have led to AHE contributions to the switching trace.

By looking more into detail in the obtained results we may surprisingly notice that the switching trace is not flat as one would expect (measurements reported in 48). First of all, in order to increase data precision without introducing distortions in their tendency (for the sake of a better understanding) was applied a Savitzky–Golay filter to the reference and switching curves. What does the Savitzky–Golay filter is performing a convolution by taking into account successive adjacent data sets (the number of points is user defined) and fitting such a sub-set with a low-degree polynomial exploiting the linear least squares method [45]. As we may see in the time interval corresponding to the sent pulse, the switching curve displays a deviation from the reference. Such a deviation should suggest the presence of a magnetic behavior in the device, however, as already explained during the MOKE results presentation, for the used parameter no switching should be observed. In order to check if such observations were related or not to the samples themselves, some measurements were performed without having any device mounted and contacted on the samples holder. The results of this type of measurements are reported in Figure 49.

We may see from the plots that no pattern may be identified in the behavior of the switching curve. Despite the noise, if we imagine to average such traces, we would obtain a more or less flat behavior (i.e. no switching), in agreement with the expectations. As a results, the justification underlying the obtained curves (Figure 48), have to be searched in the interaction between the specimen and the setup. Probably what we see is a voltage offset intrinsic to the measurement during the pulse sampling, due to the signal travelling across the sample which could be visualized as a resistance. It means that while the measurement is performed (i.e. during the pulse) the sampled Hall voltage presents a positive offset. This offset could cause the flat trace to be shifted a bit away from the

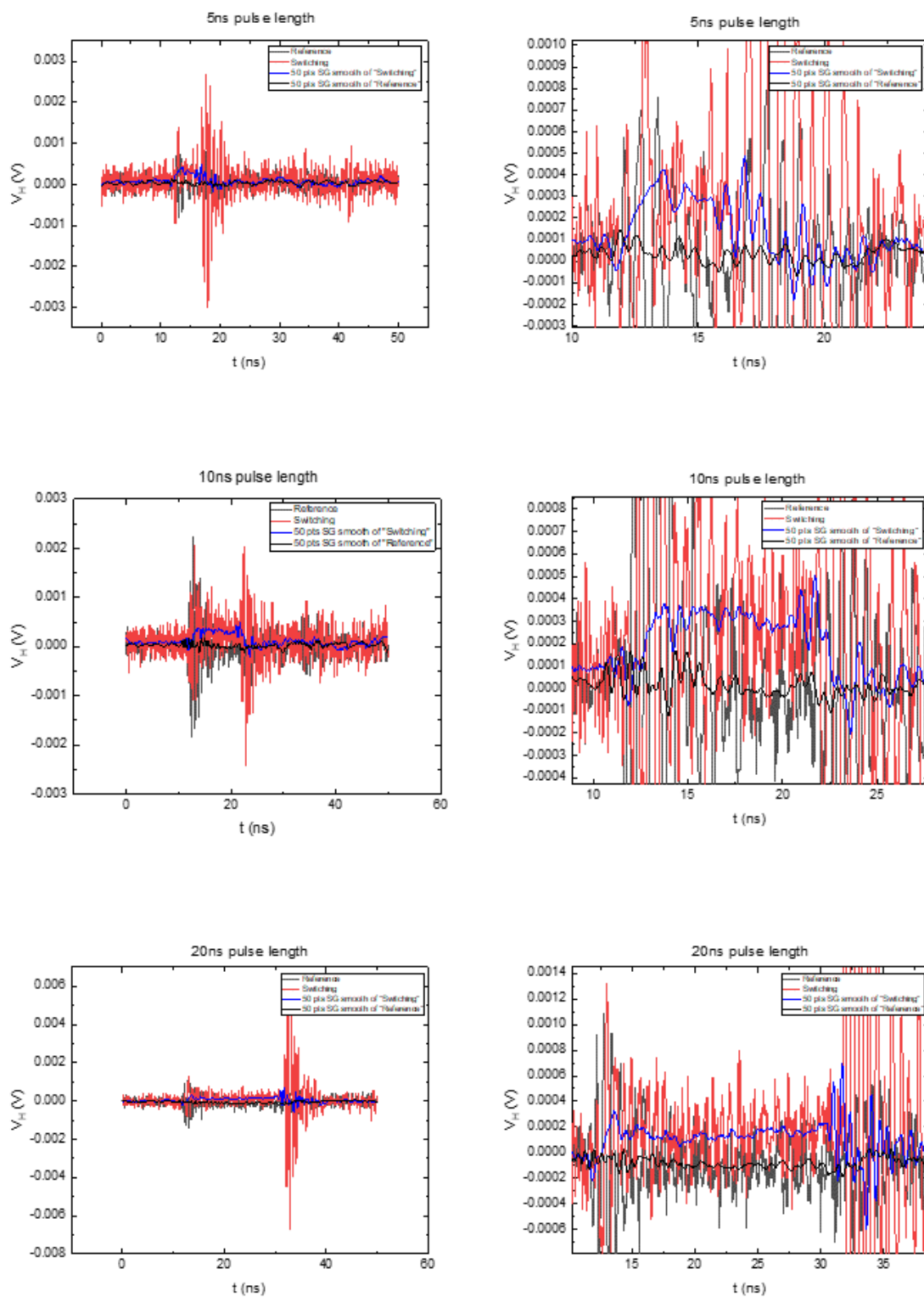


Figure 48: Hall cross TR switching traces for 31V pulses at different pulse lengths. The blue curves refer to the switching signal while the black ones to the reference signal.

reference trace. Such a phenomenon would explain why the switching trace rises and falls

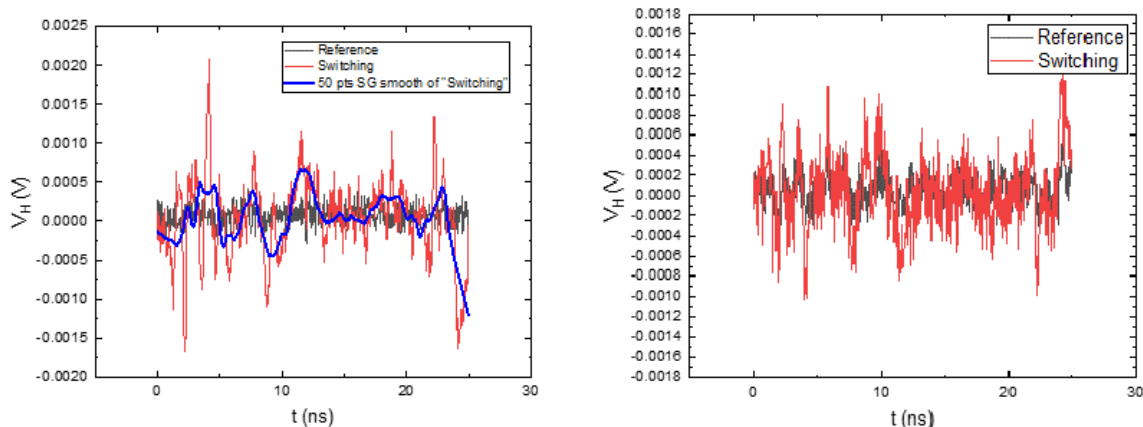


Figure 49: TR switching analysis with no sample mounted on the sample holder. The setup was left in an open circuit condition while performing the measurement. In both pictures the black traces represent the reference and the red traces the switching. The blue trace is the smoothing of the switch trace obtain after having applied the Savitzky–Golay filter. Both measurements where done in the same conditions, sending $\pm 30\text{V}$ set/reset pulses 20ns long. The external field was equal to $\pm 30\text{mT}$ while acquiring the background signals and $< 1\text{mT}$ during the switching protocol.

so quickly, making the switching trace of an almost rectangular shape.

4.3.3 Switching trace of Hall bars

One of the major difficulties when performing TR measurements on Hall bars is the asymmetry of the structures. As already explained in 3.3, the whole measuring setup relies on the symmetry of the system, which allows to avoid current shunting events and enables the measurement of the Hall voltage across the device. The symmetry breaking introduced by Hall bars, leads to the suppression of the virtual ground at the center of the structure. Indeed, the two voltage pulses of opposite polarity injected from the two extremities of the structure do not meet anymore in the perfect middle of the one (50). A solution to such a problem is represented by the addition of an attenuator to the setup. More precisely, it can be attached to the first balun of the setup, on the side that finds in direct contact with the shorter arm of the Hall bar. In such a way the stronger pulse (i.e. the one that has to travel less across the Hall structure) is attenuated and comparable in amplitude with the one that has to travel across a longer path and therefore loses amplitude components along the way.

The measurement in both type 1 and type 2 Hall bars cases where performed with and without attenuators, demonstrating that the dimensions of the devices is such that it is not introduced a too dramatic attenuation of the pulse travelling the short path. In the following only the more relevant results will be presented.

Type 1 Hall bars Some of the results obtained for type 1 Hall bars are reported in Figure 51. Overall, we may notice that the behavior of the obtained curves is really similar to those observed with the Hall crosses. Indeed, we may see that the switching trace abruptly rises in correspondence of the pulse start. Similarly, as soon a the pulse

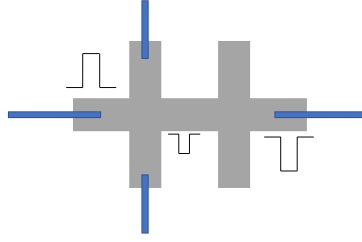


Figure 50: Hall bar contacted for TR measurements. The blue lines represent the wiring of the device. From the left side comes the positive pulse while from the right side comes the negative one. Since the transverse signal is sampled at the level of the first transverse arm of the structure, the two pulses have not the same amplitude at the point where the measurement is done (for instance, in this case we may see that the positive pulse has a larger amplitude with respect to the negative one).

time window comes to an end, also the switching signal goes back to the initial level with a quite rapid fall. Across the measurement (i.e. in the pulse time window) the switching trace maintains what may be considered as constant behavior looking at the smoothed curves. If the justifications given for the Hall crosses' behavior is correct, applying the same reasoning to the Hall bars, we may conclude that no magnetic behavior is observed either for the Hall bars.

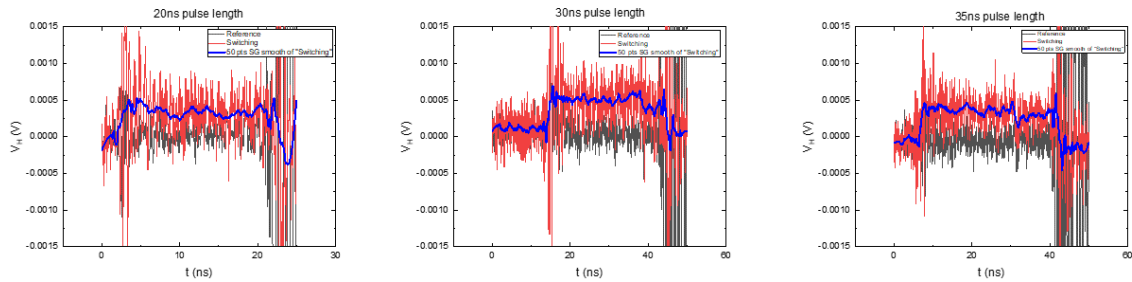


Figure 51: TR switching measurement for a type 1 Hall bar with a 2dB attenuator inserted in the setup in order to balance the pulses in the structure. Black curves are the reference trace, red curves the switching trace while blue curves represent the smoothed switching traces. From left to right we find the results for respectively 20 ns, 30 ns and 35 ns pulse lengths. In all the three cases the pulse amplitude was equal to 50V.

Type 2 Hall bars As far as the results concerning the type 2 Hall bars are taken into account, also in this case no clear magnetic behavior can be observed. As we may see from the results reported in Figure 52 the plots are similar to those obtained after the analysis of the type 1 Hall bars. Therefore the same considerations apply. The only difference in this case is the reversed polarity of the offset, which could be due to the possibly reversed injected current polarity or swept transverse voltage contacts.

We could conclude that the TR characterization does not seem to be a suitable technique for the investigation of in-plane magnetic samples. The reasons could be multiple. First of all it should be implemented a system in which only the second harmonic signal can be observed. This would allow to eliminate the first order contribution which results to be

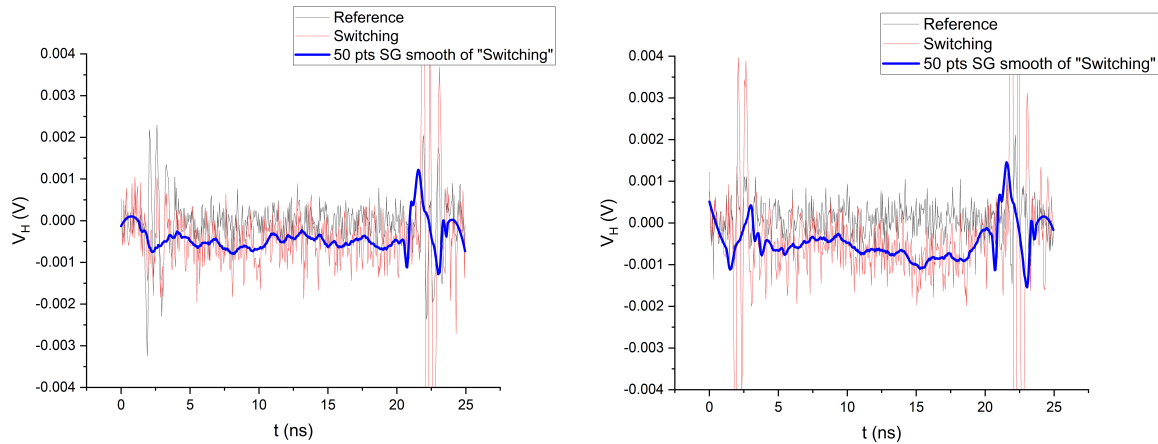


Figure 52: TR switching measurement for a type 2 Hall bar without any attenuator inserted in the setup. Pulse length of 20ns and pulse amplitude of 20V.

meaningless in IMA samples because of their geometry and how it impacts Equation 3.5. However, this implementation results to be particularly difficult if not impossible to be realized. Indeed, with the TR setup we are looking at the time evolution of the signal while the separation of the harmonic components would require an uncoupling of different frequency components. This last point translates into a Fourier transformation of the time-evolving signal.

Furthermore, the variations of the transverse voltage V_H , associated to a magnetic behavior of the in-plane devices, results to be in the order of magnitude of few mV, if not less. Such values are comparable with possible noise contributions and offsets adding up to the signal. This places the TR characterization of this particular kind of devices at the edge of the TR setup resolution.

Additionally, with the TR setup there is no possibility to check in a unique way if the \vec{M} reversal is really taking place or not. A solution could be represented by the implementation of a new setup that combines the time-resolved and the magneto-optical characterization. In such a way, by optically checking the state of the samples before and after the sent pulse, we are able to associate the electrical signal to an on going magnetic behavior without having any doubt.

A last possibility that has to be mentioned is the one that actually a switching is taking place in the Hall bars, but its dynamics is so fast that is achieved within the few first ns of the injected pulse. We are confident to exclude this possibility since we have dealt mainly with y-type switching during the TR observations, which we have seen having a dynamics evolving on much greater time scales than 1ns (2.4.3).

5 Conclusions and outlook

In this thesis we investigated the current-induced switching of the magnetization in in-plane magnets (IMA, i.e. magnets having the anisotropy easy axis laying in the xy plane). The main interest of such a study falls in the domain of the development of MRAMs, a kind of Random Access Memories for data storage based on the magnetic properties of the materials. This kind of memories reveal to be appealing because of their advantages in terms of energy expenditure, a topic which is becoming a more and more important concern in nowadays technology development given the environmental issues that we are facing.

In order to be able to perform the analysis of our interest, first of all we fabricated samples that we thought to be suitable for this type of study. The requirement for such structures was to be able to generate Spin Orbit Torques, the physical phenomenon exploited for magnetization (\vec{M}) reversal in this thesis experience. Usually, for such purposes, are employed heavy metal (HM)/ferromagnet (FM) heterostructures.

Through a photolithographic process in clean room were obtained Hall bars and Hall crosses. The starting point were multi-layer stacks deposited on Si substrates. Such deposited stacks presented the bi-layer made out of Pt/Co. Several samples were deposited, each having varying thicknesses of Pt and Co.

As far as the geometry is concerned, the analyzed Hall crosses presented central ellipses with three possible orientations: 0° (long axis aligned along x-axis), 90° (long axis aligned along y-axis) and 45° (long axis shifted by 45° with respect to the x-axis).

The thesis experience took advantage of three main techniques: the harmonic Hall voltage measurement (coinciding to a static electric characterization), the Magneto Optical Kerr Effect microscopy (corresponding to an optical characterization) and the time-resolved measurements (representing the dynamic electric characterization).

Each technique led us to a progressive improvement in the understanding of the fabricated devices:

- Thanks to the static electric characterization we were able to define some basic properties of the samples, namely the magnetization anisotropy orientation, the magnitude of the switching mechanism and the contributions due to different Spin Orbit Torque components to the phenomenon.
- The magneto-optical characterization allowed us to confirm the presence of the magnetization reversal allowing to exclude electrical noise contributions from the previous observations.
- The time-resolved characterization was thought to be a good solution to overcome the difficulty in the analysis represented by the resistance equivalence of the initial and final switching states.

The main results lead to the conclusion that the magneto-optical method was the best in order to observe uniquely the switching and retrieve the conditions for which it takes place. Despite the TR method seeming to be the most promising one, it didn't lead to unquestionable results about the \vec{M} reversal. Such problems could come from the inadequacy of both samples and measurement setup. As far as the devices are concerned, we have seen that the Hall crosses revealed to get damaged before any magnetic property variation

could even be observed. Fabricating devices having bigger central ellipses could be a useful improvement or even devices presenting a thicker Pt layer. On the other side, modifying the TR setup also could be an advancement. Indeed, the time-resolved setup was initially developed in order to analyze Perpendicular Magnetic Anisotropy (PMA) samples. The signal coming from IMA devices finds at the edges of the resolution achieved by the instruments making up the setup.

In the following we report some suggestions for future improvements and a possible continuation of this project.

- Performing the analysis of stacks having different thicknesses of Pt/Co. We can already make some assumptions on the possible outcomes. Indeed, thicker Co layer would provide a larger magnetic volume for the switching. On the other side, thicker Pt layer would decrease the resistance of the device. More Pt would lead to a higher Spin Orbit Coupling, meaning more Spin Orbit Torques. However, we could also experience a decrease of the contributions produced by the Anomalous and Planar Hall Effects: more current would be dissipated across the structure, affecting less the oscillation of \vec{M} around its equilibrium point.
- Implement a TR setup including a magneto-optical check of the magnetic state of the sample before and after the supposed switching.
- Analyzing Hall bars having different aspect ratios to understand better the impact of the geometry on the behavior of the devices.
- Substituting the Pt with an antiferromagnet (e.g. IrMn) that could introduce an exchange bias in the system with a subsequent unidirectional anisotropy due to interface coupling. As a consequence, could be induced an orientation of the magnetization easy axis in such a way to increase the PHE contributions to the harmonic Hall voltage signals.
- Improve the understanding of the anisotropy orientation in the observed devices and underlying reasons, aided also by simulation software.

Overall, there are still a lot of open questions concerning IMA devices that are waiting for an answer. Keeping alive the investigation would not only allow us to better understand the mechanisms underlying some fundamental physical phenomena (namely the SOT), but also would allow to improve market technologies in such a way to be more compatible with current needs.

6 References

- [1] Taylor, P. Volume of data/information created, captured, copied, and consumed worldwide from 2010 to 2020, with forecasts from 2021 to 2025. <https://www.statista.com/aboutus/our-research-commitment/3282/petroc-taylor> (2022). Accessed: 2023-05-10.
- [2] Diény, B. *et al.* Opportunities and challenges for spintronics in the microelectronics industry. *Nature Electronics* **3**, 446 – 459 (2020).
- [3] S., F., T., A. & C., Z. A spin–orbit torque switching scheme with collinear magnetic easy axis and current configuration. *Nature Nanotech* **11**, 621–625 (2016). URL <https://doi.org/10.1038/nnano.2016.29>.
- [4] Iacovacci, V., Lucarini, G., Ricotti, L. & Menciasci, A. Magnetic field-based technologies for lab-on-a-chip applications. In Stoytcheva, M. & Zlatev, R. (eds.) *Lab-on-a-Chip Fabrication and Application*, chap. 3 (IntechOpen, Rijeka, 2016). URL <https://doi.org/10.5772/62865>.
- [5] Bruno, P. Geometrically constrained magnetic wall. *Phys. Rev. Lett.* **83**, 2425–2428 (1999). URL <https://link.aps.org/doi/10.1103/PhysRevLett.83.2425>.
- [6] Ohsumi, H. Magnetoelastic effect in holmium studied by x-ray diffraction. *Journal of the Physical Society of Japan* **71**, 1732–1739 (2002). URL <https://doi.org/10.1143/JPSJ.71.1732>.
- [7] Meiklejohn, W. H. & Bean, C. P. New magnetic anisotropy. *Phys. Rev.* **102**, 1413–1414 (1956). URL <https://link.aps.org/doi/10.1103/PhysRev.102.1413>.
- [8] Ruiz, E. 9.20 - exchange coupling in di- and polynuclear complexes. In Reedijk, J. & Poeppelmeier, K. (eds.) *Comprehensive Inorganic Chemistry II (Second Edition)*, 501–549 (Elsevier, Amsterdam, 2013), second edition edn. URL <https://www.sciencedirect.com/science/article/pii/B9780080977744009220>.
- [9] Gambardella, P. & Miron, I. M. Current-induced spin–orbit torques. *Philosophical Transactions of the Royal Society A: Mathematical, Physical and Engineering Sciences* **369**, 3175–3197 (2011). URL <https://royalsocietypublishing.org/doi/abs/10.1098/rsta.2010.0336>.
- [10] Manchon, A. & Zhang, S. Theory of spin torque due to spin-orbit coupling. *Phys. Rev. B* **79**, 094422 (2009). URL <https://link.aps.org/doi/10.1103/PhysRevB.79.094422>.
- [11] Manchon, A. & Zhang, S. Theory of nonequilibrium intrinsic spin torque in a single nanomagnet. *Phys. Rev. B* **78**, 212405 (2008). URL <https://link.aps.org/doi/10.1103/PhysRevB.78.212405>.
- [12] Han, W., Maekawa, S. & Xie, X.-C. Spin current as a probe of quantum materials. *Nature Materials* **19**, 139–152 (2019). URL <https://doi.org/10.1038/s41563-019-0456-7>.
- [13] Sala, G. *Magnetization dynamics induced by spin and orbital currents in ferro- and ferrimagnets*. Doctoral thesis, ETH Zurich, Zurich (2022).
- [14] Avci, C. O. *Current-induced effects in ferromagnetic heterostructures due to spin-orbit coupling*. Doctoral thesis, ETH Zurich, Zürich (2015).
- [15] Dyakonov, M. & Perel, V. Current-induced spin orientation of electrons in semiconductors. *Physics Letters A* **35**, 459–460 (1971). URL <https://www.sciencedirect.com/science/article/pii/0375960171901964>.
- [16] Sinova, J. *et al.* Universal intrinsic spin hall effect. *Phys. Rev. Lett.* **92**, 126603 (2004). URL <https://link.aps.org/doi/10.1103/PhysRevLett.92.126603>.
- [17] Nagaosa, N., Sinova, J., Onoda, S., MacDonald, A. H. & Ong, N. P. Anomalous hall effect. *Rev. Mod. Phys.* **82**, 1539–1592 (2010). URL <https://link.aps.org/doi/10.1103/RevModPhys.82.1539>.

-
- [18] Mihai Miron, I. *et al.* Current-driven spin torque induced by the rashba effect in a ferromagnetic metal layer. *Nature Mater* **9**, 230–234 (2010). URL <https://doi.org/10.1038/nmat2613>.
- [19] Bychkov, Y. A. & Rashba, E. I. Properties of a 2d electron gas with lifted spectral degeneracy (1984).
- [20] Bihlmayer, G., Noël, P., Vyalikh, D. V., Chulkov, E. V. & Manchon, A. Rashba-like physics in condensed matter (2022-10).
- [21] Manchon, A. & Zhang, S. Theory of nonequilibrium intrinsic spin torque in a single nanomagnet. *Phys. Rev. B* **78**, 212405 (2008). URL <https://link.aps.org/doi/10.1103/PhysRevB.78.212405>.
- [22] Manchon, A., Koo, H. C., Nitta, J., Frolov, S. M. & Duine, R. A. New perspectives for rashba spin-orbit coupling. *Nature Materials* **14**, 871–882 (2015). URL <https://doi.org/10.1038/nmat4360>.
- [23] Böhnert, T. *et al.* Magnetothermopower and magnetoresistance of single co-ni/cu multilayered nanowires. *Phys. Rev. B* **90**, 165416 (2014). URL <https://link.aps.org/doi/10.1103/PhysRevB.90.165416>.
- [24] Binda, F. *Molecular beam epitaxy and spin-orbit torques of topological insulator heterostructures*. Doctoral thesis, ETH Zurich, Zurich (2022).
- [25] Ralph, D. & Stiles, M. Spin transfer torques. *Journal of Magnetism and Magnetic Materials* **320**, 1190–1216 (2008). URL <https://doi.org/10.1016/j.jmmm.2007.12.019>.
- [26] Manchon, A. *et al.* Current-induced spin-orbit torques in ferromagnetic and antiferromagnetic systems. *Reviews of Modern Physics* **91** (2019). URL <https://doi.org/10.1103/RevModPhys.91.035004>.
- [27] Miron, I. M. *et al.* Perpendicular switching of a single ferromagnetic layer induced by in-plane current injection. *Nature* **476**, 189–193 (2011). URL <https://doi.org/10.1038/nature10309>.
- [28] Lee, K.-S., Lee, S.-W., Min, B.-C. & Lee, K.-J. Threshold current for switching of a perpendicular magnetic layer induced by spin Hall effect. *Applied Physics Letters* **102**, 112410 (2013). URL <https://doi.org/10.1063/1.4798288>.
- [29] Liu, L. *et al.* Spin-torque switching with the giant spin hall effect of tantalum. *Science* **336**, 555–558 (2012). URL <https://www.science.org/doi/abs/10.1126/science.1218197>.
- [30] Grimaldi, E. *et al.* Single-shot dynamics of spin-orbit torque and spin transfer torque switching in three-terminal magnetic tunnel junctions. *Nat. Nanotechnol.* **15**, 111–117 (2020). URL <https://doi.org/10.1038/s41565-019-0607-7>.
- [31] Fukami, S., Anekawa, T., Ohkawara, A., Zhang, C. & Ohno, H. A sub-ns three-terminal spin-orbit torque induced switching device. *2016 IEEE Symposium on VLSI Technology* 1–2 (2016). URL <https://ieeexplore.ieee.org/document/7573379>.
- [32] Lee, J. W. *et al.* Enhanced spin-orbit torque by engineering pt resistivity in Pt/Co/AlO_x structures. *Phys. Rev. B* **96**, 064405 (2017). URL <https://link.aps.org/doi/10.1103/PhysRevB.96.064405>.
- [33] Conte, R. L. *Magnetic nanostructures with structural inversion asymmetry*. Ph.D. thesis (2016).
- [34] Avci, C. O. *et al.* Unidirectional spin hall magnetoresistance in ferromagnet/normal metal bilayers. *Nature Physics* **11**, 570–575 (2015). URL <https://doi.org/10.1038/nphys3356>.
- [35] Avci, C. O. *et al.* Interplay of spin-orbit torque and thermoelectric effects in ferromagnet/normal-metal bilayers. *Phys. Rev. B* **90**, 224427 (2014). URL <https://link.aps.org/doi/10.1103/PhysRevB.90.224427>.

-
- [36] Binda, F. *et al.* Spin-orbit torques and magnetotransport properties of α – Sn and β – Sn heterostructures. *Phys. Rev. B* **103**, 224428 (2021). URL <https://link.aps.org/doi/10.1103/PhysRevB.103.224428>.
- [37] Posti, R. *et al.* Odd symmetry planar Hall effect: A method of detecting current-induced in-plane magnetization switching. *Applied Physics Letters* **122**, 152405 (2023). URL <https://doi.org/10.1063/5.0143904>.
- [38] Li, D. *et al.* Roles of joule heating and spin-orbit torques in the direct current induced magnetization reversal. *Scientific Reports* **8** (2018).
- [39] Fert, A., George, J.-M., Jaffres, H. & Faini, G. Spin injection and experimental detection of spin accumulation. *Journal of Physics D: Applied Physics* **35**, 2443 (2002). URL <https://dx.doi.org/10.1088/0022-3727/35/19/319>.
- [40] Islam, M., Pikul, M. & Wang, X. Thermally assisted magnetization reversal of a magnetic nanoparticle driven by a down-chirp microwave field pulse. *Journal of Magnetism and Magnetic Materials* **537**, 168174 (2021). URL <https://www.sciencedirect.com/science/article/pii/S0304885321004509>.
- [41] Zheng, Z. *et al.* Anomalous thermal-assisted spin-orbit torque-induced magnetization switching for energy-efficient logic-in-memory. *ACS Nano* **16**, 8264–8272 (2022). URL <https://doi.org/10.1021/acsnano.2c02031>.
- [42] Jacot, B. J. *et al.* Systematic study of nonmagnetic resistance changes due to electrical pulsing in single metal layers and metal/antiferromagnet bilayers. *Journal of Applied Physics* **128**, 173902 (2020). URL <https://doi.org/10.1063/5.0026147>.
- [43] Churikova, A. *et al.* Non-magnetic origin of spin Hall magnetoresistance-like signals in Pt films and epitaxial NiO/Pt bilayers. *Applied Physics Letters* **116**, 022410 (2020). URL <https://doi.org/10.1063/1.5134814>.
- [44] Neumann, L. & Meinert, M. Influence of the Hall-bar geometry on harmonic Hall voltage measurements of spin-orbit torques. *AIP Advances* **8**, 095320 (2018). URL <https://doi.org/10.1063/1.5037391>.
- [45] Savitzky, A. & Golay, M. J. E. Smoothing and differentiation of data by simplified least squares procedures. *Analytical Chemistry* **36**, 1627–1639 (1964). URL <https://doi.org/10.1021/ac60214a047>.
- [46] Lienig, J. & Thiele, M. *Fundamentals of Electromigration-Aware Integrated Circuit Design* (Springer Cham, 2018). URL <https://doi.org/10.1007/978-3-319-73558-0>.

Appendices

A Photolithographic process for device fabrication

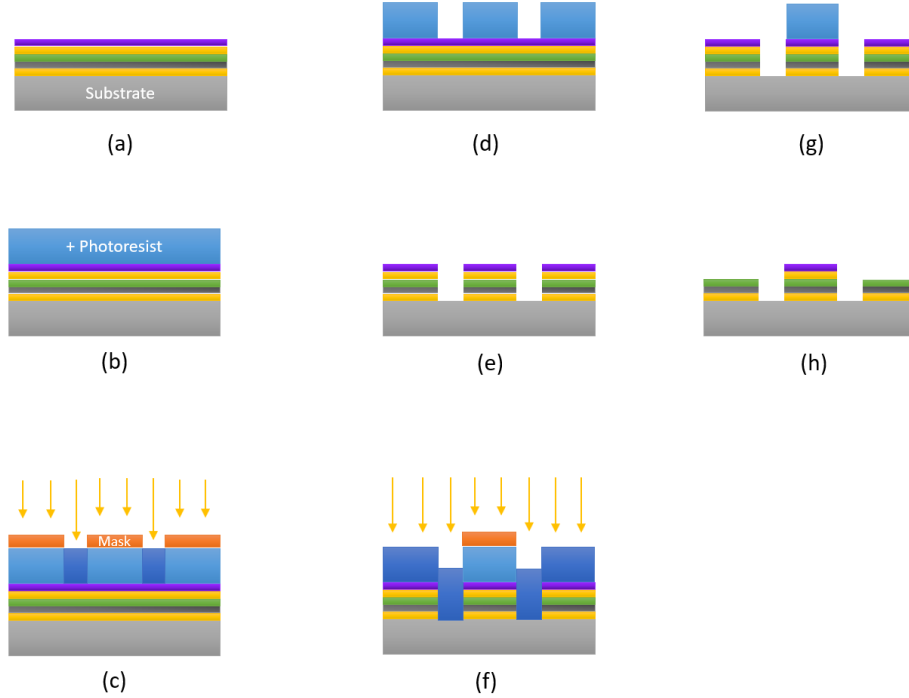


Figure 53: Schematics of the photolithographic process for device fabrication. **(a)** Deposition of the stack. **(b)** The photoresist is applied. **(c)** The resist is exposed through a mask. **(d)** Development of the photoresist. **(e)** Ar ion etching. **(f)** The photoresist is applied and exposed once again. **(g)** Only the unexposed regions will preserve the photoresist. **(h)** The final structure is obtained.

In Figure 53 we may find the photolithographic procedure referred to the two step fabrication process. In **(a)** is represented the deposition of the stack over the Si substrate. In yellow Cr, in gray Pt, in green Co and in purple Si_3N_4 (only the Pt and Co layers vary in thickness through the different samples [Table 1]). In **(b)** the positive photoresist (PR) AZ 1505 is applied over the cleaned stack using a spinner-bench. We remind that in a positive PR the portion of the PR that is exposed to light becomes soluble to the PR developer. In order to obtain a properly cleaned sample before starting the photolithography, is used ultrasound-bathing first in acetone and then in isopropanol for 3min each. The recipe for the PR application is the following: ramp up the spinner speed in 5sec to the target velocity of 4000rpm/sec, then continue the spinning for 45sec at 4000rpm/sec. After the spinning has finished the photoresist has to be baked for 60min at 90° . If we see that the photoresist didn't span correctly it could mean that some H_2O vapor is stuck on the surface. To solve this issue, one could try either to bake the sample at 180° for 1/2 min, or to perform some O_2 plasma ashing for 60 sec at 1 mbar pressure and 150 W power. In **(c)** the sample is exposed through a mask (more details in B) put in contact with it for 10sec with a dose of 12.3 mJ/cm^2 . In **(d)** the exposed photoresist is eliminated immersing the sample in AZ 400 K 1:4 developer (i.e. one part developer, four parts of water) for 10/12sec. In **(e)** the unprotected sample regions are etched away exploiting

Ar ion etching. The precise timing depends on the thicknesses of the stack that has to be eliminated, but it can range from 3min 30sec to 5min. The excess photoresist is eliminated with ultrasound bathing in acetone for 3min. In (f) the PR is applied and exposed once again with the same recipe as previously. In (g) we see that only the unexposed regions will preserve the PR after development. In (h) the final shape is obtained by a final etching procedure.

B Masks used for sample fabrication

The used masks for sample exposure have been fabricated via laser writing at ETH facilities. In this case, is performed a photolithographic process where a thin chromium layer over a silica substrate is patterned according to the desired mask shape. The design of the mask is obtained with the help of a CAD tool. The .gds file generated after the design procedure is converted into a compatible format and transmitted to the software of the laser writing system. The system exposes the photoresist via direct laser writing with a laser beam, technique that allows to achieve better quality results with a resolution of 10 – 100 nm.

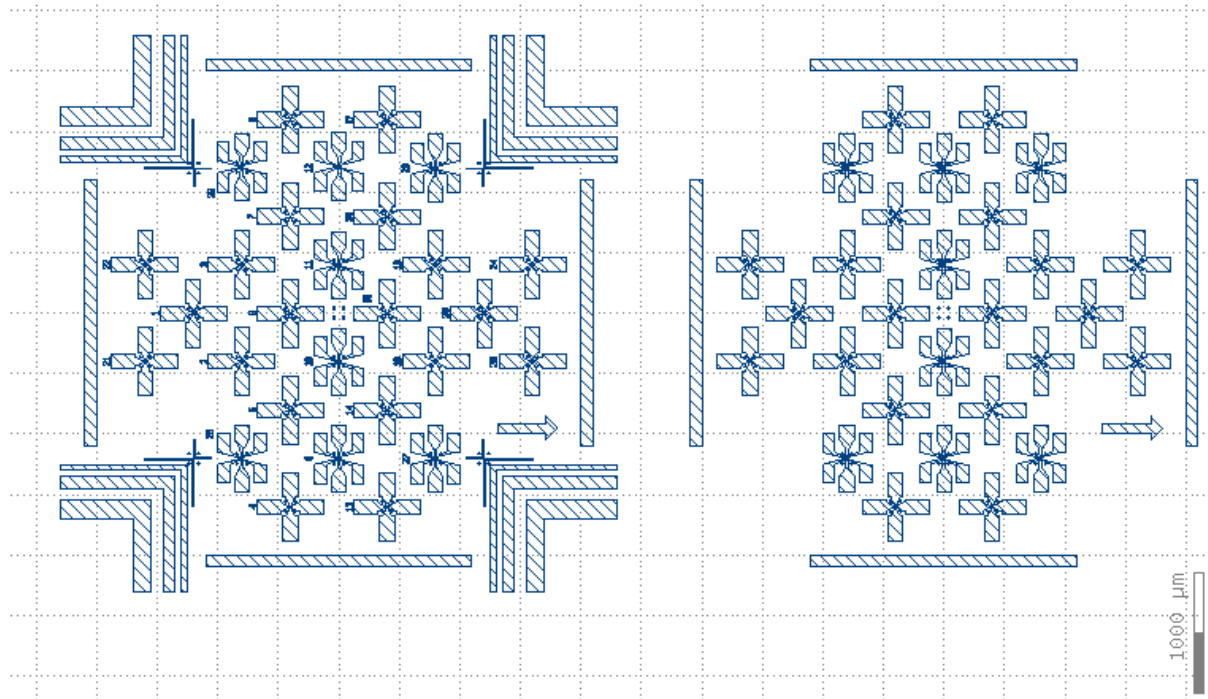


Figure 54: Mask used for two step sample fabrication.

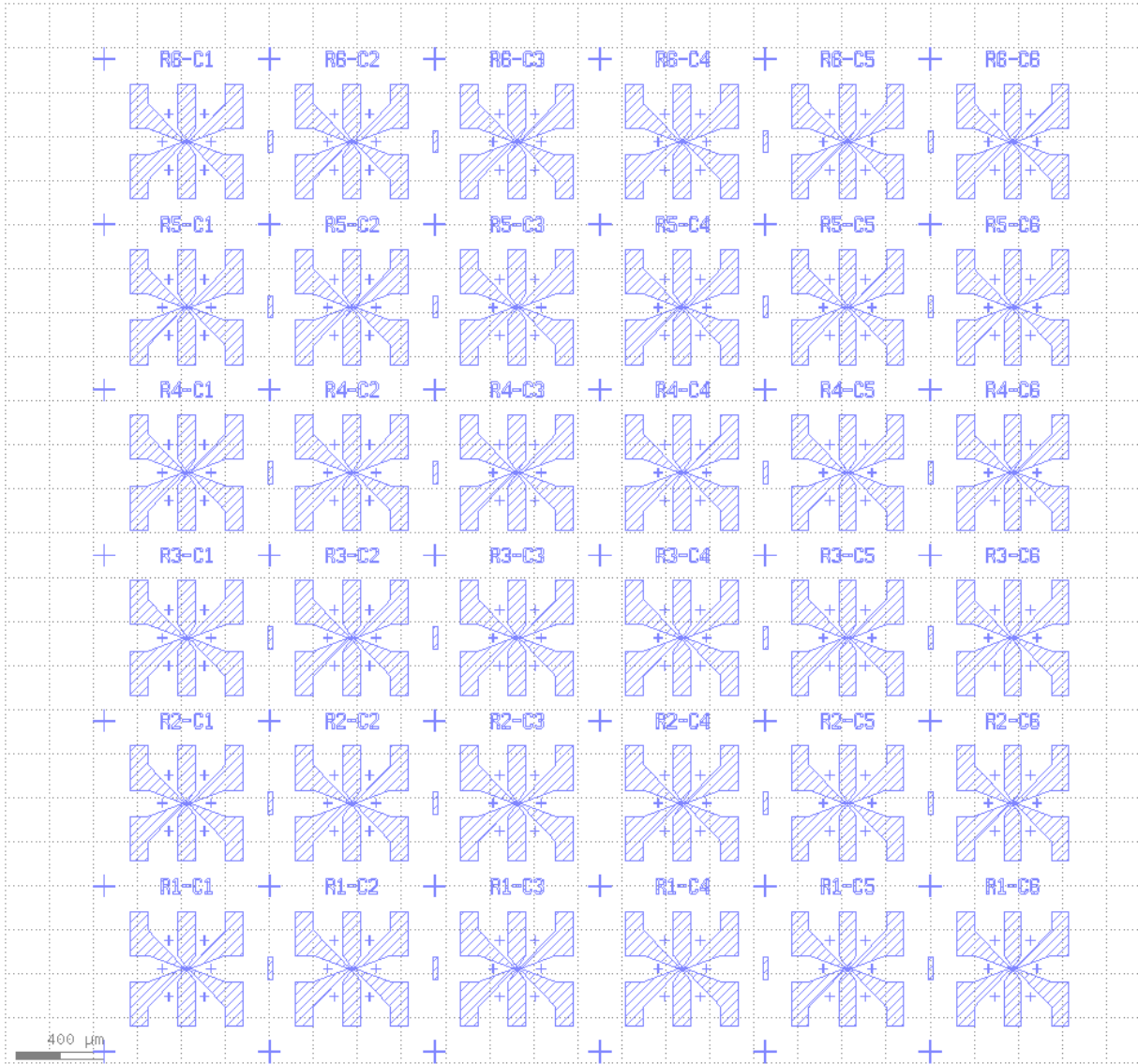


Figure 55: Mask used for one step sample fabrication.

C Electromigration

The main reason of failure that has been encountered throughout the magneto-optical analysis of the devices is represented by electromigration (EM). EM may be encountered also during static measurements if the device undergoes too high currents in dc pulse measurements or electrostatic discharges during its handling (e.g. during the wire bonding or the mounting of the sample in the instrumental setup). For this reason it is worth to explain the physical reasons underneath such a phenomenon.

Electromigration is defined as the process in which we assist to material migration due to chemical, thermal, mechanical and electrical phenomena. Material migration refers to the forced material transport in solid bodies and represents one of the most critical problems in nowadays interconnections in Integrated Circuits [46]. From a physical perspective, this phenomenon may be understood taking into account that the current flow in a conductor generates two forces:

- **the electrostatic force** F_{field} , which is due to the electric field arising in the

material;

- **the wind force** F_{wind} . This force is caused by the momentum transfer from the flowing conduction electrons to the static ions making up the crystal lattice. It is called wind force since it acts as a wind along the direction of the current flow (the electron wind). This force plays a main role in the electromigration process. As a consequence, the material transport takes place in the direction of the electron motion (i.e. from negative (cathode) to positive (anode) electric poles of the device).

In order for electromigration to take place, the F_{wind} has to overcome the activation energy necessary to start the diffusion process. Such energy is the outcome of the balance among the diffusion processes in several different directions, namely the diffusion within the crystal, along the grain boundaries and the surfaces. The component having the highest energy requirements will be the dominant one. It is important also to keep in mind that the diffusion process is highly inhomogeneous, affected by the nonuniformities present in the material, which could result also because of design issues such as mechanical tension gradients, temperature distributions or manufacturing damages. The inhomogeneities induce a divergence in the diffusion flow. The main side effect is the depletion and accumulation of material in their proximity. Typical structures that may be found are voids (in case of depletion processes) and hillocks (in case of accumulation). We conclude by noting that also Joule heating contributes to electromigration enhancement. The thermal contribution to F_{wind} by lowering the activation energy bringing a thermal contribution to the F_{wind} .

What happens in the proposed results, is that subsequently to the application of a too high voltage or current or too long voltage pulse we assist to the induction of the EM. This process causes an open circuit in the device, not allowing anymore to perform the measurements and therefore destroying the DUT.

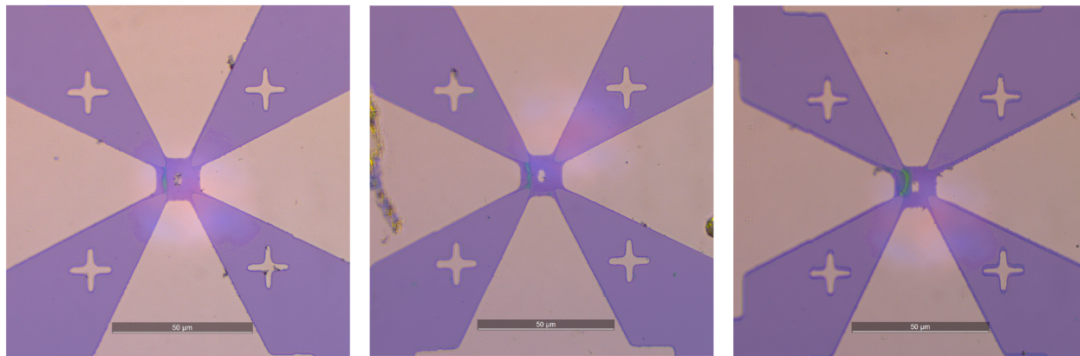


Figure 56: Electromigration (EM) in 90° Hall crosses. The iridescent areas coincides with the spots where EM caused a depletion of Pt leading to an open circuit in the structure.

